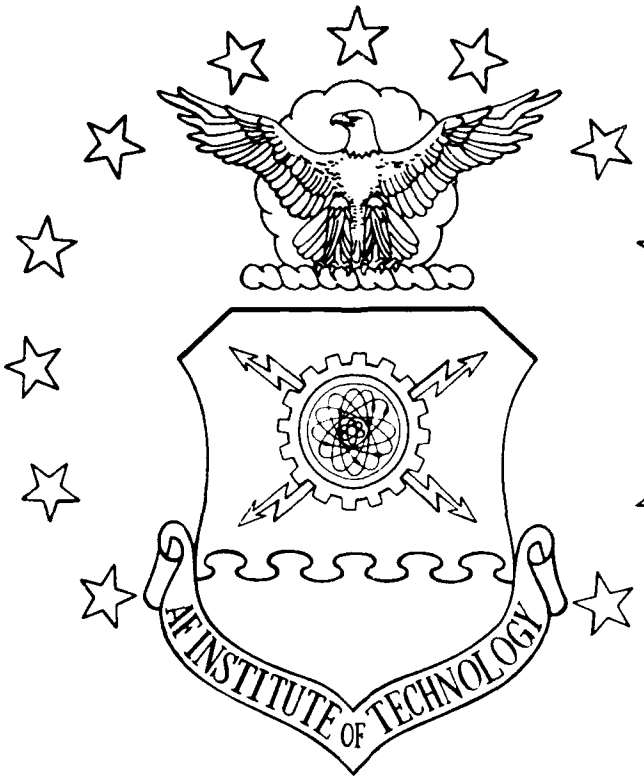

*Original contains color plates: All DTIC reproductions will be in black and white.

DEPARTMENT OF THE AIR FORCE

AIR UNIVERSITY

AIR FORCE INSTITUTE OF TECHNOLOGY

Wright-Patterson Air Force Base, Ohio

AFIT/GA/ENY/90D-03

(1)

MATERIAL PROPERTIES OF SILICON CARBIDE FIBERS WITH CONTINUOUSLY APPLIED SOL–GEL ALUMINA COATINGS

THESIS

Christian C. Daehnick
Captain, USAF

AFIT/GA/ENY/90D-03

Approved for public release; distribution unlimited.

AFIT/GA/ENY/90D-03

MATERIAL PROPERTIES OF SILICON CARBIDE FIBERS WITH CONTINUOUSLY APPLIED SOL–GEL ALUMINA COATINGS

THESIS

Presented to the Faculty of the School of Engineering

of the Air Force Institute of Technology

Air University

In Partial Fulfillment of the

Requirements for the Degree of

Master of Science in Astronautical Engineering

Christian C. Daehnick

Captain, USAF

December, 1990

Acknowledgements

This thesis, in particular the collection and evaluation of the experimental data, was an involved process that I could not have completed on my own. I am particularly indebted to my advisor, Dr Anthony Palazotto, for his overall support and guidance, to the other members of my reading committee for their efforts to keep the work intellectually rigorous, and to numerous people at the Materials Lab, especially Dr. Paul Jero, Mr George Hartman, and Mr Cameron Begg for their advice and assistance in the many details of the experimental work from initial sample fabrication to the operation of electron microscopes. I also want to thank my wife Janet for her patience and understanding during the writing of this text.

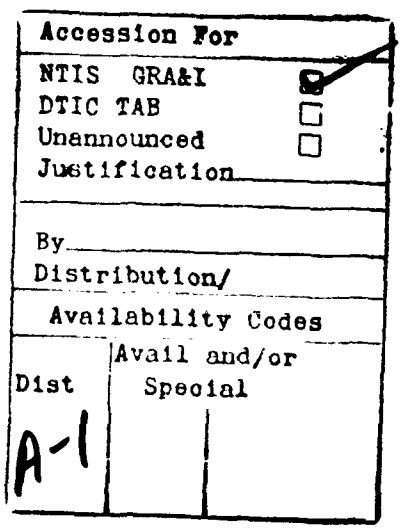

Table of Contents

List of Figures

List of Figures (continued)

List of Figures (continued)

List of Tables

List of Tables (continued)

Table Page

List of Symbols

Symbol	Meaning
δ	displacement of a fiber in a push-out test
L_o	free length of a fiber
P	load (subscript identifies specific object)
p	pressure
r	radius (subscript identifies specific object)
E	Young's modulus (subscript identifies material)
μ	effective friction coefficient in a push-out test
σ	stress (subscript identifies specific object)
σ	standard deviation
G	shear modulus (subscript identifies material)
G_{II}	strain energy release rate for mode II crack propagation
x'	characteristic crack separation distance
V	volume (subscript identifies specific object)
x	in general, refers to a measurement
$\bar{x}$	mean value of a set of measurements
ν	Poisson's ratio (subscript identifies material)
α	thermal expansion coefficient (subscript identifies material)
a	radius of an uncoated fiber
b	radius of a coated fiber
u	induced displacement (subscript identifies material)
e	strain (subscript identifies material)
A_x, B_x, C_x	unknown constants (of integration or otherwise)
A, B, ... M	(without subscripts) fiber series designators
d	fiber diameter
t	coating thickness

Abstract

An investigation was conducted to determine the effect of non-α-alumina coatings applied under varying conditions on some of the properties of silicon carbide fibers. Limited characterization of the coatings by optical, scanning electron, and transmitted electron microscopy as well as energy-dispersive x-ray analysis was performed. Tensile tests were used to determine changes in elastic modulus, ultimate strength, and strain to failure of the coated fibers relative to the uncoated fibers. The coatings were found to lower the mean value of the measured properties as their thickness increased, but the measurements were not accurate enough to determine if this corresponded to a simple rule of mixtures relationship or not. For the same reason, no definitive statements can be made about the properties of the coating itself. A two-dimensional plane strain analysis incorporating thermal residual stresses was also performed to determine possible failure points.

MATERIAL PROPERTIES OF SILICON CARBIDE FIBERS WITH CONTINUOUSLY APPLIED SOL-GEL ALUMINA COATINGS

Introduction

The original objective of this experiment was to investigate the possibility of developing an interlayer for a ceramic matrix composite that would have two basic desirable properties: a resistance to oxidation (important in a high-temperature oxidizing environment), and the ability to cause deflection of cracks propagating in a ceramic (or glass, as a model) matrix composite, hence improving the toughness and strain to failure of the composite. As such, it was to build on work being done at the Air Force Wright Research and Development Center Materials Laboratory (WRDC/ML); effectively, to combine research into microporous alumina coatings with work on the behavior of interfaces in glass or ceramic composites. From an analytical standpoint, it would attempt to bridge the gap between the primarily empirical work of the ceramicist and the macromechanical world of solid mechanics without delving into complex micromechanical models. In this sense, the experiment was originally intended to relate the behavior of an alumina interlayer to a model developed at WRDC/ML from extensive experience with glass matrix composites using carbon interlayers (12).

In the course of the experiment, however, two large obstacles became apparent. First, as there was no prior experience with the use of alumina coatings as an interlayer in a composite, there were no answers to such questions as what material properties the interlayer would have, first as a coating on a silicon carbide fiber and then after manufacture into a composite. It was initially assumed that the coatings could be made

microporous (hence relatively weak), but this had not been experimentally verified, nor was there any feeling for what the composite densification process—the hot pressing of the matrix component material (glass powder) with the fibers—would do to the coatings. In practice, an attempt was made to perform fiber push-out tests on a composite made with the alumina-coated fibers, but the results were inconclusive: in almost all cases, the matrix cracked before the coated fiber could be debonded ıg its length, so no comparison could be made to carbon interlayer composite behavior. Besides this, examination of the interlayer after matrix failure showed that the interlayer did not fail in a predictable way. Furthermore, the loads recorded were so much higher than for push-out tests on composites with carbon interlayers that there seemed little reason to hope for a weak interface from these particular coatings.

From an analytical point of view, the problem quickly proved insurmountable: a macromechanical approach may have been feasible but would have contributed little to an understanding of the problem, while a sufficiently detailed micromechanical solution to the problem of crack initiation and propagation through an interlayer would not only have been beyond the scope of this experiment but involved too many unknowns to be realistically attempted.

Rather than attempt a trial and error approach to finding a type of alumina (or other non-oxidizing) fiber coating that would in fact serve as a weak interlayer, the project was revised to study the properties of the coated fibers before composite densification, with the hope that this would provide some insight into the properties of the coating itself and perhaps the behavior that could be expected in a composite. This study was carried out by performing tensile tests on uncoated fibers and fibers with coatings of varying thicknesses applied under varying conditions. Analytically, the problem was scaled down to a two-dimensional axisymmetric plane strain analysis, with thermal residual stresses superimposed, of the fiber/coating system, with the goal of identifying possible failure locations of the fiber coating system under load.

Even with a reduced scope, however, the problem is not a simple one. By the nature of the fiber coating process, it is virtually certain that the coatings are not composed of α-alumina (the thermodynamically stable phase) but of preliminary phases; their material properties will therefore not necessarily be those of α-alumina, so an accurate theoretical prediction of coated fiber tensile properties (ultimate stress, strain to failure, and elastic modulus), is not, strictly speaking, possible. An attempt was made instead to compare measured values to a simple rule of mixtures calculation, with the properties of the coating varied. Furthermore, the coatings were thin, resulting in small volume ratios (no higher than nine percent) with respect to the fiber, and a significant number of potential error sources was identified. As a consequence, numerous individual tensile tests had to be run to achieve statistically significant differences in mean values of the measured properties, with the consequence that relatively few data points (13 in all) were obtained for the number of tests done (over 300), and only a small range of coating conditions and thicknesses could be tested.

Historical Development

The field of brittle matrix composites is one of great current interest because of the potential for combining high strength matrix materials with reinforcing agents that improve the toughness—defined as the ability to withstand local overstress without catastrophic failure (11)—and strain-to-failure of the composite material. An understanding of the behavior of such composites is far from complete, however, and there is a particular need to study the behavior of composites suitable for high temperature environments.

Several studies have been conducted (1, 3, 4, 7, 13, 14, 15, 16) on continuous fiber-reinforced ceramic composites, particularly on the behavior of silicon carbide fibers with carbon-rich outer layers, such as Textron SCS-6 fibers, in a glass matrix. Additional studies have been done on other fiber/matrix combinations. This work has served as the basis for theories on the desirable interface properties for fibers in a ceramic matrix (11, 12). The presence of a carbon outer layer, which becomes an interlayer in a ceramic or glass matrix composite, leads to a weak interface which in turn has been identified as a key factor in improving ceramic composite toughness and strain to failure (11). For high temperature oxidizing environments, however, such carbon interlayers would not be suitable, since the fibers, matrices and interlayers would probably need to be oxidation resistant (8). It has been suggested (8) that by introducing a non-oxidizing coating onto a non-oxidizing fiber before the composite is densified (laid up and hot pressed, typically, as explained in Chapter IV), an oxidation resistant ceramic composite could be created.

Importance of the Interface

The basic idea of a continuous fiber-reinforced ceramic composite is that a crack in the matrix material will be deflected along one of the reinforcing fibers, causing fiber pullout and preventing catastrophic failure of the composite. For a fiber coated with a

material different from the matrix or the bulk of the fiber itself, this can happen in one of three ways: debonding at the fiber/coating interface, fracture of the coating, or debonding at the coating/matrix interface. Empirical evidence suggests (11) that the nature of the fiber/matrix interface is important to improving the toughness and strain to failure of a continuous fiber reinforced ceramic matrix composite; specifically, a weak interface (one that readily allows fiber pullout while remaining strong enough for load transfer) is a desirable feature in such composites.

Carbon interlayers have been shown (7, 11) to be effective in producing a weak interface. These coatings are not suitable for high temperature oxidizing environments, however. Elevated temperature tension tests of such a composite (15, 16) show that the composite becomes brittle in air at 1000 °C, that the strength and strain to failure were decreased substantially, and that this was accompanied by the disappearance (oxidization) of the carbon interlayer.

Alumina Interlayers

In engineering a suitable oxidation-resistant interlayer, three mechanisms may possibly produce a weak interface (8): microporous interlayers, reactive interlayers that lose volume, and interlayers with ductile particles. Recent experiments at WRDC/ML have shown that continuously-applied sol-gel coatings are able to produce thin, reasonably uniform alumina coatings on single fibers (8), while experiments with sol-gel derived yttrium-aluminum-garnet (YAG) thin films indicated that microporosity could be achieved and the coarseness of the pores controlled as a function of sintering (heat treatment) temperature (9). With these studies as a basis, an attempt was made to create a weak alumina coating for silicon carbide fibers.

By a simple rule of mixtures calculation (see *Theoretical Considerations*) it can be shown that an increase in porosity of a ceramic material will lead to lower strength and

modulus. A porous ceramic coating could in this way be made weaker than either the fiber or the matrix, thus leading to a weak interface and increased composite toughness. Prior research at the Materials Lab led experimenters there to believe that alumina coatings applied with the sol-gel coating techniques could have anywhere from 20% to 60% porosity (air to alumina volume fraction). Predicting the exact effect of this porosity on the ability of a crack to propagate through the coating, even if the average pore size and the properties of the coating (Poisson's ratio, shear modulus, etc) were known, remains a daunting task, however. Given that the material properties, pore volume fraction, and pore size of a sol-gel derived alumina coating were unknown, analytical determination of the strength of an alumina interface, or even of the viability of this approach, could not be made.

Alumina, as an oxide, would certainly not be vulnerable to a high-temperature oxidizing environment; however, numerous questions arose as to its ability to serve as a weak interface—particularly between a silicon carbide fiber and a glass matrix—under any circumstances, what properties the coating would have, and how these might be affected by changes in initial coating conditions, and the temperature and pressure of the composite formation (densification) process.

Limited research (13) has shown that alumina fibers and glass matrices have an undesirably strong interface. Because of the YAG thin-film studies, however, it was felt that the alumina coatings could be made porous, possibly creating an interface weaker than that of an alumina fiber in a glass matrix. Some preliminary work (push-out tests) was done to explore the performance of alumina-coated silicon carbide (SCS-0) fibers in a glass matrix; indications were that the interface was not weak—push-out loads appeared to be several times those for SCS-6 fibers—but matrix failure on 90% of the push-outs made even an estimate of interface properties somewhat problematic. Questions arose as to the effect of the densification of the composite on the porosity of the alumina, the mismatch in thermal expansion coefficients between alumina and the other materials, and the possibility of a reaction between the alumina and the borosilicate glass.

It was therefore decided to remove the glass matrix from the problem and study the effect of alumina coatings applied by the continuous sol-gel coating process on the ultimate stress, strain to failure, and elastic modulus of silicon carbide fibers. This was accomplished through tensile testing of coated and uncoated Textron SCS-0 fibers. Variation of the above properties with coating thickness, as well as with changes in the heat treatment temperature and sol-gel concentration, was also investigated.

Predictability of Results

Originally, it was hoped that enough tests could be performed to provide the basis for an empirical relation between coating parameters and interface properties. This idea was abandoned, however, because of the large number of variables involved and the difficulty of obtaining sufficiently accurate experimental data. Among the obstacles were a lack of any good method of determining shear modulus of the coating, the need to expand the range of coating thicknesses, heat treatment temperatures and sol concentrations tested, and the uncertainty (without further, modified, tests) of the effect of heat treatment temperature and variation of sol concentration on coating properties. For example, the actual amount of sintering of a batch of coated fibers could not be accurately determined due to large temperature variations within the furnace. This was not considered critical as long as the temperature profile remained constant throughout the coating of an individual batch of fiber, however, it would play havoc with any attempt to derive a relationship between coating properties and heat treatment temperature.

Although the properties investigated do not bear directly on the question of whether alumina could be made to function as a weak interface—specifically, shear properties were not investigated—this study does provide some insight into the variation of those properties with respect to variables in the coating process. An attempt was made to anticipate and minimize experimental variations, and to conduct a sufficient number of

tests to give some statistical validity to the mean values measured. As is usually the case in experimental work, however, not all developments could be anticipated, and the data is not as complete as was expected. Nonetheless, some interesting features of the alumina coatings were discovered, and the results of this work may be of use in guiding future experiments.

Theoretical Considerations

The purpose of this section is not to derive a theory that will predict coating and coated fiber material properties as a function of initial conditions, much less predict what effect coating a fiber in a given way will have on that fiber's performance in a continuous ceramic matrix. Although these are all questions that relate to this experiment, an analytical solution to any of them is beyond the scope of this work. Instead, this section will concentrate on the theoretical concerns of most use in conducting the experiment: statistical analysis of the data and simple one-dimensional (rule of mixtures) calculations of combined material properties. This is extended somewhat through the application of a two-dimensional plane strain analysis to the fiber/coating system, from which some information about the location of the initial failure in the tensile tests may be inferred. As an introduction, however, it is appropriate to review some of the analytical and empirically-derived theories about continuous fiber-reinforced ceramics and their components.

This experiment (in the form of the push-out tests) was initially designed to observe behavior as predicted by models developed at the Materials Lab (12). Specifically, (12) describes how the load versus deflection curve in a fiber push-out (or pull-out) test can, after accounting for load train compliance, be predicted if the material and interface properties of a fiber/matrix composite are known. Conversely, if the actual load versus deflection curve behaves qualitatively as expected, the data can be used to extract interface properties. Without going into the derivation of the equations, this may be accomplished as follows.

An expression for the displacement of the free fiber end (i.e., the one being pushed) can be written. This displacement, once the initial debonding of the fiber from the matrix has begun, will be due to compressive strain in the free length of the fiber plus the sum of the displacements over the debonded portion, and can be written:

$$\delta = \frac{L_o P_a}{\pi r^2 E_f} + \frac{1}{2\mu k \pi r E_f}\left[P_a - P_d - P^* \ln\left(\frac{P_a + P^*}{P_d + P^*}\right)\right] \quad (1)$$

where

L_o is the free length of the fiber

P_a is the applied load

r is the radius of the fiber

E_f is the Young's modulus of the fiber

μ is the friction coefficient of the interface, and

P_d is the critical force in the fiber at the crack tip for the crack to propagate.

The two other parameters are defined as follows:

$$k = \frac{E_m \nu_f}{E_f(1 + \nu_m) + E_m(1 - \nu_f)} \quad (2)$$

with E_m the Young's modulus of the matrix, ν_f the Poisson's ratio of the fiber, and ν_m the Poisson's ratio of the matrix; and

$$P^* \equiv \frac{\sigma_N \pi r^2}{k} \quad (3)$$

where σ_N is the radial (normal) stress. This can be thought of in pull-out tests as the point at which the Poisson's contraction from the axial load exactly cancels the radial normal stress.

Even if the material properties (moduli and Poisson's ratios) are known, three unknowns remain in Equation (1): P_d, P^*, and μ. Kerans argues in (12) that P^* and μ can be calculated from the non-linear portion of the experimental load versus displacement curve before the peak load (corresponding to full fiber debonding and push-out) is reached, and once this is done, P_d can be determined from Equation (1) for the entire progressive debonding curve. Furthermore, the strain energy release rate for mode II interface crack propagation (G_{II}) can be calculated as follows:

$$G_{II} = \frac{1}{4\pi^2 r^3 E_f}\left[(P_d + P^*)\left(\frac{2\mu k L_d P^*}{r} + P_d\right)\exp\left(\frac{2\mu k L_d}{r}\right) - P_a P^*\right] \quad (4)$$

where L_d is the length of fiber over which debonding has progressed, and the other terms

are as defined before. By setting μ to zero in Equation (4), G_{IIc} of the interface, a true material constant, is found to be:

$$G_{IIc} = \frac{P_d^2}{4\pi^2 r^3 E_f} \tag{5}$$

Those interested in further discussion of these equations are referred to (12); the purpose of their inclusion here is to show that they assume, among other things, that a) the fiber can be treated as a homogenous entity with a known modulus and Poisson's ratio, and b) that the load versus displacement curve for the push-out tests, after subtracting load train compliance (the extension or contraction under load of mechanical linkages in the load train), will show initial linearity, then a non-linear region (whether or not there is a noticeable initial debonding point) until the peak load is reached. Neither of these very important assumptions could be verified in the initial push-out tests of alumina-coated silicon carbide fibers, so this approach was not pursued further.

A second possibility considered was to attempt to determine properties of the fiber/coating interface directly by adapting the so-called ACK model, named after the authors of Reference (1). Again, without going into details, the model argues that the distance between cracks in one part of a bimaterial system that has been subjected to stress has a characteristic range, i.e., that multiple cracks visible in a matrix (or in this case the fiber coating) will be separated by a distance of between x' and 2x', where:

$$x' = \left(\frac{V_m}{V_f}\right)\frac{\sigma_{mu} r}{2\tau} \tag{6}$$

and V_m/V_f is the coating (matrix) to fiber volume fraction, σ_{mu} is the ultimate stress of the coating, r is the fiber radius, and τ is the maximum shear stress which the interface can sustain. From measurement of the crack separations in the coating by means of a strain stage under a microscope, this would provide some insight into the nature of the fiber/coating interface, but it does assume that the ultimate stress of the coating is a known quantity. Because this is not necessarily so, and because of practical difficulties in

setting up the experiment, this avenue was also not pursued further. In a similar vein, the analytical model proposed in (10) was interesting, but not readily testable.

Finally, some research was done to determine if any other efforts had approached a similar problem and might be adapted to describing the failure of the matrix material during the fiber push-out tests (see *Results and Discussion*). The types of theories considered in this sense were those on residual stress induced fracture (3,4), crack propagation in bimaterial systems (5), friction effects (14), and stress field computation (24). None of these suggested a straightforward way to explain the behavior of the push-out samples, but the latter did serve as the inspiration for the two-dimensional plane strain analysis of the fiber/coating system as described below.

As regards the coatings themselves, an analytical solution to the effect of changes in sol concentration and heat treatment time and temperature on the properties of the alumina coatings and the coated fibers would have been of great interest. Unfortunately, the coating method used precluded the presence of α-alumina (the thermodynamically stable state and the one for which data on material properties exists). Research has shown (20) that α-alumina nucleates from boehmite (the first solid phase of alumina encountered in the sol-gel process) through the intermediate phases of γ-, δ-, and θ-alumina. This process takes place slowly at lower temperatures, with α-alumina first detectable after 15 *hours* of heat treatment at 1040 ^{o}C (20); clearly, α-alumina will not be present in the coatings prepared for this experiment. As to which phase would be present, and what its properties might be, the total Gibbs free energy change for the formation of a new phase in a gel can be determined as a function of crystal defects energy, volume, surface area, interface energies of the new and parent phases, and the strain energy created by a physical mismatch in spaces occupied by the new and parent phases (20). With a sufficiently accurate measurement of heat transferred to the coating (a problem given the furnace temperature profiles; see *Experimental Procedure*), an attempt could have been made to determine the actual phase present, but, although the

preliminary phases of α-alumina have been studied as described in (20), it was clear that there was insufficient information—and more important, little reason—to attempt an analytical description of the coating properties.

Furthermore, the coatings (with one exception) were not applied in a single pass, but in multiple passes, which meant that the first coat applied would be subjected to n times the amount of heat treatment as the nth coat. The effect this would have on the coating, i.e., in terms of layering or other phenomena, could not be predicted. Another complication arose with the hot pressing of the samples for push-out tests; although the hot press temperature (800 °C) was lower than the coating temperature for the fiber series used (A-C), there may have been an effect on the coating structure. Even an attempt to describe coating thickness as a function of sol concentration, coating speed/heat treatment time, and heat treatment temperature was problematic; Hay (8) describes an empirical relationship, but this does not take into account the effects of multiple passes. As will be shown in *Results and Discussion*, the relationship between coating thickness and the other parameters (when multiple coatings are applied) does not appear to be linear, but insufficient data was taken to derive an empirical model.

Statistical Analysis of Data

Because of the numerous variables and uncertainties present in the experiments, a statistical analysis was used to determine if there was in fact any difference between the different cases tested. In doing this, the following elementary statistical concepts were employed.

Averaging. A simple (non-weighted) average was used to obtain the mean value for the ultimate stress, strain to failure, and elastic modulus within a particular population. For the the purposes of this study, each fiber series constituted a separate population. The median values of each of these measurement sets was also computed to give an indication of the skewness of the data.

Standard Deviation of the Population about the Mean. Henceforth referred to simply as the standard deviation, this was computed in the usual way as

$$\sigma = \sqrt{\frac{1}{N}\sum_{i=1}^{N}(x_i - \bar{x})^2} \qquad (7)$$

where N is the number of measurements in the population, x_i is each individual measurement, and $\bar{x}$ is the average of the measurements.

Standard Deviation of the Mean. The standard deviation is a good measure of the variance in the process (the coating and testing of the fibers) but does not suffice to show a statistically significant difference between mean values when the change from one population to the other is on the order of one standard deviation or less. To do this, a concept known as the standard deviation of the mean or the standard error of the mean is employed. This is simply defined as

$$\sigma_m = \frac{\sigma}{\sqrt{N}} \qquad (8)$$

but requires a short discussion.

The standard deviation of the mean is an indication of how reliable the mean itself is, in other words, how close the mean of a set of measurements is likely to be to the true value of the mean of a very large number of measurements (23). For this concept to have any value in the context of this study, the mean of the data must be of some use in the first place. For example, the mean value of a large number of coin tosses will approach 1/2 (heads being assigned a value of one and tails a value of zero), but this value does not represent a likely result of a coin toss. The mean of the ultimate stress, strain to failure, and elastic modulus of ceramic fibers, on the other hand, is thought to have some value. First, a sufficient number of trials would be expected to show a normal (Gaussian) distribution about the mean value, and second, in fiber reinforced composites a large number of fibers is present, and describing their properties in terms of a mean value is commonly accepted practice; material properties such as elastic modulus, Poisson's ratio, ultimate stress, etc are of necessity the average of numerous measurements.

The data must also be suitable for the standard deviation of the mean to be an appropriate quantity to quote, though. In general, this means that the data should be normally distributed (21:92). However, the Central Limit Theorem states that the mean $\bar{x}$ will possess a sampling distribution that is approximately normal, *regardless of the probability distribution of the sampled population*, if the population is sufficiently large (17:295). In general, the larger the population, the closer the distribution of $\bar{x}$ will be to normal, and the more skewed the distribution of the sampled population, the larger that population will need to be for the distribution of $\bar{x}$ to be normal. As a rule of thumb, a sample size of 30 is usually assumed sufficient for a normal distribution of $\bar{x}$ (17:295). With this in mind, sample sizes of 30 were selected for tensile tests of fiber series G through M. Sufficient amounts of fiber were not available to test the same sample size for fiber series A through F, and the effect of this is documented in *Results and Discussion.*

Rule of Mixtures Calculations

The only predictive calculation done for this study was a rule of mixtures calculation. This type of calculation states simply that the properties of a combination of two materials will be a weighted average of the component properties, with the weighting based on volume fractions. In the case of the elastic modulus, for example, this rule states that

$$E = \frac{V_1}{V_1 + V_2} E_1 + \frac{V_2}{V_1 + V_2} E_2 \qquad (9)$$

where E is the combined modulus, and the subscript 1 and 2 denote the volume or modulus of material 1 and 2 respectively. Of course, this is a very simplistic calculation: it assumes a uniform mixture of the (isotropic) component materials. The effects of geometry are completely ignored, and as a result this theory would not be expected to precisely predict the behavior of a silicon carbide fiber with a thin coat of alumina of

indeterminate phase (and thus indeterminate properties). Given the extreme difficulty of approaching the behavior of the coated fibers in any other way, however, this was chosen as a benchmark to which to compare the experimental data. The combined (coated fiber) elastic modulus was predicted in this way, using the modulus of the coating as a variable, and an estimate of the effective coating modulus was computed from the experimental data for use in the two dimensional plane strain calculations. Because the rule of mixtures does not account for the thermal residual stresses which will be present in the coatings, it was felt that calculation of ultimate stress in this way would not be worthwhile.

Two Dimensional Plane Strain Analysis

A somewhat more realistic analysis takes account of the cylindrical geometry of the problem and the presence of two distinct materials rather than a mixture. Thermal residual stress can also be incorporated through superposition of loads, as shown below. This approach also makes some significant assumptions that limit its applicability, but it does offer some insight into the behavior of the tensile test specimen, namely the transverse stresses that arise due to differences in modulus and Poisson's ratio of the two materials. The derivation below follows Chawla (2:186-196) which, although it describes a fiber in a unit element of matrix material, is actually a better description of the behavior of a coated fiber.

Assumptions and Variables. First, the coated fiber, henceforth referred to as the composite, is assumed to be axisymmetric with no variations in diameter along its length. This is a reasonable assumption, but does not take into account the effect, if any, of lumps in the coating (see *Results and Discussion*). Further, the composite is assumed to be uniaxially strained; again a reasonable assumption, but not completely true because physical misalignment of the fiber in the testing apparatus will cause some off-axis loading. Good experimental technique should keep this to a minimum, however. The

two materials are assumed to be characterized by the (temperature-independent) elastic properties E (axial Young's modulus), ν (Poisson's ratio) and α (the coefficient of thermal expansion). It is also assumed that no debonding or cracking of the coating occurs—at least not before the load at which the stresses will be evaluated. The latter is a reasonable assumption in itself as long as the coating has not cracked from thermal residual stress before loading even begins, but the load at which to evaluate the stresses is questionable, since it is unknown at what point the coating begins to crack. Better knowledge of the coating properties, on the other hand, would enable an estimate to be made from these equations as to what load on the coated fiber would be required to exceed the ultimate stress of the coating.

Finally, the fiber is treated as a monolithic element, which it is not. The Textron silicon carbide fibers are produced by pulling a carbon core with a nominal diameter of 35 μm through a chemical vapor deposition (CVD) apparatus to apply the silicon carbide. As a result, the fiber itself is actually made up of two components, but the general assumption is that it behaves as a monolithic element. The Poisson's ratio and modulus of this fiber would ideally be constant from batch to batch, but it appears (see *Results and Discussion*) that at least the modulus is not.

Derivation of Equations. To begin, consider a fiber of radius a with a coating applied so that the overall radius is b (Figure 1). Each component of this composite structure will have, in general, different material properties E, ν and α (coefficient of thermal expansion). Because of the geometry of the problem, cylindrical coordinates (r, θ, z) are the natural choice. Two types of stresses will be considered: those resulting from a mismatch in thermal expansion coefficients during the coating process (thermal residual stresses), and those resulting from a uniaxial load applied in the z (axial) direction (the tensile tests). Expressions for the thermal residual stress will be presented

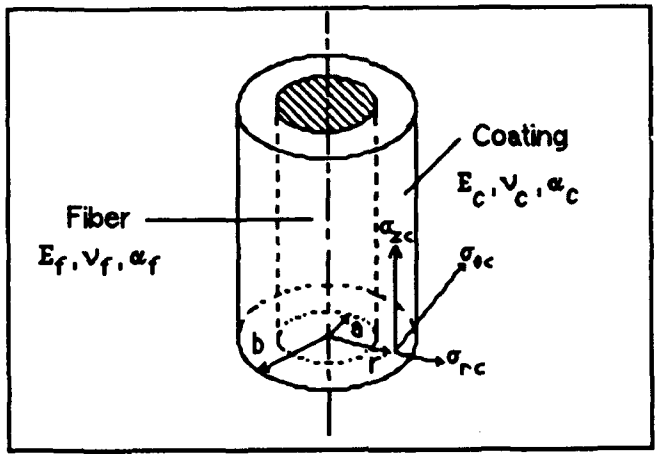

Figure 1. Sectional View of a Coated Fiber

first, since these stresses are of course already present before the fiber is subjected to an axial load.

The derivations presented below are in summary form. A more complete derivation may be found in Appendix A.

Thermal Residual Stress Equations. Assuming that the stresses take the form of the Lamé solution for a cylinder under radial stress at the boundary, the components can be written

$$\sigma_{r_1} = A_1 + \frac{B_1}{r^2} \tag{10}$$

$$\sigma_{\theta_1} = A_1 - \frac{B_1}{r^2} \tag{11}$$

$$\sigma_{z_1} = C_1 \tag{12}$$

$$\sigma_{r_2} = A_2 + \frac{B_2}{r^2} \tag{13}$$

$$\sigma_{\theta_2} = A_2 - \frac{B_2}{r^2} \tag{14}$$

$$\sigma_{z_2} = C_2 \tag{15}$$

It can be seen immediately that $B_1 = 0$; otherwise, stresses would be infinite at the axis of symmetry (r =0). By applying the following boundary conditions

$$\sigma_{r_1} = \sigma_{r_2} \qquad \text{at } r = a \tag{16}$$

$$\sigma_{r_2} = 0 \qquad \text{at } r = b \tag{17}$$

and the condition that the the resultant of the axial stress of a section z = constant of both cylinders must be zero, the number of unknown constants can quickly be reduced to two, and the stress component expressions written as

$$\sigma_{r_1} = \sigma_{\theta_1} = A_2\left(1 - \frac{b^2}{a^2}\right) \tag{18}$$

$$\sigma_{z_1} = C_2\left(1 - \frac{b^2}{a^2}\right) \tag{19}$$

for the fiber, while the expressions for the coating become

$$\sigma_{r_2} = A_2\left(1 - \frac{b^2}{r^2}\right) \tag{20}$$

$$\sigma_{\theta_2} = A_2\left(1 + \frac{b^2}{r^2}\right) \tag{21}$$

$$\sigma_{z_2} = C_2 \tag{22}$$

where the sub-subscript 1 denotes fiber and 2 denotes coating. The remaining two unknown constants are determined by applying two more boundary conditions, namely

$$u_{r_1} = u_{r_2} \qquad \text{at } r = a \tag{23}$$

$$e_{z_1} = e_{z_2} \qquad \text{at } r = a \tag{24}$$

to the expressions for the strains derived from Hooke's law

$$e_r = \frac{\sigma_r}{E} - \frac{\nu}{E}(\sigma_\theta + \sigma_z) + \alpha\Delta T \tag{25}$$

$$e_\theta = \frac{\sigma_\theta}{E} - \frac{\nu}{E}(\sigma_r + \sigma_z) + \alpha\Delta T \tag{26}$$

$$e_z = \frac{\sigma_z}{E} - \frac{\nu}{E}(\sigma_r + \sigma_\theta) + \alpha\Delta T \tag{27}$$

with Equations (18) through (22) substituted as appropriate. This results in two equations for the two unknowns that can be written in matrix form as

$$\begin{bmatrix} 2\left[\frac{\nu_2}{E_2} - \frac{\nu_1}{E_1}\left(1 - \frac{b^2}{a^2}\right)\right] & -\left[\frac{1}{E_2} - \frac{1}{E_1}\left(1 - \frac{b^2}{a^2}\right)\right] \\ \left[\frac{(1-\nu_1)}{E_1}\left(1 - \frac{b^2}{a^2}\right) - \frac{(1-\nu_2)}{E_2} - \frac{(1+\nu_2)}{E_2}\frac{b^2}{a^2}\right] & \left[\frac{\nu_2}{E_2} - \frac{\nu_1}{E_1}\left(1 - \frac{b^2}{a^2}\right)\right] \end{bmatrix} \begin{bmatrix} A_2 \\ C_2 \end{bmatrix} = \begin{bmatrix} (\alpha_2 - \alpha_1)\Delta T \\ (\alpha_2 - \alpha_1)\Delta T \end{bmatrix} \tag{28}$$

The inverse of the first term may be found analytically (most likely using a symbolic manipulator like Macsyma) and used to premultiply both sides, in which case A_2 and C_2

can also be written analytically, and general expressions for the stresses obtained directly from Equations (18) through (22). However, since all the values in the matrix as well as α_1, α_2 and ΔT have either been assumed as constant material properties or are known from the experiment, it is easier to solve for the numerical values of the quantities in the matrix. The inverse of the resulting (much simpler) matrix will be used to premultiply both sides of Equation (29), leading to values for A_2 and C_2 and subsequently for the stress components; this is done in *Results and Discussion.*

Equations for Stress under an Axial Load. To distinguish these equations from the thermal residual stress derivations, the sub-subscripts used will now be "f" for the fiber and "c" for the coating. Since axial symmetry has been assumed, stress will be a function only of r, and the relation for each coordinate axis is

$$\begin{aligned} \sigma_r &= K[(1-\nu)e_r + \nu(e_\theta + e_z)] \\ \sigma_\theta &= K[(1-\nu)e_\theta + \nu(e_r + e_z)] \\ \sigma_z &= K[(1-\nu)e_z + \nu(e_\theta + e_z)] \end{aligned} \tag{29}$$

where
$$K \equiv \frac{E}{(1+\nu)(1-2\nu)} \tag{30}$$

is the bulk modulus.

The strains can be written in terms of displacements u_r as:

$$e_r = \frac{du_r}{dr} \qquad e_\theta = \frac{u_r}{r} \qquad e_z = \text{constant.} \tag{31}$$

Substituting these into equations (29) gives

$$\begin{aligned} \sigma_r &= K\left[(1-\nu)\frac{du_r}{dr} + \nu\frac{u_r}{r} + \nu e_z\right] \\ \sigma_\theta &= K\left[\nu\frac{du_r}{dr} + (1-\nu)\frac{u_r}{r} + \nu e_z\right] \\ \sigma_z &= K\left[\nu\left(\frac{du_r}{dr} + \frac{u_r}{r}\right) + (1-\nu)e_z\right] \end{aligned} \tag{32}$$

The only equilibrium equation for this problem is

$$\frac{d\sigma_r}{dr} + \frac{\sigma_r - \sigma_\theta}{r} = 0. \tag{33}$$

Substituting the first two Equations (32) into Equation (33) and simplifying gives a second order differential equation for the radial displacement u_r:

$$\frac{d^2u_r}{dr^2} + \frac{1}{r}\frac{du_r}{dr} - \frac{u_r}{r^2} = 0 \tag{34}$$

This has a solution of the form

$$u_r = Cr + \frac{C'}{r} \tag{35}$$

which, like the other equations, is valid for either the fiber or the matrix. Consequently, expressions can be written for the radial displacement in each component as:

$$u_{r_f} = C_1 r + \frac{C_2}{r}$$

$$u_{r_c} = C_3 r + \frac{C_4}{r}, \tag{36}$$

where the sub-subscript *f* identifies the fiber and *c* the coating. Using the boundary conditions of the problem, the constants, displacements, and stress components of the coated fiber under axial stress can now be solved for. The boundary conditions are:

$$u_{r_f} = 0 \qquad \text{at } r = 0 \tag{37}$$

$$u_{r_f} = u_{r_c} \qquad \text{at } r = a \tag{38}$$

$$\sigma_{r_f} = \sigma_{r_c} \qquad \text{at } r = a \tag{39}$$

$$\sigma_{r_c} = 0 \qquad \text{at } r = b \tag{40}$$

Equation (37) comes from the fact that radial displacement must go to zero at the axis of symmetry; Equation (38) and (39) from the requirement for continuity, thus equal radial stresses and strains in both materials, at the interface; and Equation (40) from the radial stress at the free surface being zero.

Applying Equation (37) to the first of Equations (36) shows that

$$\boxed{C_2 = 0} \tag{41}$$

otherwise, u_{r_f} would go to infinity at $r = 0$. From Equations (36) and (38)

$$\boxed{C_1 = C_3 + \frac{C_4}{a^2}} \tag{42}$$

Applying the first of Equations (36) and Equation (41) to the first of Equations (32) gives

$$\sigma_{r_f} = K_f(C_1 + \nu_f e_z)$$

or

$$\sigma_{r_f} = K_f\left(C_3 + \frac{C_4}{a^2} + \nu_f e_z\right) \tag{43}$$

when Equation (42) is used to substitute for C_1.

Using the second of Equations (36) in the first Equation (32) leads to

$$\sigma_{r_c} = K_c\left(C_3 - \frac{C_4}{r^2}(1 - 2\nu_c) + \nu_c e_z\right) \tag{44}$$

Now, applying Equation (40) to Equation (44) and solving for C_3:

$$\boxed{C_3 = \frac{C_4}{b^2}(1 - 2\nu_c) - \nu_c e_z} \tag{45}$$

The remaining boundary condition, Equation (39), is now used to relate equations (43) and (44) at r = a:

$$K_f\left(C_3 + \frac{C_4}{a^2} + \nu_f e_z\right) = K_c\left(C_3 - \frac{C_4}{a^2}(1 - 2\nu_c) + \nu_c e_z\right)$$

After substituting for C_3, this leads to a value for C_4:

$$\boxed{C_4 = \frac{e_z(\nu_c - \nu_f)\, a^2\, b^2\, K_f\, V_f}{b^2\, K_f\, V_f + a^2\,(1 - 2\nu_c)(K_f\, V_f + K_c\, V_c)}} \tag{46}$$

Numerical values can now be found for each of the unknown constants, and the stress components can be solved for from Equations (43) and (44) in the radial direction. In the tangential direction

$$\sigma_{\theta_f} = K_f(C_1 + \nu_f\, e_z) = \sigma_{r_f} \tag{47}$$

$$\sigma_{\theta_c} = K_c\left[C_3 + (1 - 2\nu_c)\frac{C_4}{r^2} + \nu_c e_z\right] \tag{48}$$

and in the axial direction

$$\sigma_{z_f} = K_f[(1 - \nu_f)\, e_z + 2\nu_f C_1] \tag{49}$$

$$\sigma_{z_c} = K_c[(1 - \nu_c)\, e_z + 2\nu_c C_3] \tag{50}$$

It is interesting to note that the axial stresses are constant, but not equal. As mentioned above, a more detailed derivation of these equations can be found in Appendix A.

Material, Equipment and Experimental Procedures

Although two types of experiments were conducted—push-out tests and tensile tests—all of the useful data came from the tensile tests. Nonetheless, to give a complete picture of the investigation, a discussion of the procedures used in the push-out tests is included here as well.

Material

Two basic materials were used in the experiments: the colloidal suspension (sol) of aluminum isopropoxide and the Textron SCS-0 fibers. In addition, a glass powder was used to form the glass composite for the push-out tests.

The alumina sol was made by a standard technique (8, 9); for this experiment, previously prepared sols of known concentration were used.

The fibers used for this investigation were a non-commercial product of Textron, Inc. which has been made available to WRDC/ML for research purposes. This fiber, designated SCS-0, is made by chemical vapor deposition (CVD) of silicon carbide on a carbon filament core. What differentiates this fiber from Textron's commercial products is that those fibers (SCS-2, SCS-6, etc.) are given a final fine-grained carbon-rich coating to heal flaws in the fiber surface (6). As a result, the commercial fibers have higher break loads, and tend to exhibit more uniformity in fiber diameter and material properties such as ultimate stress and elastic modulus, than SCS-0. The carbon coating is vulnerable to oxidation, however, making SCS-0 the logical choice for this experiment. Textron's testing procedures (see Appendix B for a brief discussion of how these related to the testing procedures used for this experiment) are geared to producing the commercial fibers; as a result, although data on ultimate stress for the SCS-0 fibers was available (6), it did not correspond well to the measured data on the two uncoated fiber series (see Appendix B). The diameter measurements given by Textron did agree with those made in this experiment.

Finally, the glass powder used to create the coated fiber/glass matrix composite was a non-commercial potassium borosilicate mixture produced by Corning Glass, and designated "Type 118 RED," or more commonly "Type D". This particular type has a coefficient of thermal expansion (CTE) which closely matches that of the silicon carbide (SiC) fibers, while other types (118REA, 118REB,118REC, and 118REE) had either greater or lesser CTE's.

The table below summarizes the material property values used in calculations for this experiment. These values are the ones currently in use by the Materials Laboratory in their work, and have to some extent been verified by testing. It is recognized, however, that these numbers are not the only possible values; α-alumina, for example, can have a wide range of modulus values depending on the porosity and grain size (22), and the same is true for other ceramic materials.

TABLE 1. SUMMARY OF MATERIAL PROPERTIES

Material	Elastic Modulus (GPa)	Poisson's Ratio	CTE* (25-500 ° C)
α-Alumina	275.0	0.22	7.0×10^{-6}/°C
Textron SiC	413.7	0.15	3.62×10^{-6}/°C
Glass (118RED)	64.2	0.20	3.66×10^{-6}/°C

*(coefficient of thermal expansion)

Experimental Procedures

Fiber Preparation. The first step in either the fiber push-out or tensile test experiments was the actual coating of the fibers with a thin layer of alumina.

Coating the Fibers. This was accomplished using a continuous coating apparatus developed by Dr Randy Hay at the USAF Materials Lab. The device, pictured in Figure 2 and shown schematically in Figure 3, consists of the following parts: a fiber supply spool, the sol-gel coating bath with a recirculating pump, the sintering (heat

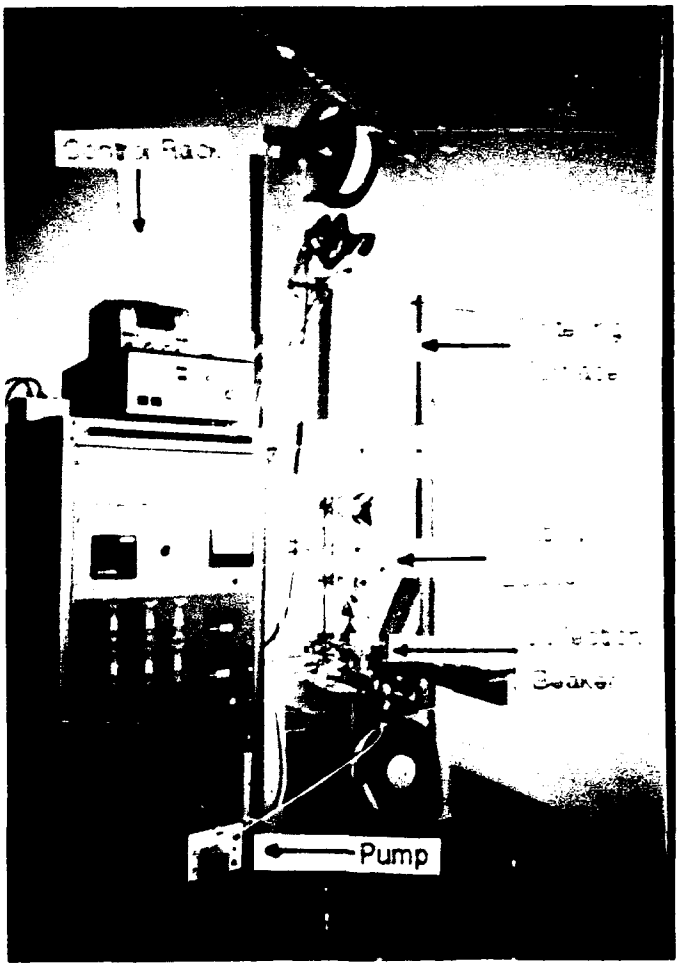

Figure 2. Sol-Gel Coating Apparatus

treatment) furnace, and the motorized fiber take-up spool. Temperature of the furnace and speed of the take-up spool can be controlled, thus both the heat treatment temperature and time can be varied; for this experiment, the take-up speed (hence heat treatment time) was kept constant while the temperature was changed for different sample batches. An additional furnace can be added between the supply spool and the sol-gel bath to burn off any debris (e.g., dust) that may have attached itself to the fiber, however it was not found (8) to have any significant effect on the coatings. (This furnace was run at a temperature lower than that of the sintering furnace, and thus should not affect on coating properties.) Use of the burn-off furnace was discontinued after the first two fiber batches.

The apparatus was loaded by hand as follows: the fiber was pulled from the supply spool to the coating bath where it was threaded through the collection beaker and the sol regulator valve located between the collection beaker and the coating beaker (Figure 3).

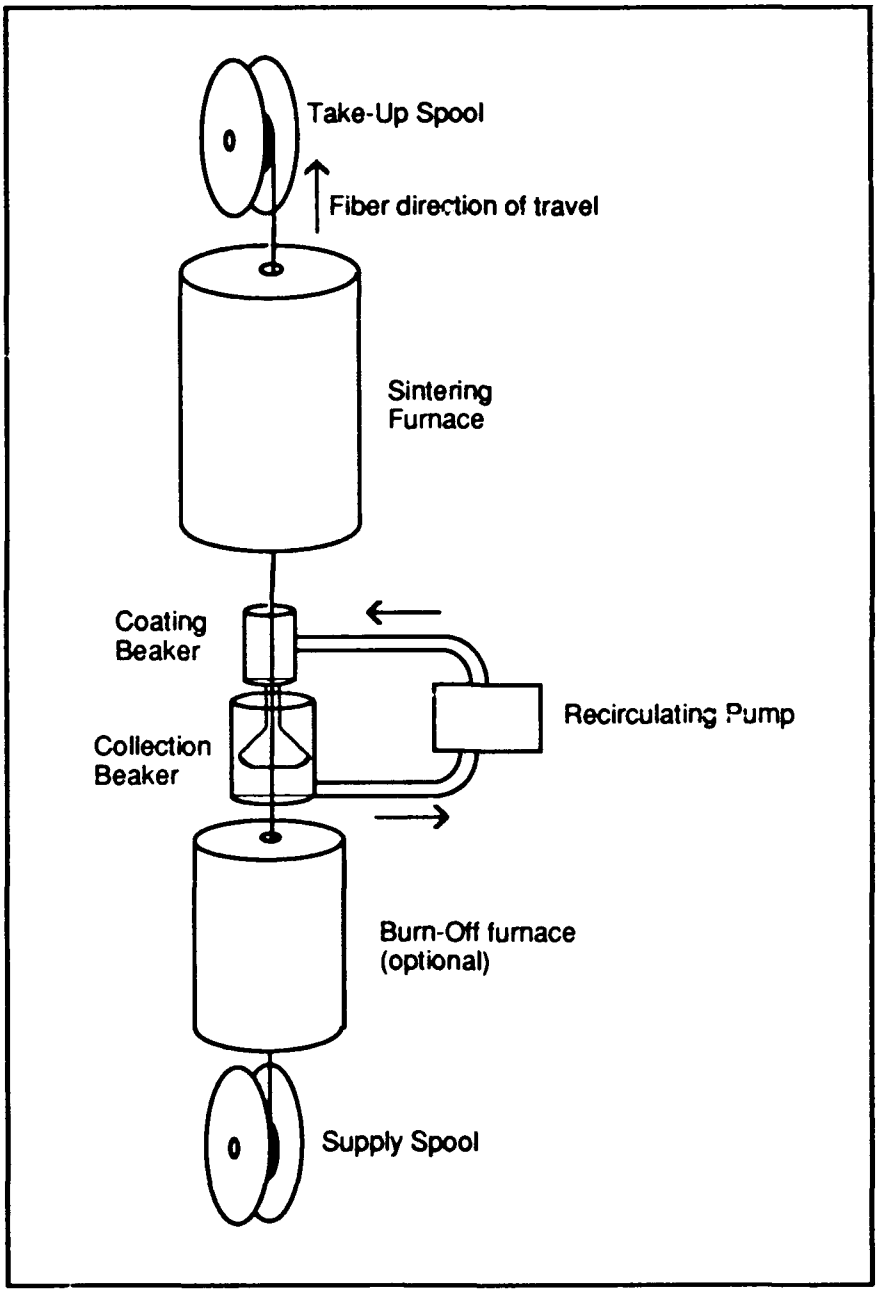

Figure 3. Coating Apparatus Schematic

From there, it was fed through the coating beaker and the sintering furnace, and pulled from the top of the furnace to the take-up spool, to which it was secured with a piece of tape. When this was complete, the take-up spool motor could be turned on and the remainder of the fiber coated at a constant speed. Because of the handling of the fiber during this process, the lead and trailing meter of each segment was discarded after the coating process was finished.

The following illustrates how a complete fiber batch was run. The total length of fiber needed for samples was first calculated, and an additional amount added to compensate for losses due to handling of the fiber during the coating process. This length was then converted to the time needed to apply a single coat, and the coating apparatus was loaded and run for this length of time. The fiber was then detached from the supply spool, and (except for fiber series A, which only had a single coat) run through the coater again as described above. When the fourth coat (in the case of fiber series H, for example) was begun, the amount of fiber being coated was kept track of by counting the number of revolutions of the take-up spool. When a sufficient length of fiber (about 2.5 meters) had received four coats, the take-up spool motor was stopped, and the fiber broken at the take-up spool. The fiber already on the spool was tagged as having four coats, and its loose end fastened down, while the remainder of the fiber (still trailing through the furnace and the coating bath to the supply spool) was fastened to a different portion of the take-up spool. The take-up motor was restarted, and the remainder of the fiber given its fourth coat, then its fifth, sixth and seventh. On the eighth coating pass, the process was repeated, and another section of fiber (series I in this case) was separated and tagged before the remaining one third of the original length of fiber was given its eighth through twelfth coats of alumina.

Coating conditions were varied as shown below in Table 2. Heat treatment time, a function of the take-up spool speed and the length of the furnace, is given for each pass

through the apparatus. The reason for the different heat treatment times is that two furnaces were used: one 0.33 meters (13 inches) long and one 0.46 meters (18 inches) long, while the take-up spool motor was run at a constant speed throughout.

TABLE 2 FIBER COATING CONDITIONS

Batch	Sol Concentration(g/l)	Furnace temp (°C)	Heating time/pass (sec)
1	72	950	20
2	72	800	20
3	36	950	28
4	36	800	28

It must be noted that the heat treatment temperatures given in Table 2 are nominal and represent neither the minimum nor maximum temperature experienced by the fiber as it passes through the furnace. The primary reason for this is the variation of the temperature profile in the furnace from the temperature as monitored by the control thermocouple. This variation is shown in Figure 4 for the .33 meter furnace (Furnace 1), and in Figure 5 for the .46 meter furnace (Furnace 2).

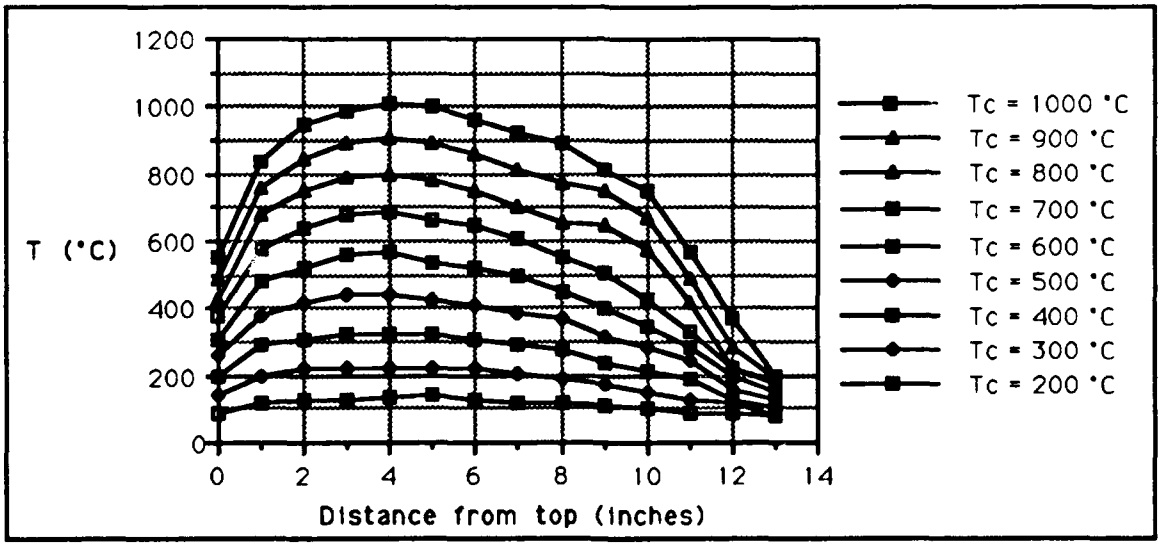

Figure 4. Temperature Variation in Furnace 1

For the .46 meter furnace, the variation was even more pronounced, and the nominal reading of the control thermocouple less representative. For example, when the

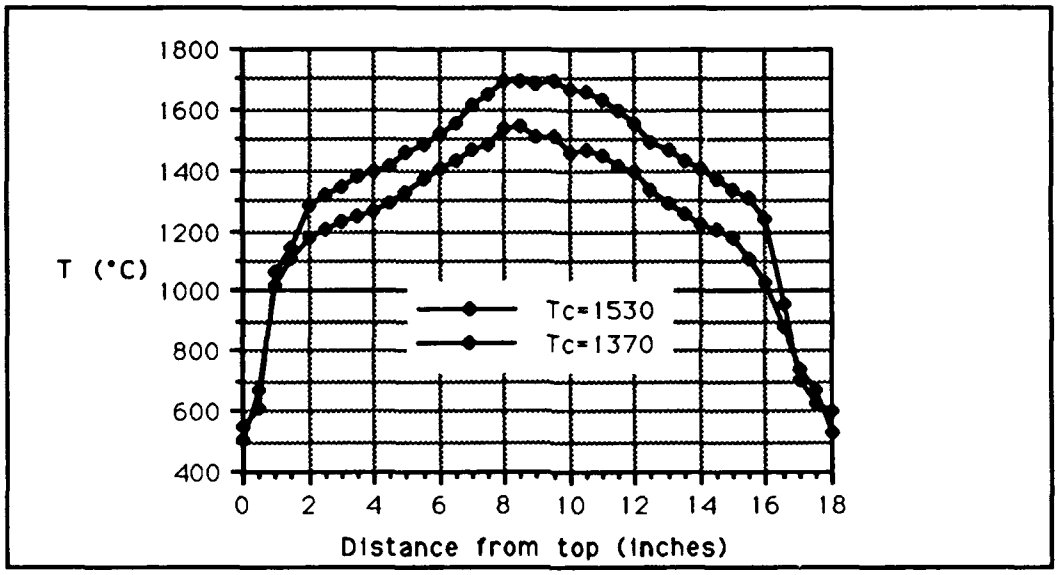

Figure 5. Temperature Profile for Furnace 2

control temperature was set to 950 °C, the actual temperature, as measured with an *accufiber* Model 10 optical fiber temperature control system, ranged from about 500 °C at the top of the furnace to 1100 °C at the hot spot. For a nominal setting of 800 °C, the variation was from about 500 °C to 920 °C. This would have been a cause for great concern if this experiment were attempting to show a theoretical relationship between coating parameters and coating thickness or material properties; however, as mentioned earlier this idea was discarded precisely because of the large number of unknowns and the difficulty of isolating variables and making sufficiently precise measurements. The only critical factor in this experiment was ensuring that the coating temperature (or temperature profile) remained constant during the processing of a particular batch, and this was in fact done.

The primary means of varying coating thickness was to run the fiber several times through the apparatus. To do this, the fiber was run through once, then the take-up spool (holding the just-coated fiber) was switched with the supply spool (which was either empty or had any remaining fiber covered with a layer of paper). The fiber was then threaded through the coater, and coated again completely. This process was repeated until the desired number of coats of alumina was applied. A byproduct of this, of course, is that on the second, third, and subsequent passes the coatings applied previously will be heat treated again and again. For a brief discussion of the possible effects of this, see *Results and Discussion.*

Sol concentration and to a lesser extent heat treatment temperature will also affect coating thickness (see Theoretical Considerations), however, the relationship is mainly empirical. To achieve comparable coating thicknesses, the fibers coated at half the sol concentration were given twice as many coating passes. A further discussion of the effect of these variables is given in *Results and Discussion.*

Table 3 below shows the effect of varying the sol concentration and heat treatment temperature between batches (as given in Table 2) as well as the number of passes on the eventual coating thickness.

TABLE 3. FIBER SERIES BREAKDOWN

Fiber Series	Batch	Number of Passes	Coating Thickness (μm)
A	1	1	.5
B	1	3	1.5
C	1	6	3.50*
D	NA	0	0
E	2	2	.5
F	2	4	1.0
G	NA	0	0
H	3	4	.5
I	3	8	1.5
J	3	12	2.5
K	4	4	.5
L	4	8	1.5
M	4	12	2.5

* more precise due to direct SEM measurements of thickness

The measurement of the coating thickness is described below.

Examination of Coatings. This step had two purposes: first, to determine if the coating was reasonably uniform and free of flaws (chips, cracks, gouges or spalling), and second, to determine the coating thickness.

Examination of the coatings was done in two stages. After the coating process was complete, two or three samples (about 3 cm in length) of fiber were examined under an optical microscope at magnifications ranging from 100x to 1000x. Three main types of flaws were noted, none of which was deemed sufficiently serious to prevent the testing of a fiber (flaking off of the coating would have been a serious flaw). The first type of flaw consisted of small (on the order of 10 μm) particles on the surface of the fiber; these were also seen on uncoated fibers and were probably dust particles. These were found mainly at lower coating temperatures, but did not occur in large numbers, did not seem to lead to coating irregularities, and were not accounted for in subsequent testing. The second type of flaw occurred when thermal residual stresses in the coating caused circumferential cracking (Figure 6). Only one fiber series was seen to have this problem: series C,

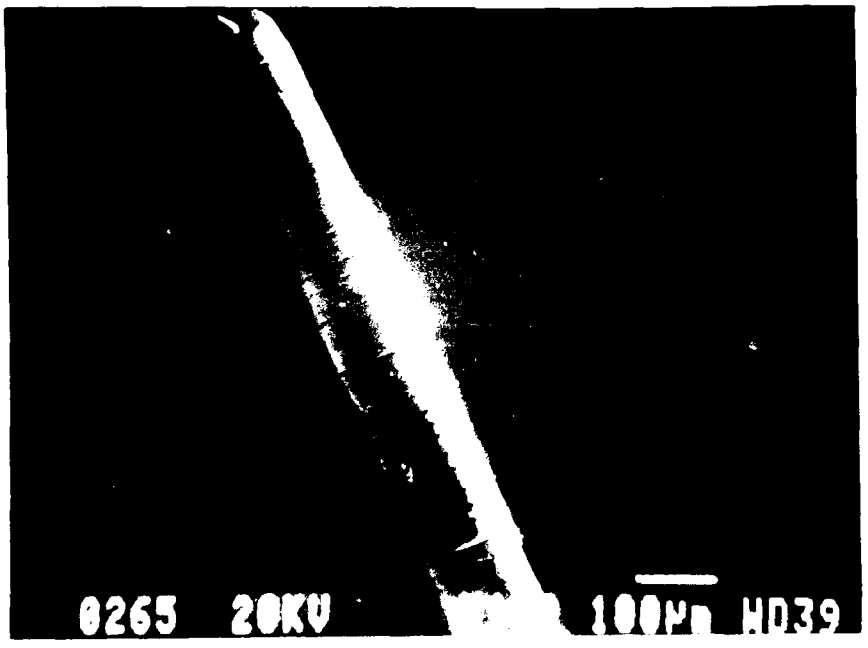

Figure 6. Circumferential Cracking of the Alumina Coating from Thermal Residual Stress

which had the largest number of coats at the high sol concentration. The effect of this flaw is discussed further in *Results and Discussion*. Finally, any obvious irregularity in the surface was looked for. An SEM photomicrograph of one such irregularity is shown in Figure 7; this is actually an accretion, probably of alumina, on the silicon carbide fiber after the bulk of the coating has spalled away (see *Results and Discussion*). This

Figure 7. Irregularity in the Alumina Coating

accretion may have been caused by a partially evaporated "glob" of sol from the surface of the coating bath adhering to the fiber and being heat treated; subsequent coats would probably have covered it and resulted in a coating bulge on that portion of the fiber. It is unknown why it would remain attached to the fiber when the rest of the coating did not. It is possible that one of the aforementioned "dust particles" served as a nucleus for this accretion, but this fiber was from series C, for which the burn-off furnace was used, and examinations of those fibers before and after coating actually revealed fewer "dust" particles than in subsequent series.

In general, it is difficult to say whether the coatings were sufficiently free of flaws or not as few criteria have been established. In an optical microscope under reflected white light, the uniformity of coating thickness can be determined from color shifts in the interference patterns (8) if the coatings are not too thick; experience suggests a coating thickness of less than 3 μm is necessary for an interference pattern to appear. Using this and the other criteria in (8): the "near complete absence of bubbles and other inhomogeneities," the coatings were determined to be reasonably uniform.

The second stage of the coating examination process was primarily for the purpose of coating thickness measurement, but in practice also served as a second check for any fiber flaws. A word about coating thickness measurements in general is in order: it is recognized that these measurements could be a major weakness in a study such as this for three reasons. First, calculations of stress and therefore modulus are strongly dependent on the cross-sectional area used, hence errors must be kept to an absolute minimum. The second reason, which is also a complication to the first, is that any method of measuring coating thickness will have some element of subjectivity; the only way to deal with this is to take multiple measurements. Finally, given the microscopic size of the coatings and the relatively huge length of the fiber over which they are supposed to be uniform, the possibility of non-uniformities is hardly insignificant. It is possible that variations in coated fiber diameter, which were not accounted for in the calculation of fiber tensile properties, account for a some of the variance in the data. This area is considered further in *Results and Discussion.*

Coating thickness was measured in two ways. The primary method was to use an optical microscope with a digital micrometer attached to the specimen platform. After properly aligning the fiber, at 50x magnification, with crosshairs in the eyepiece, magnification was increased to 400x and the fiber was focused on at its widest point (i.e. the point which clearly defined edges appeared to extend farthest to either side). The crosshairs were then aligned with one edge of the fiber, the micrometer zeroed, and the

crosshairs moved to the opposite edge of the fiber by traversing the specimen platform. When the crosshairs were aligned with this edge, the value on the micrometer (which was displayed to the nearest .001 mm or 1 μm) was read off. This process was repeated three times for each fiber measured, and those values were averaged. Three fibers were measured from each of fiber series A-F, and six fibers each from series G-M. These sets of measurements, each one already an average, were then averaged again to come up with an average diameter for the fiber. The diameter for the uncoated fiber that served as the basis for the fiber series was then subtracted from this value, and the difference divided by two to come up with the values shown in Table 3. As a check on the accuracy of this method, two fibers each from fiber series I and J were measured using a similar technique on a Bausch and Lomb microscope with a Vickers-AEI image splitting eyepiece and calibrated lenses. Materials Lab personnel claim that this system has a nominal precision of 0.1 μm. In the four cases measured, the diameter measurements obtained in this manner to within less than 1 μm with those measurements obtained in the first way. Since the precision of the original diameter measurements was 1 μm, the data seemed to agree well, and the values given in Table 3 were used for subsequent calculations of cross-sectional area, ultimate stress and modulus. Since twice the coating thickness accounts for the diameter change, an accuracy of 0.5 μm in thickness is considered reasonable.

Two other methods were used to check coating thickness. For fiber series C, which was used in a sample prepared for push-out tests, a coating thickness of 3.5 μm was measured, again using an optical microscope, when viewing the fiber in cross section after it had been imbedded in the matrix material and polished (see below for a description of this procedure). Finally, some sample fibers were examined in a scanning electron microscope (SEM) as described at the end of this section, but again only the thickness of fiber series C could be directly measured.

Fiber Push-Out Tests. Though they did not result in any useable data, the fiber push-out tests consumed a great deal of experimental time. Their failure also provided the rationale for the testing of the fibers alone, since the introduction of a matrix material added further unknowns to an already complex problem. For this reason, a brief description of the procedure follows.

Specimen Preparation. Following coating of the fibers (in this case fibers A-D), the fabrication of a glass-matrix composite was begun. The process consisted of winding the fibers onto a motorized mandrel, cutting them into sections, laying them up with glass powder in a die, and hot pressing them.

The apparatus used to wind the fibers onto a mandrel was similar to that shown in Figure 8, the only difference being the size of the mandrel used. For this experiment,

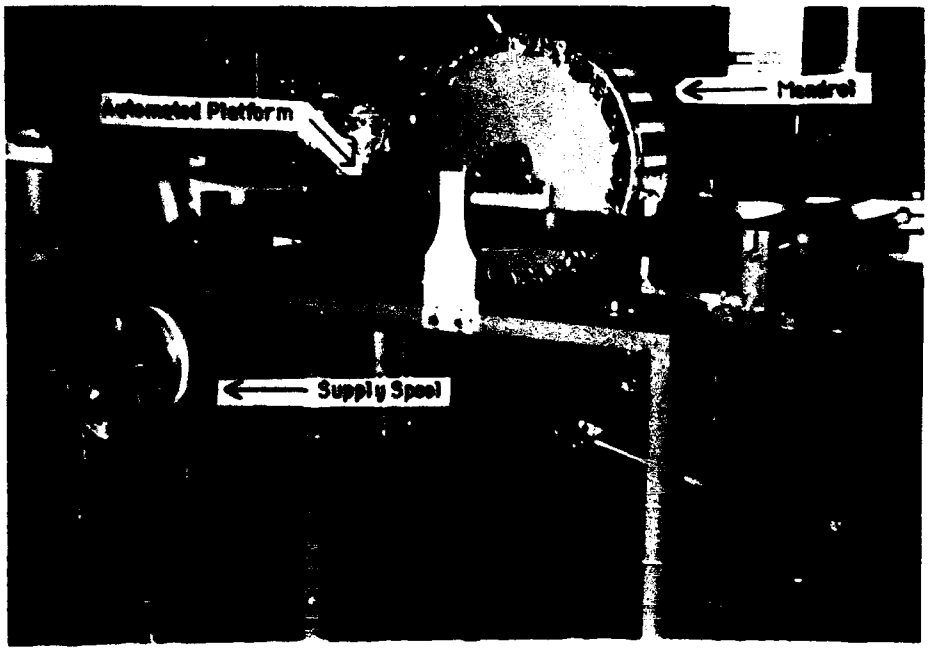

Figure 8. Fiber Winding Apparatus.

the mandrel used was eight inches in diameter; the one pictured is 18 inches in diameter. The mandrel was prepared by wrapping it in aluminum foil, then running a strip of

double-sided tape along each edge. Single-sided cellophane tape was then placed perpendicular to these strips at 1.25 inch (center-to-center) intervals, sticky side up; these latter strips would hold the fibers together after they'd been cut. The fiber was then run from the supply spool to the mandrel and attached to one of the horizontal strips of tape. The mandrel was then started at a slow speed, pulling the fiber onto it; spacing between subsequent rows of fiber was achieved by an automated platform that moved the mandrel to one side by 1.1176 mm (44 mils) in two increments per revolution. After approximately three meters of one fiber series had been wound onto the mandrel, the fiber was broken, the mandrel advanced farther to the side to leave a gap, and the fiber from the next series attached. In this way, approximately three meters each of fiber series A-D were wound around the mandrel as shown in Figure 9 below.

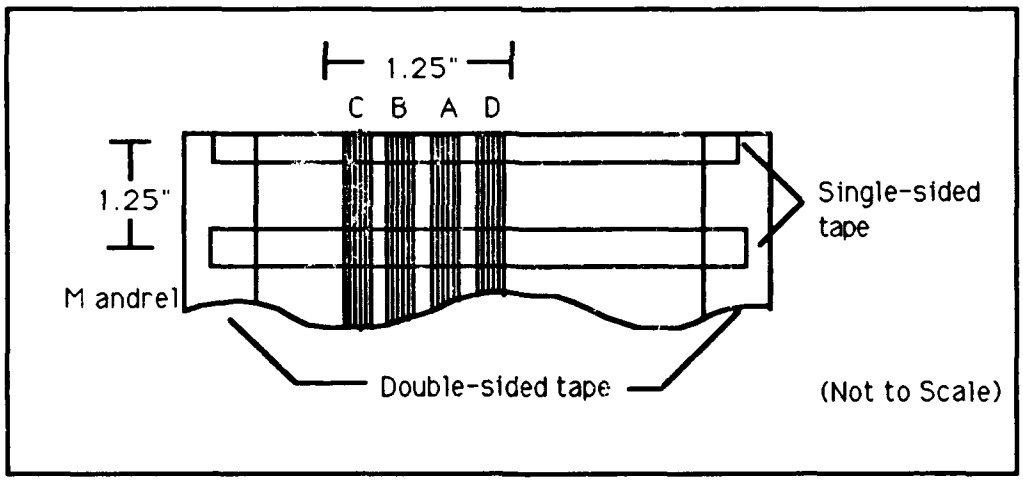

Figure 9. Fiber Winding Order

This is a representation of the top of the mandrel as if viewed from the right side of Figure 8. Referring to Figure 8, the light colored horizontal stripes on the mandrel are single sided tape, and some fiber (from a different experiment) can be seen wrapped around the near side of the mandrel.

When the fibers were all wound, the sheet of aluminum was removed from the mandrel (after cutting the fibers in one place) and laid flat. Using a paper cutter, the fibers were then cut into segments at the locations of the single-sided tape. When this was complete, the result was 21 squares of 25 fibers about 32 mm long; in other words, a layer of fibers ready to fit into a 1.25 by 1.25 inch die.

Die preparation consisted of calculating the amount of glass powder needed to give the desired sample thickness (6 mm) after hot pressing. This was done by computing the volume in cm^3 (0.6 • 3.175 • 3.175) of the finished sample, subtracting the volume of the fibers (number N • $\pi r^2 l$) and multiplying the resulting volume by the final density of the glass (2.3 g/cm^3) to give the total mass of glass powder required. The die was then assembled as follows: a molybdenum foil liner was inserted into the die, then a ram was inserted into one end. Three squares of graphite foil are then placed on top of the ram, followed by a square of molybdenum foil. The first layer of glass powder (one eighth of the total) is poured on top of this, following which the first layer of fibers is laid into place. After carefully removing the remaining cellophane tape from the fiber ends with tweezers while holding the fibers in place with a special tool, more glass powder is added, then two Saphicon™ fibers were laid crosswise (relative to the silicon carbide fibers) to ensure that different layers of fibers would not mix during hot pressing. This sequence was repeated for seven fiber layers, then another piece of molybdenum foil was laid on top of the stack, followed by three more layers of graphite foil. Finally, the upper ram was inserted into the die. A cross-sectional view of this stack is seen in Figure 10 below.

The die was then wrapped in an insulating blanket and placed into the hot press, an induction-heating chamber with a hydraulic ram. The chamber was first evacuated with a vacuum pump, then filled with argon as the temperature approached the desired value. Because the fibers were coated at a (nominal) temperature of 950 degrees centigrade, the hot press was run at 850 °C to avoid further changes in the coatings. Once the induction

furnace reached this temperature, approximately 500 psig were applied to the die via the hydraulic ram. The die was kept at that temperature and pressure for 20 minutes, then the

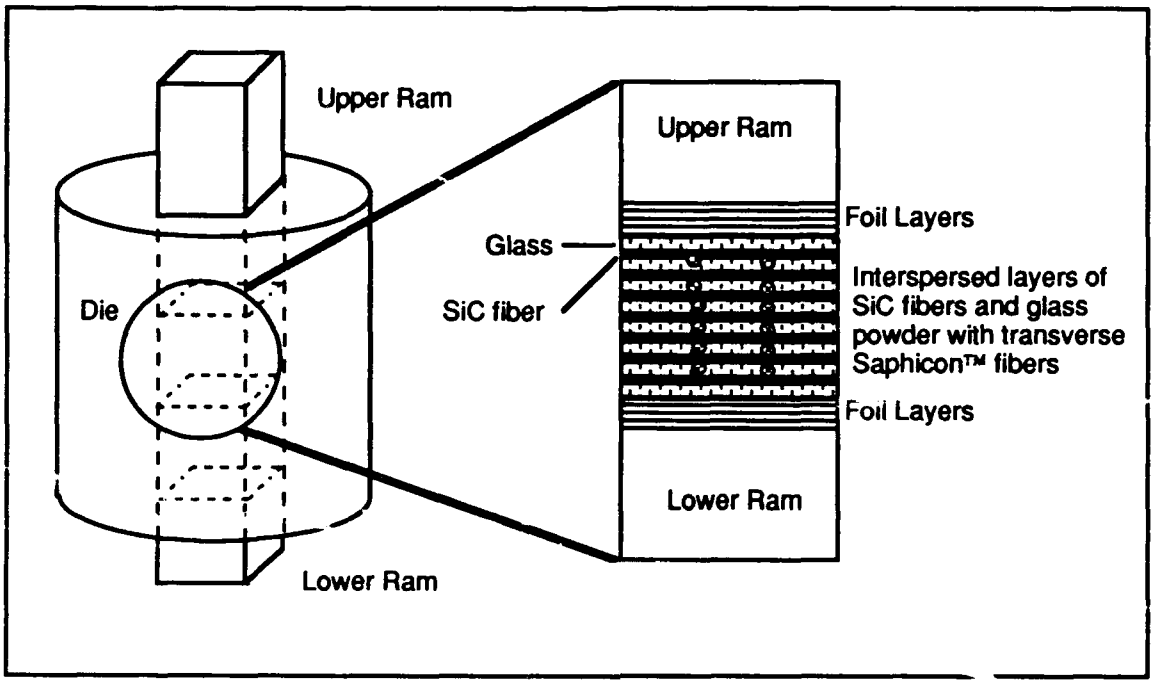

FIgure 10. Hot Press Die Cross-section

furnace was shut down and the chamber allowed to cool (with the die remaining under pressure) to room temperature. Timing is done manually, and the ram pressure, once set, is not adjusted. The latter fact means that pressure actually will drop during hot pressing, but this is allowed because it has been found that attempts to keep the pressure constant usually result in squeezing the molten glass out of the sample area and ruining the specimen.

After removing the "densified" sample from the die, the truly tedious part of the experiment began. A section of the sample (transverse to the fibers) was sliced off using a diamond-toothed saw. This section was then mounted in a microscope slide for easier handling, then ground and polished using successively finer grinding wheels and diamond pastes, finally with a 6 μm paste. When the sample surface appeared reasonably free of

scratches and other imperfections, it was photographed and a row of fibers selected for push-out attempts. This row was then mounted over a groove on a small metal block (this was to provide support to the remainder of the sample while still allowing the fiber to be pushed out the bottom; the metal block also was sized to fit into the grips on the testing machine).

Push-Out Testing. The sample, mounted on its metal block, was placed into the platform visible below the indentor in Figure 11. The pushout tester was an Instron

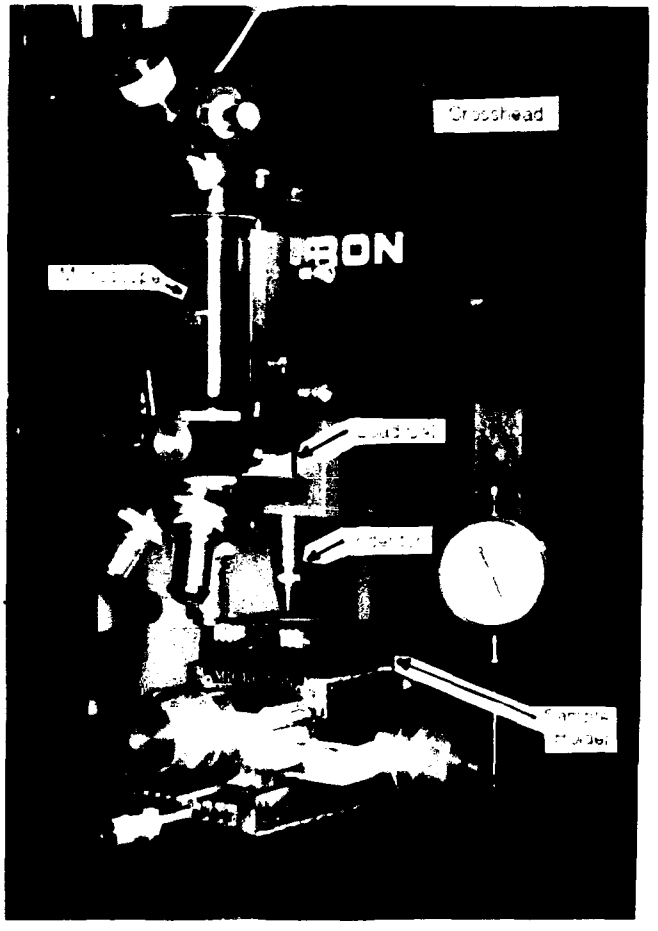

Figure 11. Instron Testing Machine Indentor Setup

1137 universal testing machine attached to both a chart recorder and a Zenith Z-100 computer used for data collection. The microscope shown in Figure 4-10 was used to check indentor alignment. Since the tip of the indentor (a 5 mil piece of tungsten wire) could not be viewed directly, it was first carefully aligned by pressing it into the epoxy holding the sample in place on the metal block. The location was checked relative to the crosshairs in the microscope, then any adjustments necessary were made. In this way, the alignment was set so that the crosshairs could be placed over a particular fiber, the sample pushed under the indentor, and the indentor lowered onto it without striking the surrounding glass. Despite the close tolerances (an indentor diameter of 127 μm and a fiber of 135-150 μm) this could be achieved on almost every attempt.

When alignment was set and a fiber selected, the indentor was lowered into position, and the Instron machine turned on. This pushed the indentor tip down until it was manually stopped, ideally after the fiber was pushed out of the glass. Theoretically, this should occur after the fiber debonds; in practice, it only happened (for the alumina-coated fibers) when the glass matrix broke. Data recorded were the load as measured by a load cell above the indentor and time (which could be converted to crosshead displacement using the testing machine speed). A qualitative presentation of the outcome of these tests is given in *Results and Discussion.*

Tensile Tests. Following the failure of the pushout tests, it was decided that perhaps a simpler investigation of coated fiber properties could be made to yield useful results. Two ideas were considered: simple tension testing to determine fiber modulus, strain to failure, and ultimate stress, and a test involving observation of the coatings while the fiber was under stress (by placing a strain stage in an optical or electron microscope) to find coating cracks and possibly derive some information on the strength of the fiber/coating interface via the ACK model (see *Theoretical Considerations*). Because of the experimental difficulty of the latter, particularly uncertainty as to whether cracking would be observed before the fiber broke, the tension test was tried.

Sample Fabrication. Preparation of the samples for testing was much simpler for this experiment than for the push-out tests. Once the fibers were coated, they were broken into segments of about 75 mm in length and fastened using epoxy to paper testing tabs. The tabs were 51 mm (two inches) in length and had a 25 mm (one inch) central cutout. The finished sample looked like the one in Figure 12.

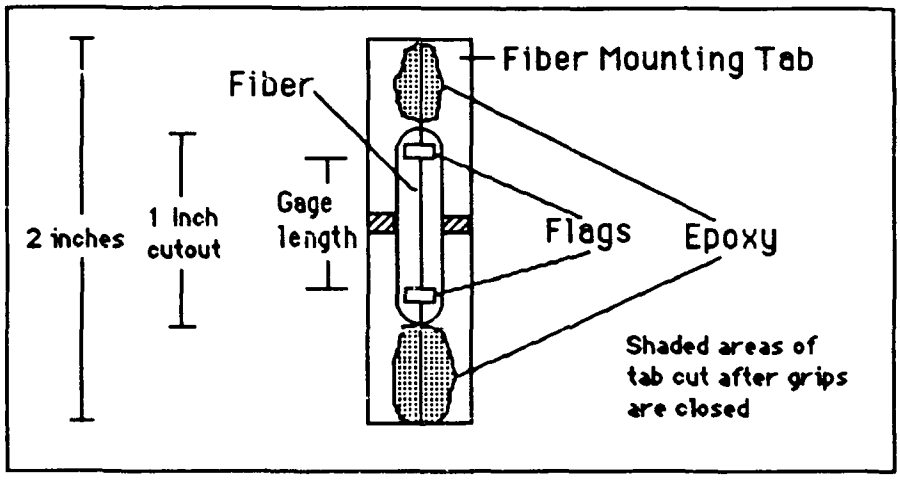

Figure 12. Tension Test Sample

After the epoxy had cured (24 hours) the excess fiber extending beyond the end of the tab was carefully cut off. By using the longer initial length, it was hoped that the central section (which would become the tested gage length) would be relatively free of bending or other stresses induced when breaking the 75 mm section off of the spool. The two objects marked "flag" in Figure 12 were small (approximately 2 by 5 mm) cardstock tabs attached to the fiber with DUCO® cement. Their purpose was to provide reference points for the laser extensometer used to measure fiber gage length and extension. This arrangement was found to be the most reliable method of ensuring that extension measurements were accurate. The problem was that the grips of the testing machine, described below, would crush an unprotected fiber even if lined with aluminum foil. By attaching the fibers to the cardstock testing tabs as described above, damage to the fiber

from the grips was eliminated; unfortunately, the cushioning effect was such that it was possible for the fiber to actually pull out of the epoxy. Although the laser extensometer could be set to read the distance between the edges of the cutout in the testing tab, fiber slippage would result in larger extension readings than the fiber was actually undergoing, hence a misleading strain measurement. The cardstock flags attached to the fiber eliminated this effect: by measuring the distance between the flags as the original gage length and then recording the extension of that length, only the actual extension of the fiber was measured. A slippage of the fiber in the epoxy would show up as a contraction in the length of the portion of the fiber being measured and not (falsely) as an increase in the length of the section under examination. As a consequence, the linearity of the stress-strain curve was improved and the strain to failure measurements made as accurate as possible.

It is recognized that this system is not without flaws. Although the length of fiber bonded to the flag was small, and extension of the fiber rarely exceeded 180 μm (approximately 1% of a nominal gage length of 18 mm), the stress produced as a result was occasionally sufficient to debond the flag from the fiber. If this happened to the upper flag, the effect was a much lower than average strain to failure, and a steep stress-strain curve. If the bottom flag slipped, the strain-to-failure was much higher than average, and the stress-strain curve very shallow. In either case, the values were easily separated from "good" data by the fact that the slope of the stress-strain curve was more than two times lower or higher than the mean value for a given fiber series, and the data was rejected. In the case where both fibers may have slipped, the data was quite noisy, but could not be rejected. Forty samples using the following combinations of bonding (fiber to test tab), grips and measurements were tried: steel grips/epoxy bonding/no flags, steel grips with aluminum foil inserts/epoxy bonding/no flags, steel grips with aluminum foil inserts/superglue bonding/no flags, steel grips/epoxy bonding/flags; the results

obtained by using the flags were more consistent and reproducible than those of any other method.

Test Procedure. The test procedure is described in detail in Appendix B, but an outline here is in order. Following the measurement of the fiber series' average diameter, each sample was mounted in turn into an ATS testing machine (Figure 13). The complete

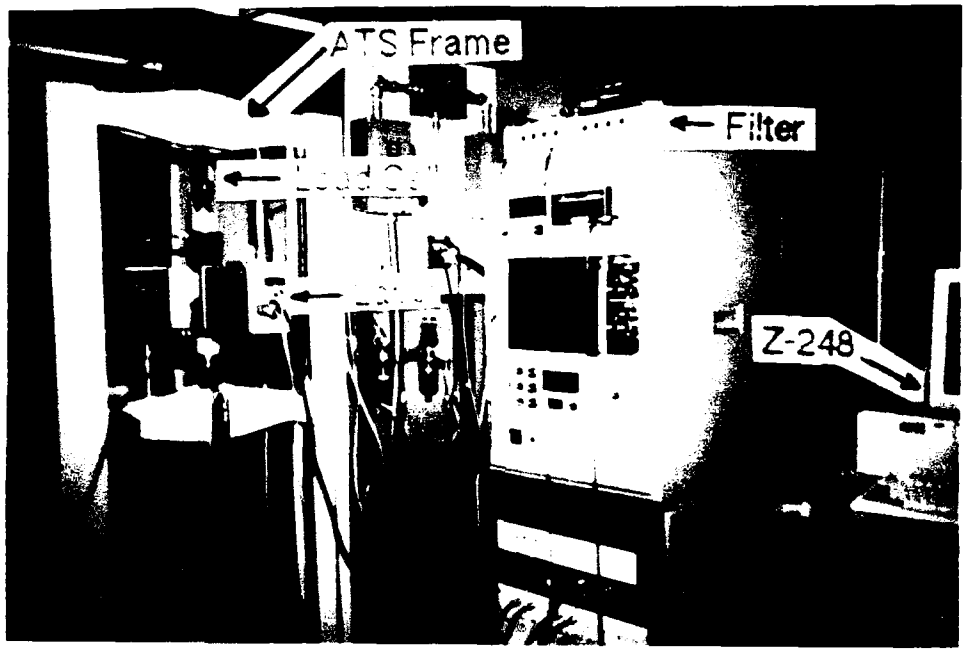

Figure 13. ATS Tension Test Setup

set of equipment included the testing frame with 100 pound load cell and a LaserMike Model 501-00 laser extensometer. The latter device uses a scanning laser beam to measure the length (and change in length, hence extension) of an object in its field of view. These were attached to a Zenith Z-248 running a modified version of the PCDAS 132 data acquisition software (see Appendix B) via a control rack that included digital readouts of load cell voltage and cross-head displacement in inches. Laser extensometer output was run through a Wavetek Model 850 low pass filter with a 10 Hz cutoff to reduce high frequency noise in the data. Load cell, crosshead displacement and extensometer outputs were recorded by the PCDAS 132 software.

Mounting of the fiber sample in the grips was done as shown in Figure 14 The crosshead, which moved the lower grip, was first raised so that the edges of the grips were separated by 1.25 inches. The sample was then positioned horizontally so that the laser scan line was parallel to the fiber and as close as possible without causing interference. Vertically, the sample was positioned so that approximately equal portions of the cardstock tab beyond the cutout were visible above and below, respectively, the top

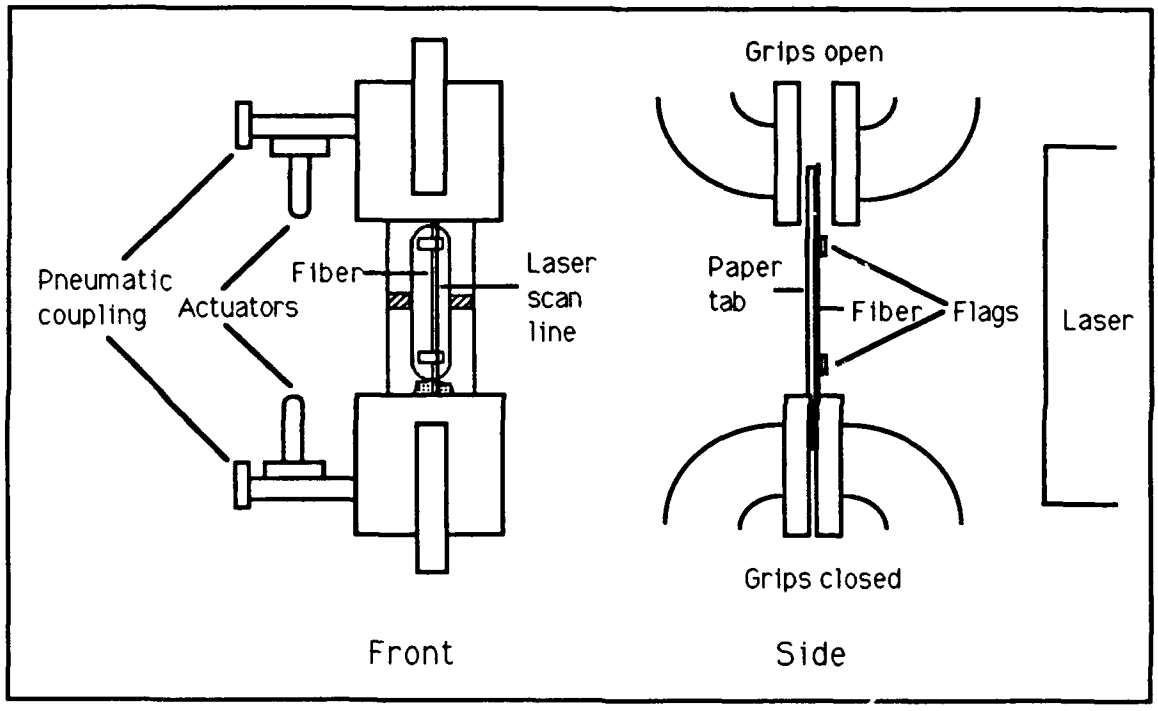

Figure 14. Sample Placement in Grips, Front and Side Views

and bottom grips. Holding the sample in this position, the lower grip was closed by actuating the pneumatic valve. Alignment was then rechecked, the laser extensometer initialized, and the upper grip closed. The load was then zeroed, and the cardstock tab cut on either side of the fiber in the shaded locations indicated in Figure 14. Care was taken to avoid putting excessive loads on the fiber during this process, and a full description of the procedure can be found in Appendix B.

With the fiber at zero load, the laser extensometer reading of gage length (between the flags) was recorded, and this information as well as sample identifying data was entered into the PCDAS 132 program. (Again, see Appendix B for a complete description of the procedure.) When this was complete, the computer was instructed to begin recording data, and the ATS machine was activated. Specifically, the crosshead holding the lower grip was placed in motion downward at a rate of approximately 0.25 mm/min (nominally 0.265 mm/min), loading and straining the fiber. The crosshead was allowed to continue in motion until the fiber failed; typically, for the samples tested, this took one to one-and-a-half minutes. At this point, the data was stored on disk, the broken sample was removed from the grips, the crosshead returned to the original position, and the process repeated for the next sample.

SEM Characterization of Fibers and Coatings. Fibers from each of the series were examined in a Japanese Electro-Optical Ltd. (JEOL) JXA 840 scanning electron microscope (SEM) operating at either 10 or 20 kilovolts. The actual operation of the microscope was performed by a Materials Lab scientist with extensive SEM experience. Energy dispersive x-ray analysis was also conducted on selected fibers, and a portion of one fiber was chemically mapped using this technique.

Fibers were prepared for the SEM by carefully cutting (with a razor knife) a segment 5-10 mm long from the sample of interest, and laying it on a conductive carbon paste that had been applied to the specimen holder. The carbon paste served to hold the fiber in place and to reduce charging under the electron beam.

Fibers and coatings were visually checked on the SEM monitor, and areas of interest were photographed. As mentioned above, some chemical analysis was also performed. The information obtained is presented in *Results and Discussion.*

Unfortunately, because of time constraints on the use of the SEM and schedule conflicts, fiber samples were not analyzed before tensile testing; in fact, the primary purpose of the SEM characterization was to examine the coatings after failure. With the

benefit of hindsight, this was not an ideal approach, since most of the coatings failed catastrophically and left little to analyze. Some leftover, undamaged, fiber was still available for testing, however, and was used for comparison purposes. Since the thrust of the thesis is not to analyze the coatings themselves, this provided adequate information, but leaves many questions unanswered. This point is covered further in *Results and Discussion*.

Some remnants of the failed push-out test samples were also observed in a low voltage Hitachi S900 SEM. The results of these observations are briefly described in *Results and Discussion* as well.

Results and Discussion

This section is divided into four parts: a discussion of sources of error in the experiment, with an emphasis on the tensile testing; a brief description of the results of the push-out tests and possible reasons for their failure; a more extensive review of the results of the fiber tensile tests; and an explanation of the relation of the two-dimensional plane strain analysis to the experimental work.

Error Sources

With the realization that the validity of the results of this study are highly dependent on the accuracy of the experimental data, every attempt was made to identify and reduce or eliminate potential sources of error. The discussion below will concentrate on the sources of error in the tensile test experiments, recognizing that there were even more possible error sources in the push-out tests.

Several sources of error were present in the experiment. These fall into two main groups: errors induced by the equipment used, and errors resulting from the manufacture of the tested sample itself. In general, those in the first group could not be controlled (aside from the usual methods of calibration) and had to be accepted. The second group was comprised of what might be termed avoidable errors, in that an ideally fabricated sample would contain none; realistically, however, the best that can be hoped for is that these errors will be small and normally distributed.

Equipment Errors. Focusing on the tensile tests, as mentioned above, there are three potential sources of equipment error. The first, common to tensile or compressive experiments, is load train compliance. This occurs when the mechanical linkages in a testing apparatus contract or stretch as a load is first applied (like the couplings on a railroad train when it is started in either direction) and as the load increases. The effect of this compliance is primarily felt when the displacement of one of the components in the

load train is used to measure the displacement of a portion of the tested sample. This problem was effectively eliminated in this experiment by measuring the initial length and the extension of the sample with a laser extensometer. Since the physical dimensions of the sample were measured directly, strain measurements were unaffected by compliance. Load measurements should not be greatly affected, if at all, since the load train and the load cell (100 pound capacity) were designed for much larger loads than were present in this test.

Accuracy of the laser extensometer is the second potential source of error. This accuracy is quoted by the manufacturer as ± 5 μm (19), and there is virtually nothing that can be done to improve this. To keep the error from being larger, the calibration was checked regularly and the extensometer was recalibrated twice during the experiment using the procedure outlined in (19). The steel rods used for calibration were provided with diameter measurements accurate to ±0.00005 inches (1.27 μm) which was sufficient to ensure that the laser was measuring to its nominal accuracy, which amounted to approximately a 0.03% error in any given length measurement.

Finally, accuracy of the load cell must be taken into account. The figures provided by the manufacturer, Interface, Inc, indicate that the load cell used had a static error band of ±0.02% and a non-linearity of ±0.02% of the rated output. This translates to an overall error of approximately ±0.022 pounds, or ±10 grams, at the break loads of the fibers (roughly 4.5 kg) for a given measurement. The load cell was calibrated prior to the experiment, and the calibration checked during the experiment.

Sample Errors. This category includes the errors that either are controllable and likely to creep in during sample fabrication or are measurable quantities. It does not include potential variations in fiber or coating material properties; since these are the quantities that the experiment is designed to measure, the overall experimental (measured) error is the best estimate of the variation in these.

The first type of sample errors are those physical variations in the tested sample. Specifically, the diameter of the fiber may vary slightly within a specific series. This could take the form of either a variation in the basic silicon carbide fiber, or in the thickness of the coating. While the latter is more likely, neither one is considered to be larger than a fraction of a micrometer ($\leq$ ~0.5 μm). In estimating the overall error, this possible variation is ignored for the reason described below.

The accuracy of the diameter measurements made on the fiber cannot be assumed to be greater than ± 1 μm, since this is generally accepted as the precision of the optical microscopes used for the measurements, and other methods (e.g., SEM) do not lend themselves to extensive sampling of diameters. In particular, the SEM cannot be used to measure a sample before testing, so even with higher precision, an equal uncertainty would remain as to the diameter variation from one portion of the fiber to another. The approach to the problem was simply to take multiple measurements and average them (see *Experimental Procedure*) Assuming an accuracy of ± 1 μm in these measurements, the small variations likely to occur in fiber diameter or coating thickness will be masked.

A related problem is whether the diameter measurements truly reflected the thickness of the coating. During mounting of the fibers on the cardboard tabs (i.e., before measuring the diameter) some of the coatings made at the lower sol concentration did flake off in the area of the fiber that was broken. The possibility exists that damage to the segment to be tested also occurred. This was precisely the reason, however, that the segments of fibers being removed from the supply spool were about 75 mm long; with an overhang of at least 25 mm on each side, the 25 mm (one inch) central section should be unaffected by any loads applied to separate the fiber segment from the main fiber for mounting. Further, the diameter measurements themselves offered an opportunity to check the coating's integrity: if the coating had flaked away, the fiber would have looked similar to an uncoated fiber. The use of an optical microscope is important in this case,

since the coated and uncoated fibers look quite similar in black and white (e.g., under an SEM), but are noticeably different in color because of the interference fringes. None of the fibers appeared to have missing or damaged coatings when the diameters were measured. Since not all fibers were checked, however, the possibility remains that a damaged coating may have gone undetected. This would be reflected in a lower than expected ultimate stress (as much as 7% for the thickest coatings at the lower sol concentration) and modulus, since the strain measurements would be unaffected. Although this possibility cannot be entirely excluded, it is not expected to be a major factor since a) no damaged coatings were seen before testing, and b) one or two that may have been damaged will not greatly affect the mean value of ultimate stress and modulus.

The remainder of the error sources are the results of imprecision in mounting and testing the fiber. These can be (and were) mostly eliminated with good experimental technique, and in general are assumed to have a negligible contribution to the overall error.

During mounting of the fiber on the cardboard tab, the fiber might become attached with a slight bending strain present. This could occur, for example, if the epoxy were beginning to harden and one end was secured with a slight misalignment relative to the centerline of the tab. It is also possible that the contraction of the epoxy as it cures could put tensile or compressive (if the epoxy spilled over the edge of the tab and effectively pulled it into a bow shape) stress on the fiber. The solution to this was threefold: first, use of a slow (24 hour) curing epoxy; second, a carefully check of fiber alignment before gluing, and third, as discussed in Appendix B, careful unloading of the fiber before tensile testing is begun to be sure that the initial load is zero. The effect of these errors if uncorrected is of unknown magnitude, but it is assumed to be virtually eliminated by the steps mentioned.

Misalignment of the mounted fiber with respect to the testing machine grips could also occur, leading to transverse loads on the fiber. This problem was reduced as much as possible by using the laser scan line of the laser extensometer to align the fiber. By doing this, the fiber itself was as close to parallel to the tension direction as possible, barring experimenter error. The laser scan line is assumed to be parallel to the centerline of the load train (the laser's platform is attached to the testing machine and cannot be tilted), while fact that the sample may have been slightly off the centerline is considered unimportant given the relative size of the fiber and the grips.

Fiber slippage in the epoxy is potentially much more serious, leading to errors of up to +20% in strain readings and in the computed modulus. As discussed in Appendix B, this problem was effectively eliminated by gluing cardstock "flags" to the fibers and measuring the extension between these flags.

Another factor that had to be eliminated by careful sample assembly was that of misaligned flags. If, instead of being perpendicular to the fiber and the laser scan line, the flags were tilted, the laser would be measuring a distance longer or shorter than the distance between the attachment points of the flag on the fiber. This could lead to an error of as much as ±2% in strain (assuming both flags were misaligned in opposite senses by about 20 degrees). The solution to this was to glue the flags on as carefully as possible to ensure that the edges to be used for measuring were perpendicular to the fiber. No attempt was made to apply a correction factor to the strain if a flag appeared slightly misaligned, however.

The flags also had to be short enough so they would not rub the sides of the gage length cutout in the cardboard tab (not so much because the friction would cause an additional load, but to keep the flags from pulling off the fiber). This was easily accomplished, and is not considered a factor in the errors.

As mentioned above, the possibility of the flags becoming detached from the fiber was perhaps the greatest concern, since movement in one of the flags could lead to an

error as large as fiber slippage in the epoxy without flags. Aside from making sure the flags were securely glued, the only solution to this problem was to attempt to recognize and eliminate bad data. See Appendix B for a further discussion of this problem.

Another potential source of error, albeit a minor one, was the possibility that the cut ends of the tabs could rub together at the beginning of the tension test and put unwanted noise in the strain data. This was solved by cutting the tabs twice on each side (Figure 12), eliminating any possibility of contact.

Finally, the possibility that a twisting or bending load (with the grips as the fulcrum) could be placed on the fiber from cutting the tab with scissors was considered. Care was taken to cut the tab as gently as possible (see Appendix B), and cutting the tabs was assumed to have a negligible effect on the fiber, especially given the fact that it is surrounded by epoxy at the point where the grips hold it.

The table below summarizes the potential error sources, their effects when known, and the solution (if any) to the problem.

TABLE 4. POTENTIAL SOURCES OF ERROR IN TENSILE TESTS

Source	Amount	Solution
Load train compliance	unknown	Use laser vice crosshead to measure strain
Laser accuracy	±5 μm*	None; keep calibrated
Load cell accuracy	±0.022%	None; keep calibrated
Variation in fiber diameter	<< 1 μm	Average measurements
Variation in coating thickness	< 1 μm	Average measurements
Accuracy of diameter measurement	±1 μm	Average measurements
Fiber bent in epoxy	unknown	Slow curing epoxy; unload fiber
Misalignment of fiber in clamps	unknown	Use laser to line up fiber
Fiber slippage in epoxy	20% in strain	Eliminate as factor by using flags
Flag not perpendicular to laser	±2% in strain	Try to eliminate by careful gluing
Flags rub cutout sides	unknown	Inspect carefully; keep flags short
Flag movement	± 20%	Attempt to recognize and drop bad data
Cut ends of paper tabs rub	unknown	Cut twice each side
Cutting tab strains fiber	unknown	Cut carefully

* From Reference (19)

Overall Error. Because so many of the errors are of unknown magnitude (although believed small), a rigorous error analysis was not attempted. . An estimate of the likely error in the stress and strain measurements can be made from the accuracies of the various measurements, however. These are given in Table 5 as fractional error percentages by dividing the various accuracies by a typical measured value.

TABLE 5. PERCENTAGE ERRORS IN MEASUREMENTS

Quantity	Fractional Error (%)
load P	0.022
radius r	0.7
length L	0.03

These percentages can now be used in a standard formula for propagation of errors (22:100):

$$\left(\frac{\sigma_Q}{Q}\right)^2 = m^2\left(\frac{\sigma_a}{a}\right)^2 + n^2\left(\frac{\sigma_b}{b}\right)^2 \qquad (51)$$

where the function $Q = a^m b^n$ and the values in brackets are the fractional errors given by Table 5. Recognizing that the stress σ is proportional to the load and to the inverse of the radius squared ($\sigma \propto Pr^{-2}$, so m = 1, n = -2), its fractional error is given by

$$\left(\frac{\sigma_\sigma}{\sigma}\right) = \left[(1)^2\,(0.022)^2 + (-2)^2\,(0.7)^2\right]^{1/2} = 1.4\%$$

For the strain,

$$\left(\frac{\sigma_e}{e}\right) = \left[(1)^2\,(0.03)^2 + (-1)^2\,(0.03)^2\right]^{1/2} = 0.042\%$$

and since the modulus is the slope of the stress vs strain curve,

$$\left(\frac{\sigma_E}{E}\right) = \left[(1)^2\,(1.4)^2 + (-1)^2\,(0.042)^2\right]^{1/2} = 1.401\%$$

The above results clearly show that the dominant error that can be accounted for is the imprecision in the measurement of the diameter of the coated fibers. Nonetheless, the overall errors are still quite small—smaller than the measured standard deviation of the means— which is not surprising given the variables in the coating process and the other errors cited above but not quantified.

Push-Out Tests

As discussed in *Theoretical Considerations*, a coating material will have desirable properties for a fiber-reinforced ceramic composite if it (the coating) serves as a weak interface between the fiber and matrix, thus increasing the likelihood of fiber debonding and pullout. In applying alumina coatings to silicon carbide fibers and placing them in a glass matrix to form a composite, the hope was that the coating itself could be made weak; in other words, of the three possible modes of coating failure—at the fiber coating interface, through the coating itself, and at the coating matrix interface—the second could be achieved. In order for this to occur, the assumption was made that the coatings would be porous, and would remain porous through the composite densification process.

Had the coatings been sufficiently weak, a phenomenon similar to that described in *Theoretical Considerations* for the push-out tests should have been observed. Instead, push out tests attempted on fiber series A-D in the same glass matrix sample showed the following:

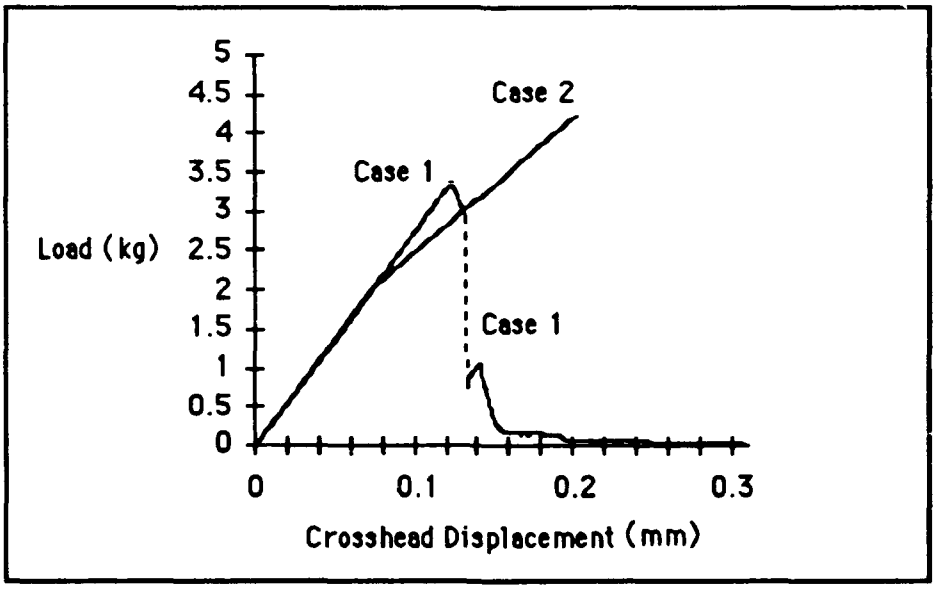

Figure 15. Fiber Push-Out Load vs Displacement Curves

The above figure is actually a composite of two push-out tests, showing two possible outcomes. In both cases, loading was initially linear with respect to the crosshead displacement. In case 1, the load continued to rise until initial debonding at the top of the fiber occurred and at the same time the glass matrix began to crack (i.e., one to three cracks began to propagate radially from the fiber/coating/matrix interfaces. These cracks rapidly led to matrix failure, as the large, rapid drop in load indicates. The small increase in load followed by a further drop to zero is probably the result of the fiber physically spreading the matrix even farther apart until there is little further resistance. The result of several such tests on a fiber reinforced glass sample can be seen in Figure 16 .

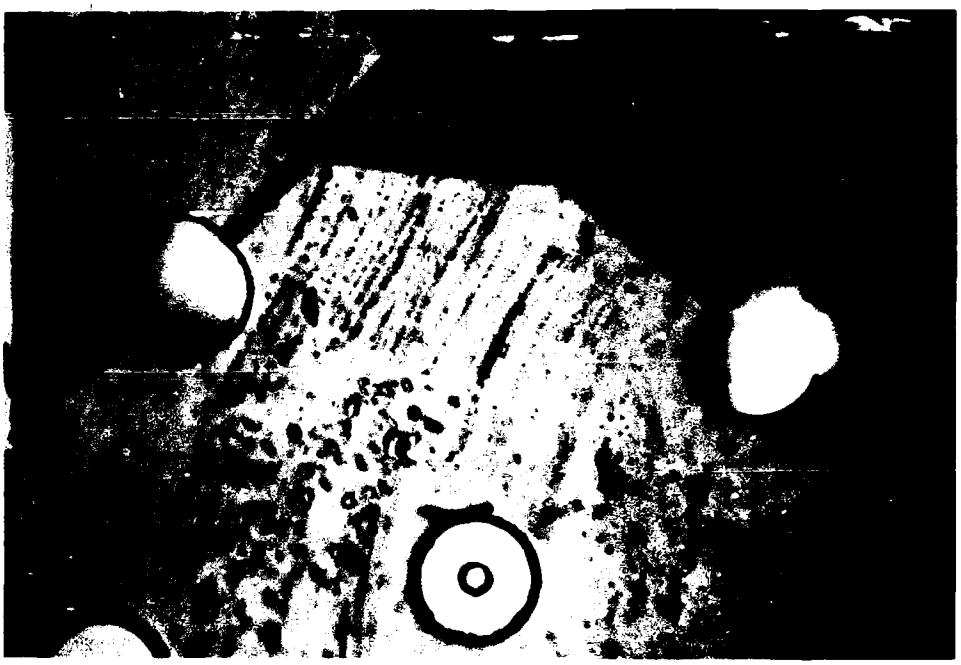

Figure 16. Glass Matrix Following Push-Out Tests (100 x Magnification)

In case 2, at about 2.2 kg of load, an initial debonding of the top of the fiber apparently occurs. This is indicated by a change in slope of the load vs displacement curve, and backed up by optical microscope examinations of fibers that had reached this point and then been unloaded; these examinations showed that the top of the fiber had been displaced downward by a few micrometers (the difference between this value and a crosshead displacement of about 80 μm at this point is accounted for by load train

compliance). Most fibers then followed a pattern similar to that of case 1, rising to an ultimate load of 3 to 4 kg, at which point the matrix cracked and either failed catastrophically or at least cracked sufficiently to allow the fiber to slide out (with varying degrees of resistance). In the specific test shown in case 2, however, the load reached almost 5 kg (the maximum for the load cell being used) without either matrix failure or full fiber debonding. Examination of this portion of the sample after it was unloaded showed that the top of the fiber had been pushed about 5 μm downward, while the bottom of the fiber was still flush with the bottom of the glass matrix. Since the sample was 1.05 mm thick, this implies a compressive strain of almost 5%. How the matrix survived without cracking in this case is unexplained.

There were also a few cases in which the fiber was apparently debonded along its entire length without causing observable cracks in the matrix. In these cases, it appeared that the fiber was pushed out of the coating at the top of the sample (i.e., the fiber/coating interface failed) as shown in Figure 17, while optical examinations of the portion of the

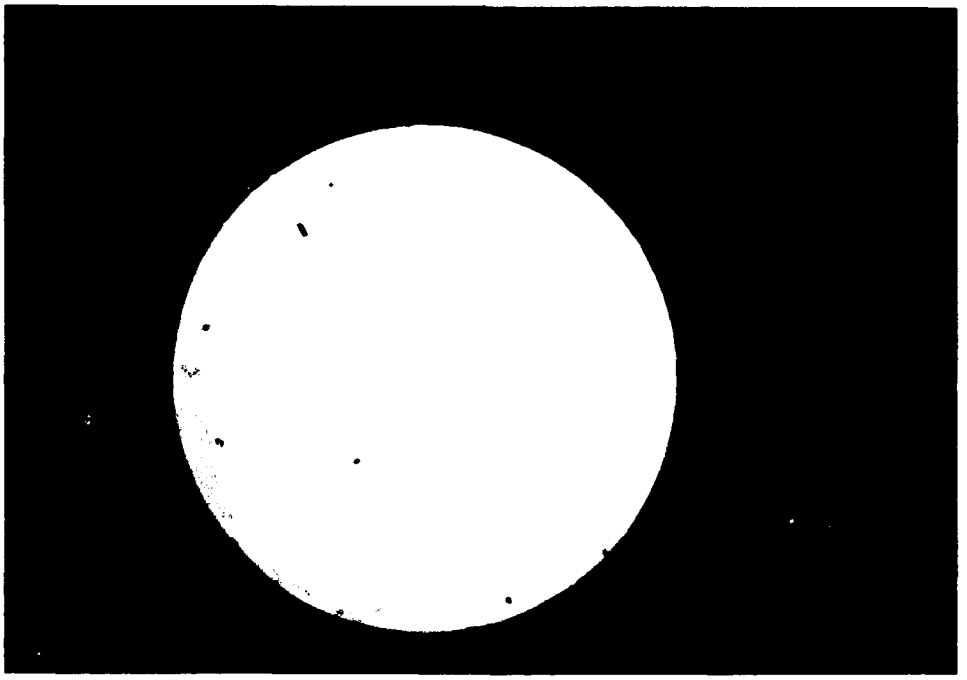

Figure 17. Fiber Pushed Out Leaving Alumina Coating Behind (400 x Magnification)

fiber that was pushed out the bottom of the matrix appeared to show at least part of the coating intact (photomicrographs taken were inconclusive, and an energy dispersive x-ray chemical analysis was not performed on this sample).

A Hitachi S900 scanning electron microscope (SEM) was also used to examine portions of the fiber/matrix composite after failure. The four photomicrographs on the next pages show some of the interesting features observed. In Figure 18, a partially pushed-out fiber is seen in a cross-section of the matrix created when the matrix failed.

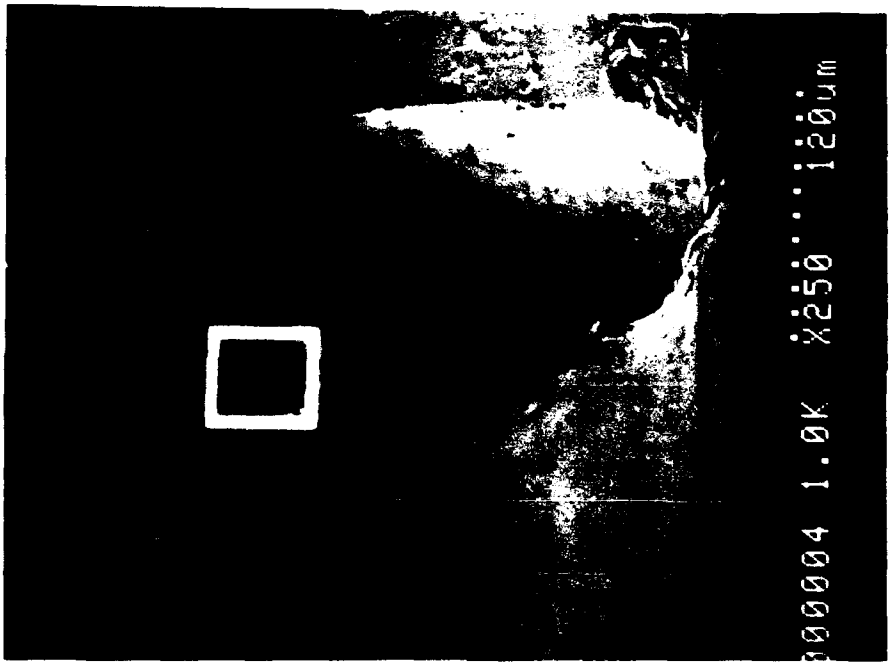

Figure 18. SEM Photomicrograph of a Partially Pushed-Out Fiber

In this case, because of the way the sample was mounted in the SEM, what was the top of the matrix is at the right side of the figure, and the "top" surface of the fiber can be seen just to the left of the white box in the photo. To the right of the "top" of the fiber in the picture is the concave channel which is all that remains of the hole out of which the fiber was pushed. Relative to the page, the fiber was being pushed to the left. An enlargement of the boxed portion of Figure 18 is shown in Figure 19. The striated surface just below center may be a cross–section of the alumina coating; the thickness is about right (this was

Figure 19. Close-Up of Fiber Channel Wall

a fiber from Series C, with an average coating thickness of 3.5 μm), and if it is in fact the coating, the apparent infiltration of the glass matrix (bottom) would provide a plausible explanation for the coating remaining with the matrix at the top of the fiber. Unfortunately, the SEM used for these pictures does not have chemical analysis capability, so the nature of the striated material could not be definitely confirmed.

Figure 20 shows the longitudinal station of the fiber where it exited the matrix; the fiber is the white band at the bottom of the photo. It appears that, as the fiber exited, it caused a wedge of the glass matrix to spall away. Unfortunately, due to electronic charging of the sample, no further detail could be gleaned from this area. Finally, Figure 21 shows a portion of the fiber that had been pushed out of the matrix (the fiber is on the top, nothing on the bottom of the photo). The ridge in the middle of the picture may be a remnant of the alumina coating; according to the scale on the photo, it ranges from two to

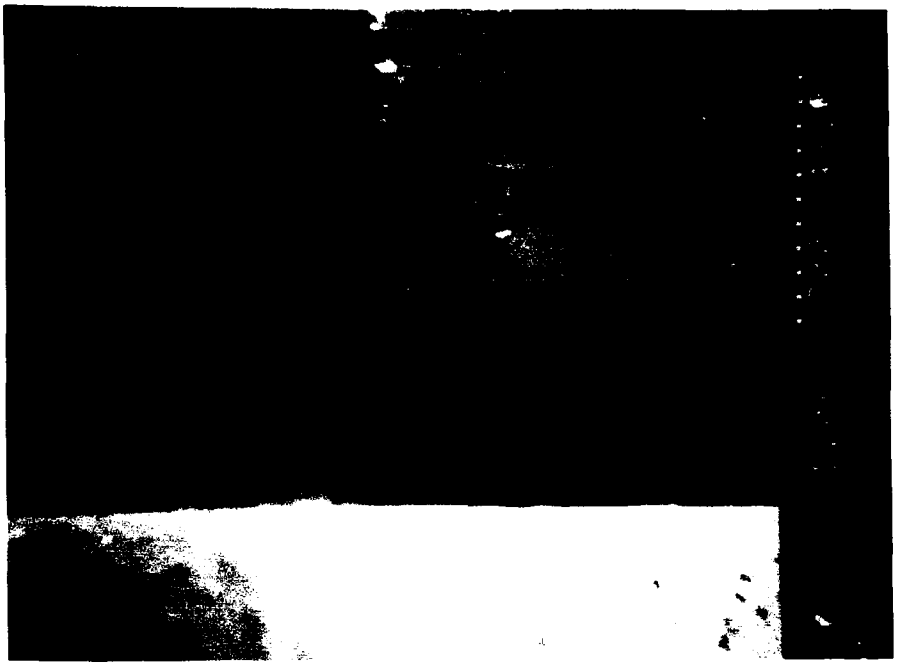

Figure 20. Fiber at Matrix Exit Point

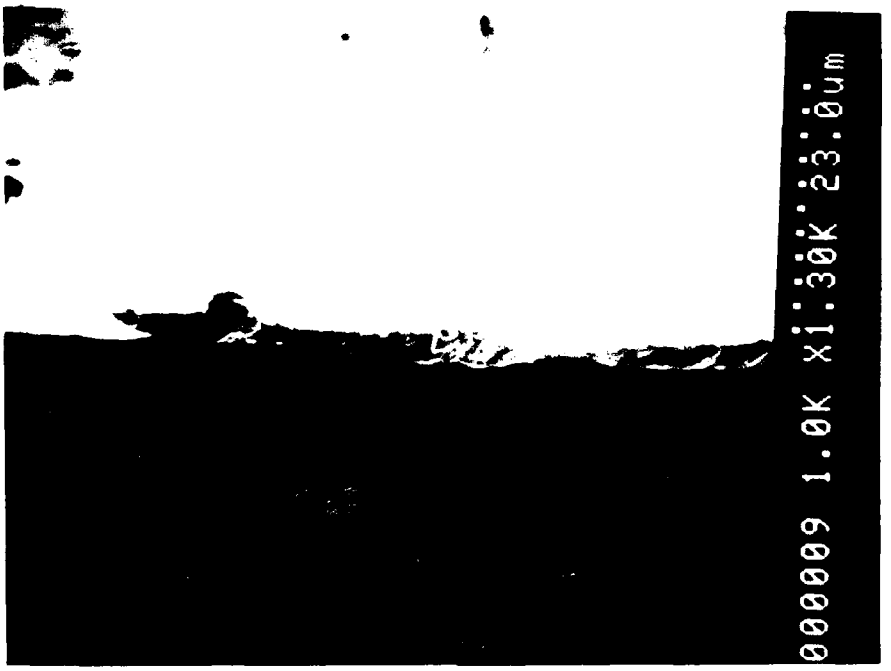

Figure 21. Possible Alumina Coating Remnant

three micrometers in thickness, which again is consistent with the coating applied to this particular fiber, particularly if some has been scraped away. Without chemical analysis, it can still not be stated with certainty that this is a portion of the coating, but that is a plausible explanation.

In an attempt to determine the porosity of the coating, Dr Randy Hay of the Materials Lab conducted a transmitted electron microscope (TEM) examination of a sample prepared from a portion of the same glass matrix composite used for the push-out tests. Figure 22 below shows a portion of the fiber with coating and a bit of the glass matrix still attached. In the photomicrograph, the dark area at the bottom is the silicon carbide

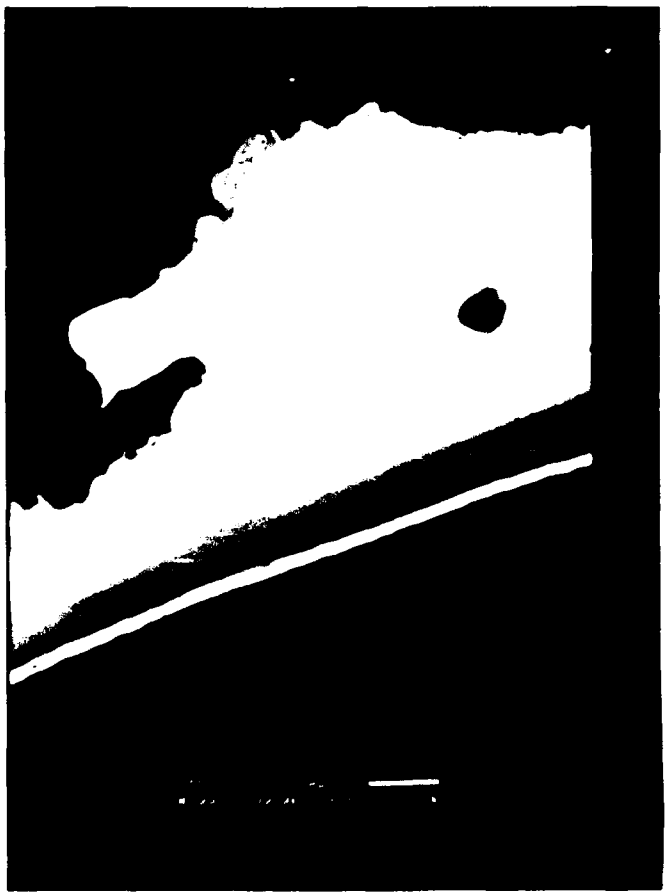

Figure 22. TEM Photomicrograph; Fiber, Coating and Matrix

fiber, the gray arc across the middle of the photo is the coating (which is about 1.3 μm thick according to the scale on the photo and indicates this fiber was from series B), and the irregularly shaped white area is a remnant of the glass matrix. Identification of these materials was confirmed by chemical analysis (electrospectrosopy). The narrow white line between the fiber and the coating is believed to show that the coating has been separated from the fiber (probably during the milling process to create the TEM specimen), but not to indicate that there is any material between the coating and fiber (e.g., glass infiltration).

The second photo (Figure 23) is a view of the coating at much higher magnification (390,000 x). As may be seen from the scale, any porosity that exists is extremely fine,

Figure 23. Alumina Coating Microstructure

perhaps on the order of 5 nanometers. It could not be determined if the coating had had this same porosity from the time of its application to the fiber, or if the composite densification process (hot pressing of the fibers into the glass matrix) may have affected

it. The practical effect of such fine porosity for the experiment was that a pore volume fraction could not be accurately estimated, and thus even a basic rule of mixtures calculation of coating modulus using alumina and air as the two materials could not be carried out.

Although many tools were available to pursue the push-out experiments and material analysis further, the prospect of multiple mode interface failure (at the fiber/coating interface and within the coating), coupled with the small number of tests that did not crack the matrix (about 10%) led to a cessation of the push-out tests and a switch to (tensile) testing of the coated fibers alone.

Tensile Test Results

A total of 295 tensile tests were performed on coated and uncoated fibers of the 13 fiber series. This does not include dozens of tests run to determine the most effective fiber mounting method (see *Experimental Procedure*) or ten tests done on SCS-6 fibers to ensure that the experimental technique was producing reasonable results (the average results of the SCS-6 tests were an ultimate strength of 3780 MPa and elastic modulus of 441 GPa, both of which are consistent with results obtained by the Materials Lab in their tests of SCS-6 fibers). Not all of the results are of equal value; fiber series A through F were made up of coated fiber left over from the push-out tests, which accounts for the variation in number of samples. Fiber series G though M, on the other hand, were coated specifically for the tensile tests, thus the number of samples in each series was held constant to the greatest extent possible (some fibers broke during handling, data for four fibers was lost due to a malfunction in the laser extensometer at the beginning of fiber series G, and three data files—each from a different series—were accidentally overwritten during data collection). These considerations aside, the variations due to experimental procedure were accounted for as described at the beginning of this chapter

and are at least consistent within a fiber "batch" (series A-C, E/F, H-J, and K-M made up the four batches, series D and G were uncoated).

Coated Fiber Properties. The data collected, as mentioned in the chapter on experimental procedures, were the coating thickness t (by subtracting the uncoated fiber diameter from the coated diameter, or by direct measurement where possible), and the ultimate stress (σ_{ult}), strain to failure (e_{ult}) and elastic modulus of the fiber (E). See Appendix B for a discussion of how each of these was obtained. The results of the tensile tests are summarized below in Table 6.

TABLE 6. SUMMARY OF TENSILE TEST RESULTS

Fiber Series	t (μm)	σ_{ult} (MPa)	e_{ult} (%)	E (GPa)
A	0.5	1944.6	0.5271	363.1
B	1.5	2029.2	0.5775	352.0
C	3.5*	1943.0	0.5525	349.0
D	0.0	2351.7	0.5983	375.5
E	0.5	2589.6	0.7239	365.4
F	1.0	2403.9	0.7290	338.7
G	0.0	2923.8	0.8379	358.0
H	0.5	2791.7	0.8246	357.8
I	1.5	2549.0	0.7879	350.2
J	2.5	2263.6	0.7134	339.8
K	0.5	2983.6	0.8918	356.3
L	1.5	2736.0	0.8180	359.3
M	2.5	2480.8	0.7979	340.1

* measured directly

Values for the coating thickness are rounded to the nearest 1/2 μm. Values for the other properties are the mean values of the data series. Although no confidence levels are attached to the individual fiber series measurements, the data for some is clearly better than for others. A complete tabulation of the collected data along with the sample size, the standard deviation of the data about the mean, the standard deviation of the mean itself, and the median value for the stress, strain and modulus for each series is presented in Appendix C.

Several questions must be addressed regarding the quality of the data. In general, it was assumed that no debonding or cracking of the coating occurs—at least not before the load at which the ultimate stress was measured. This was certainly not true for fiber series C, which had very obvious circumferential cracks resulting from thermal residual stress even before it was tested, but it may be true for the other fiber series. Since the ultimate stress of the coating itself is unknown (and no attempt was made to calculate it via the rule of mixtures; see *Theoretical Considerations*), it cannot be determined whether the coating begins to crack before the fiber fails. Examination of the fibers after testing (see below) shows that for the most part the coatings do fail catastrophically at some point during the test, but when that is cannot be determined by this testing method; this would require examination of the coatings under tension in a strain stage in a microscope.

Another significant factor in the quality of the data is the measurement of coating thickness. With the exception of fiber series C, which because of the thermal residual stress cracking left several places where the coating could be measured to tenths of a micrometer, none of the coating thicknesses could be measured directly. (This could also be done from the TEM specimen shown in Figure 22 of course, but the difficulty of making multiple TEM samples to measure different sections of the fiber means that very few data points will be recorded, and there will be no indication of how representative an individual measurement is.) The result, as described in *Experimental Procedures*, is that coating thickness can only be given to the nearest 0.5 μm (half of the resolution of the diameter measurement). Although these numbers are considered accurate, Equation (51) shows that the diameter measurements are by far the greatest single contributors to measuring error. Given the small changes observed in the ultimate stress and modulus, especially with the thinnest coatings, the measured values must be interpreted cautiously.

Finally, there is the question of how representative the tested samples were of the hypothetical universe of coated fibers. For example, in most fiber series, there are two types of stress-strain curves, those that are almost completely linear, and some with an initial non-linearity (to about 10% of the ultimate stress) of unknown cause. (This observation comes from the process of selecting the points on the stress-strain curve between which to run a least squares fit; see Appendix B.) Although there did not seem to be a correlation between the shape of the stress-strain curve and the ultimate stress, strain to failure, or modulus, intuitively the linear data seems "better." Because no relation between linearity and the measured properties was found, no adjustments were made to the data, but it does raise concerns as to whether a large number of tests would show a normal distribution.

The question of a normal distribution is important because it is a necessary assumption in most statistical work. Since the quantities listed in Table 6 are mean values, comparing them requires computation of the standard deviations. As mentioned in *Theoretical Considerations*, although a sample population of 30 or greater is generally considered sufficient to ensure that the value of the mean itself will be normally distributed, the populations tested in this experiment are either smaller or just at this level. It may be worthwhile to look at the distribution of the data about the mean for each series and relate it to a curve for a normal distribution. There are several ways to do this, but the method used here is to overlay the Gaussian curve on a five-bin histogram, as shown below in Figures 24 and 25. Figure 24 is an example of what appears to be a good distribution, while Figure 25 shows a distribution that does not look so good. Similar charts are presented for each fiber series in Appendix C.

Two notes about this method of presentation are in order: first, by plotting the distribution on a histogram with more bins, any one of the fiber series can be made to look non-Gaussian; the question is whether more bins are meaningful for such a small amount of data. In fact, the charts are somewhat misleading in identifying the better data,

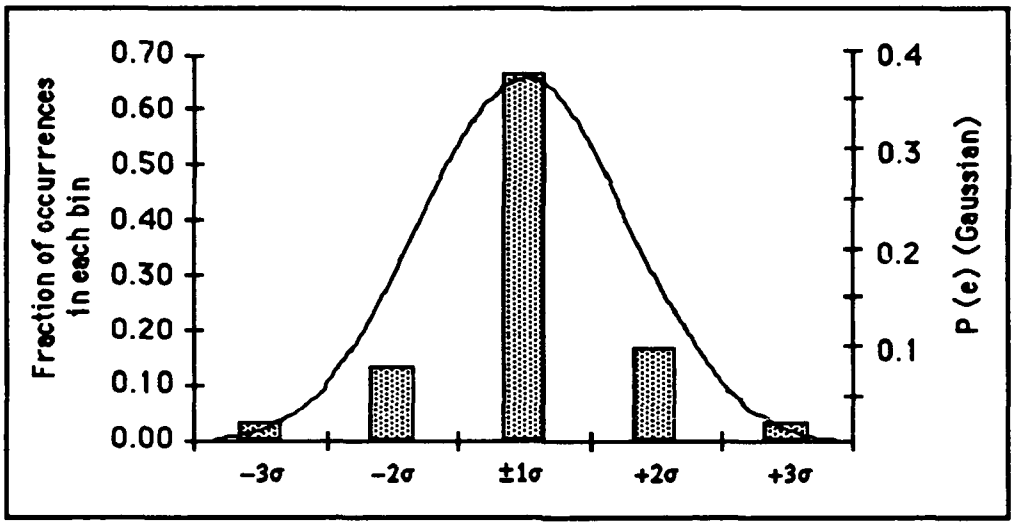

Figure 24. Distribution of Measured Modulus Values about the Mean for Fiber Series G

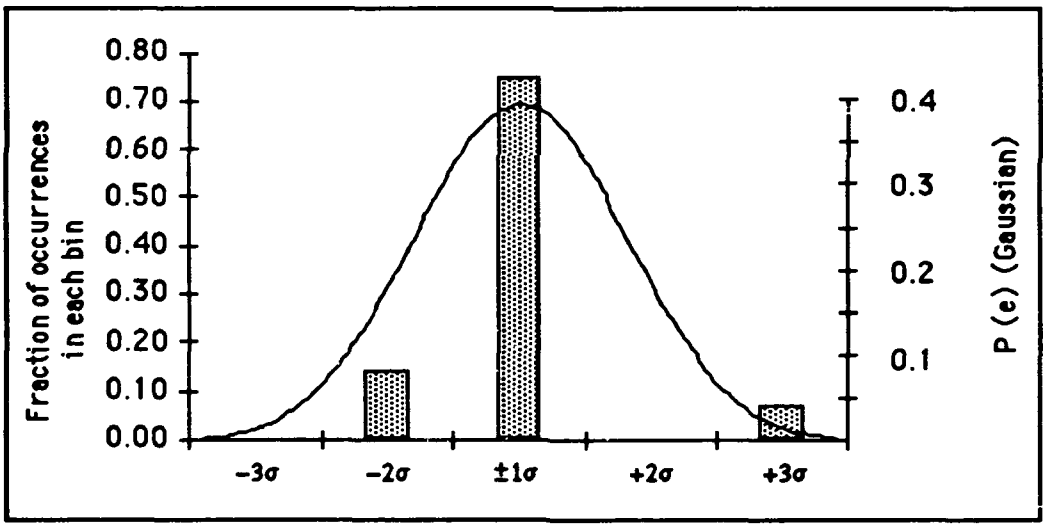

Figure 25. Distribution of Measured Modulus Values about the Mean for Fiber Series L

because they do not show the magnitude of the standard deviations. What they do show is that all the data taken (with the exception of two points in fiber series L and one in fiber series M, which were excluded from the data because they were so far from the mean) falls within three standard deviations, and the proportions within two and one standard deviations are about what would be expected from a normal distribution.

Second, only the distribution for the modulus is shown because the other data is distributed in a similar manner within each fiber series; as the slope of the stress-strain curve, the modulus was thought to be the most representative of the overall data distribution. To give an idea of the quality of the data, Table 7 lists the standard deviations of the data about the mean values presented in Table 6.

TABLE 7. STANDARD DEVIATION OF THE DATA ABOUT THE MEAN

Fiber Series	σ_{ult} (MPa)	e_{ult} (%)	E (GPa)
A	387.2	0.0959	22.7
B	266.9	0.0840	22.3
C	301.4	0.0745	23.9
D	434.2	0.1207	14.5
E	389.6	0.1179	23.2
F	307.7	0.1487	24.8
G	330.1	0.1039	14.0
H	297.5	0.0869	15.4
I	319.5	0.0925	10.4
J	254.9	0.0898	15.6
K	227.5	0.0813	15.4
L	262.1	0.1322	27.9
M	361.1	0.1237	15.3

The deviations highlight what was mentioned earlier: fiber series A through F, which came from coated fibers originally intended for the push-out tests (and were coated with the 71 g/l sol), do not appear to have data that is as good as fiber series G through M (coated with the 36 g/l sol). The distinction is particularly clear in the standard deviation of the modulus, which averages about 6.5% for the former group (fiber series D excluded) and 4.3% for the latter group (fiber series L excluded). It is not true of fiber series D, the uncoated fiber, which suggests that the sample size may not be the only factor. Coatings applied at the higher sol concentrations may in some way have more variable properties than those coated at lower concentrations. Note also that the moduli for fibers D and G, both uncoated, differ substantially; for this reason it seems important

to compare a coated fiber only to the uncoated fiber upon which it was based. There is no obvious explanation for the relatively poor performance of fiber series L.

With the aforementioned thoughts in mind, a cautious comparison of the effect of coating thickness, sol concentration, and heat treatment temperature on the coated fiber properties is in order. The following series of graphs shows the mean values of the ultimate stress, strain to failure, and elastic modulus for each fiber series. In each case, the property is plotted against the coating thickness, and the points connected by lines are those for a group of fiber series from the same coating batch. The error bars shown on the graphs are not the standard deviations of the data shown in Table 7, but the standard deviation of the mean itself as given by Equation (8).

Figure 26 shows how the ultimate stress varied as coating thickness increased. In

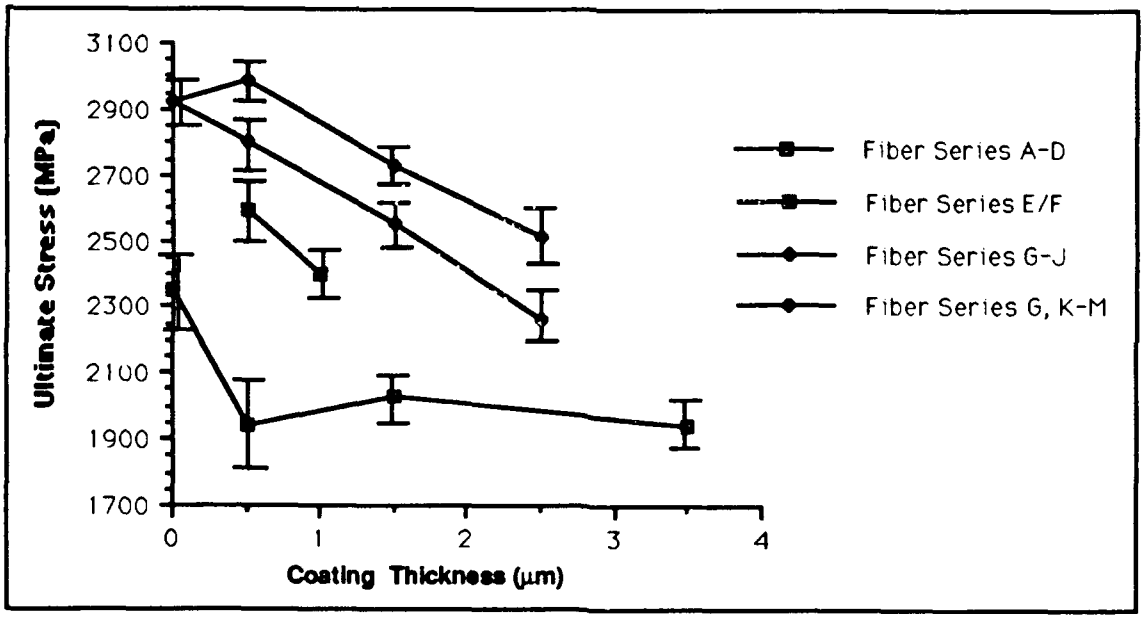

Figure 26. Ultimate Stress versus Coating Thickness

general, the alumina coating lowered the ultimate stress in a fairly linear fashion. The two exceptions to this are at the thinnest coating thicknesses, and, given the error

associated with each and with the uncoated fiber from that batch, it is difficult to say whether the large decrease seen in fiber series A-D, or the increase seen in fiber series G, K-M, is significant or not. It would be difficult to conclude from this graph that variation in coating conditions (sol concentration and heat treatment temperature) have a definite effect, however. The makings of a trend are present, and the curves are separated by one standard deviation, but more testing would have to be done to draw firm conclusions. With those caveats, the data does suggest that higher sol concentrations cause a greater decrease in ultimate stress for the same coating thickness than lower ones. It also seems to show that, at the same sol concentrations, higher heat treatment temperatures result in a lower ultimate stress for the same coating thickness.

To aid in interpreting Figure 26 and the following graphs, a modified version of Table 2 is given below:

TABLE 8. FIBER COATING CONDITIONS BY SERIES

Series	Sol Concentration(g/l)	Furnace temp (^{o}C)	Heating time/pass (sec)
A, B, C	72	950	20
E, F	72	800	20
H, I, J	36	950	28
K, L, M	36	800	28

Fiber series D was the uncoated fiber for series A through C, while G was the uncoated fiber for series H through M. The fiber that served as the basis for series E and F was not tested.

Next the effect of coating thickness and coating conditions on strain to failure is compared in Figure 27. The curves are quite similar to those in the plot of ultimate stress versus coating thickness; remarkably so, in fact, because the strain to failure measurement is completely independent of the fiber diameter measurement, and consequently has much less measurement error associated with it. This is not reflected in the standard deviations, however. In percentage terms, they are much the same for the strain data as for the stress

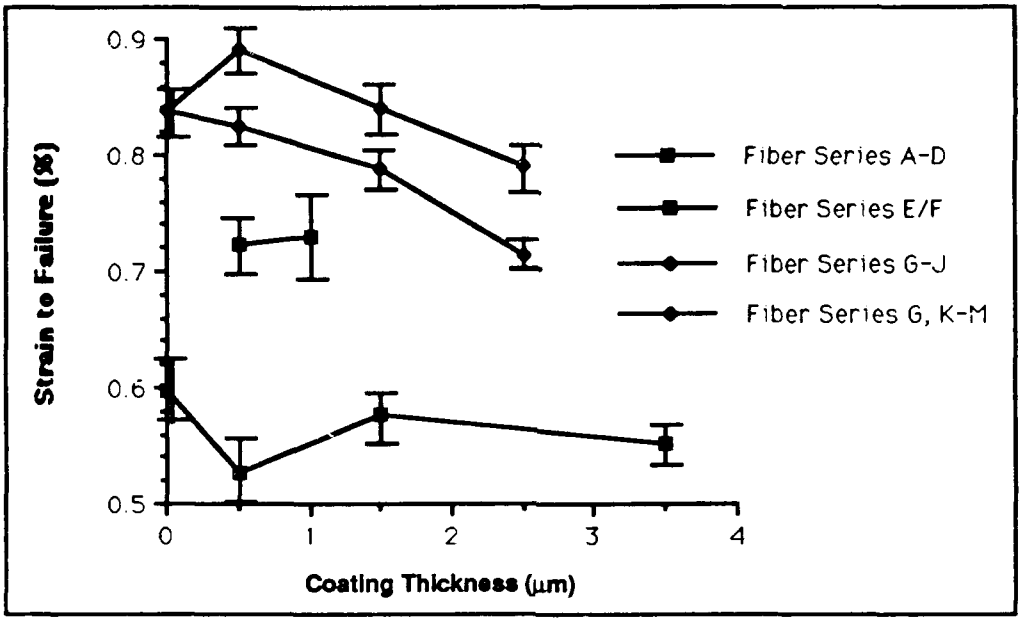

Figure 27. Strain to Failure versus Coating Thickness

data. It is reflected in the separation of the mean values, and the tentative trends noted above can be more strongly stated for the effect of coating thickness and coating conditions on the fibers. Higher sol concentrations cause a greater decrease in strain to failure for the same coating thickness than lower ones, and, at the same sol concentrations, higher heat treatment temperatures result in a lower strains to failure for the same coating thickness. The effect of coating thickness is less pronounced here than in the case of ultimate stress, however; in many cases adjacent points are separated by less than one standard deviation, and in the case of fiber series E and F, no conclusions can be drawn at all about the effect of coating thickness.

Figure 28 shows the effect of coating thickness and conditions on the elastic modulus of the coated fiber. It is immediately obvious that nothing concrete can be said about the effect of sol concentration and heat treatment time (at a given coating thickness) on the modulus; the data are statistically identical in that regard, and error bars were not drawn on this graph because the data would be indistinguishable. This is not true of the effect of

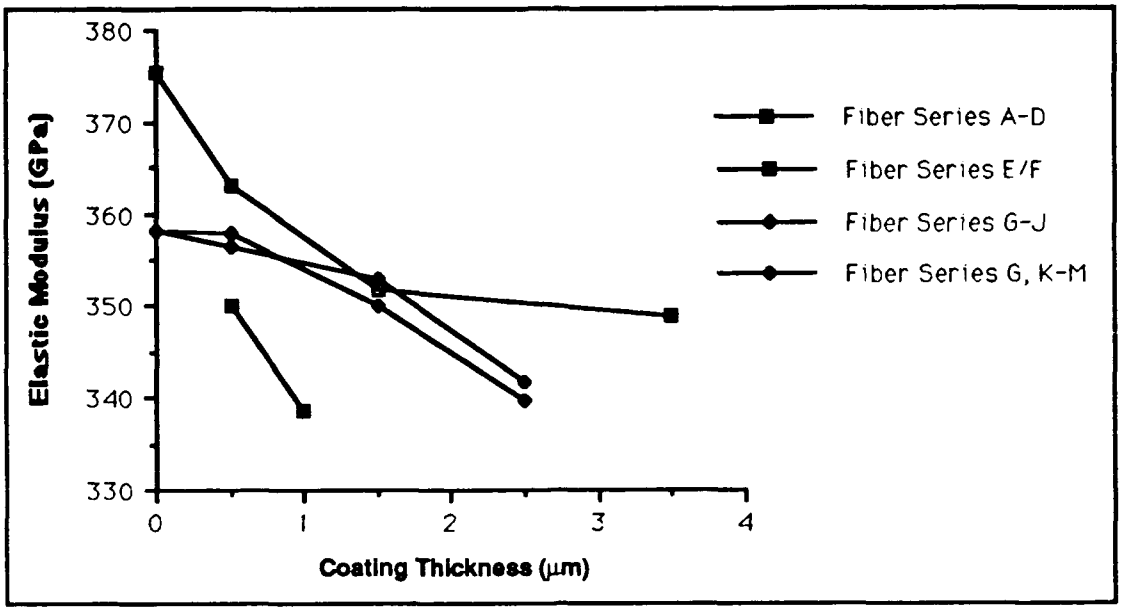

Figure 28. Elastic Modulus versus Coating Thickness

coating thickness under constant coating conditions though. Disregarding fiber series E and F because data for the uncoated base fiber for these series is not available, each of the groups of fiber series coated under the same conditions shows a monotonic decrease with coating thickness. Once again, the data for the thinnest coatings is of questionable value, however; in the case for fiber series A through D the decrease seems unusually large, while for the remaining two groups there is almost no absolute effect, let alone a statistically significant one.

Comparison to Theory. To illustrate the effect of coating thickness on the modulus, it is interesting to compare the best modulus data, that for fiber series G through J, to a rule of mixtures calculation. The effective modulus of the coating is backed out of a rule of mixtures calculation as:

$$\frac{V}{V_c}\left(E_{f+c} - \frac{V_f}{V}E_f\right) = E_c = 175.8\,\text{GPa}$$

The data for the coating and fiber volume fractions, as well as for the combined modulus, are the mean values of fiber series I, which had both the lowest standard deviation and the

closest (to the mean) median value of all fiber series. The fiber modulus comes from the mean of fiber series G, the base fiber for series I. Using this as the effective coating modulus, the rule of mixtures is again employed to plot a theoretical decrease in overall modulus with coating thickness. This is presented in Figure 29 along with a plot of the modulus variation in fiber series G-J.

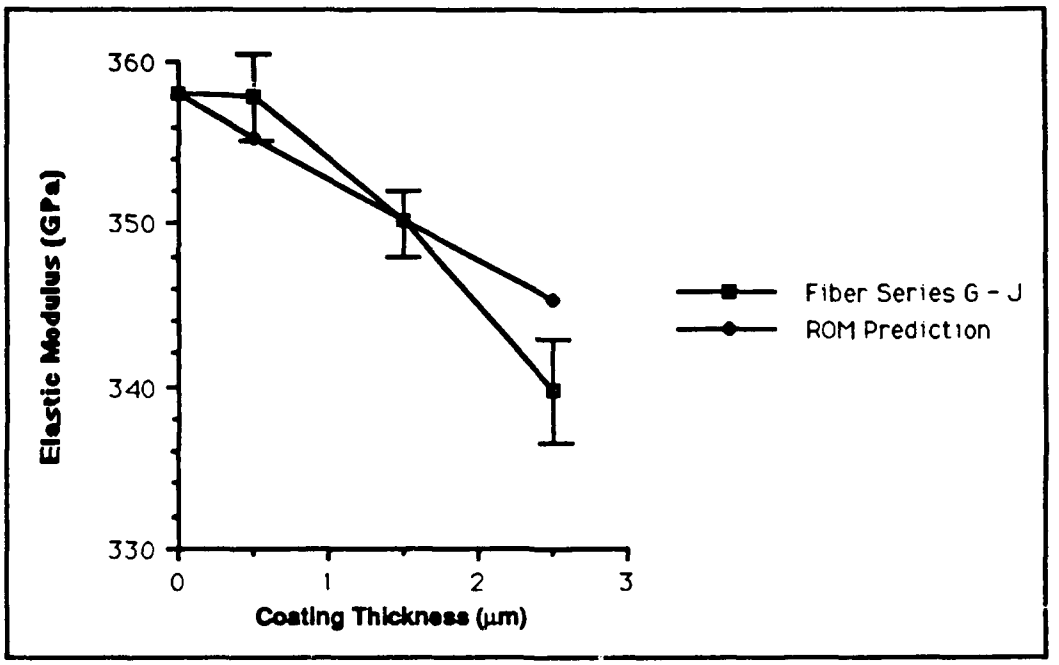

Figure 29. Elastic Modulus Variation in Fiber Series G-J versus a Rule of Mixtures Prediction

It is important to note that the error bars shown cover only one standard deviation of the mean. By extending these to two or three standard deviations, not only the rule of mixtures line shown in Figure 29, but also a rule of mixtures prediction for any effective coating modulus from zero to that of α-alumina can be accommodated. Although the trend in the data seems to suggest that the effective modulus of the coating decreases with increasing coating thickness (assuming of course that the rule of mixtures calculations have any validity in these circumstances), much more experimental data would have to be taken before this could be stated definitely.

One further interesting effect is worth mentioning. Two different sol concentrations were used, among other reasons, to see what change in the amount of coating per pass would occur. Again because data from fiber series E and F is limited, a comparison was only made at the higher coating temperature. Figure 30 shows the results.

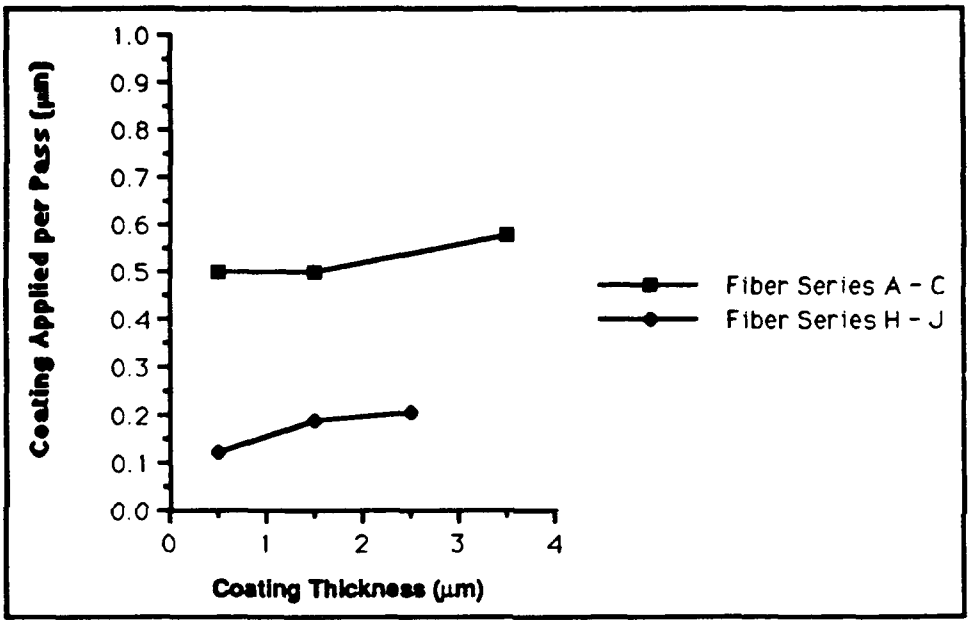

Figure 30. Coating Applied per Pass at Different Sol Concentrations

Care must be taken not to read too much into this data, since the diameter measurements on which this was based are accurate only to a micron, and the coating thickness measurements at each data point only accurate to the half micron. Dividing these measurements by the number of coating passes made to that point gives the graph in Figure 30. Two trends do seem apparent: first, the thickness of the coating applied per pass increases as more coats are applied, and second, doubling the sol concentration more than doubles the amount of coating applied per pass at the same heat treatment temperature. In terms of actual thickness, the coatings from the 71 g/l sol were as thick after three passes as those from the 36 g/l sol were after eight, and after six passes at 71 g/l, the coating was a micrometer thicker than after twelve passes at 36 g/l. No

explanation is offered for this phenomenon—it would obviously require a much more rigorous investigation—but the effect deserves consideration.

Coating Characterization. Following the tensile tests, the failed fibers were examined in a scanning electron microscope (see *Experimental Procedure*) to check the effect of the tests on the coatings. Some cracking and flaking of the coatings had been expected, but the effects were far greater.

The first location examined was at the end of a fiber where a tensile failure had occurred. One such location is shown in Figure 31.

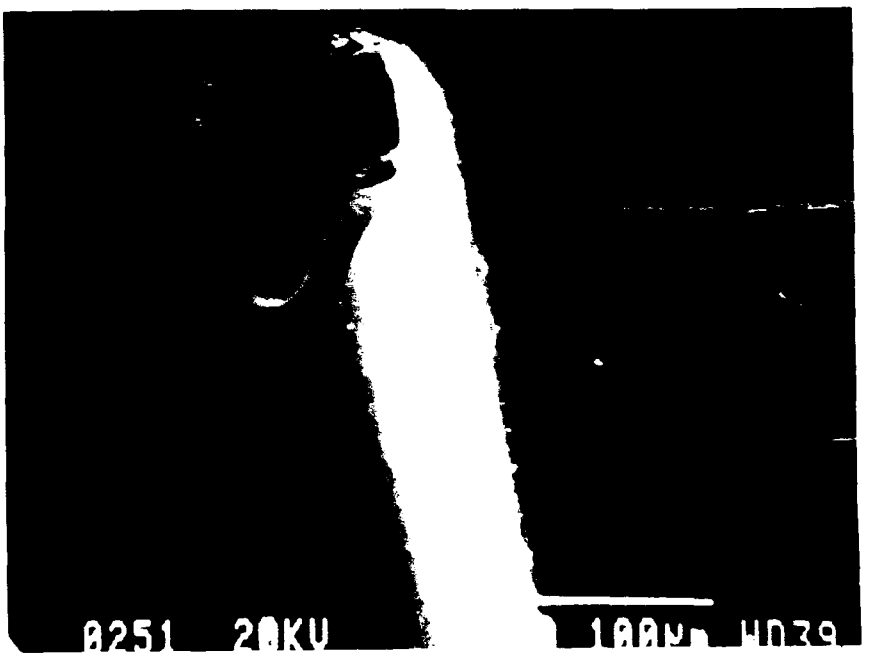

Figure 31. Fiber Series B Tensile Failure Location

The structure of the fiber is clearly visible in this picture: the dark area at the center is the carbon core, which is surrounded by silicon carbide. By looking at this picture alone, it is not possible to tell if any of the coating is left; in fact, most of it seems to have spalled off except for a ridge visible on the right side of the fiber. That some alumina is still present is confirmed by the x-ray mapping photograph shown in Figure 31. The three elements

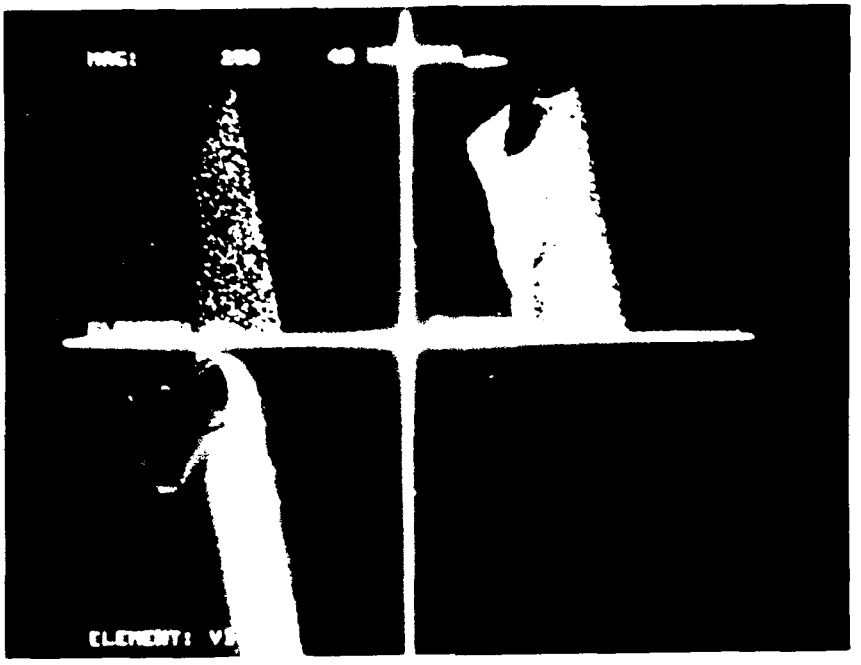

Figure 32. Energy Dispersive X-Ray Mapping of Failure Location

pictured are, clockwise from the lower left corner: the video image, the return from the x-ray counter of alumina-characteristic energy, and the silicon return. The alumina coating that remains is really only a trace, as the strength of the silicon return indicates.

Another typical break is shown in Figure 33. The carbon core of the fiber is seen clearly here sticking out of the silicon carbide, and again there is nothing but a trace of the alumina coating; this was confirmed by the energy dispersive x-ray analysis that was done at the locations where these pictures were taken (see *Experimental Procedure*). In fact, the only appreciable amount of coating found on any of the fibers after tensile testing is seen in Figure 34. In this case, it appears that an upper layer of coating may have flaked off (note the debris in the lower center of the photo, though this may not be alumina. In any case, the coating visible has circumferential cracks similar to those seen on fiber series C (this fiber was from series E). It is unknown if these cracks are the

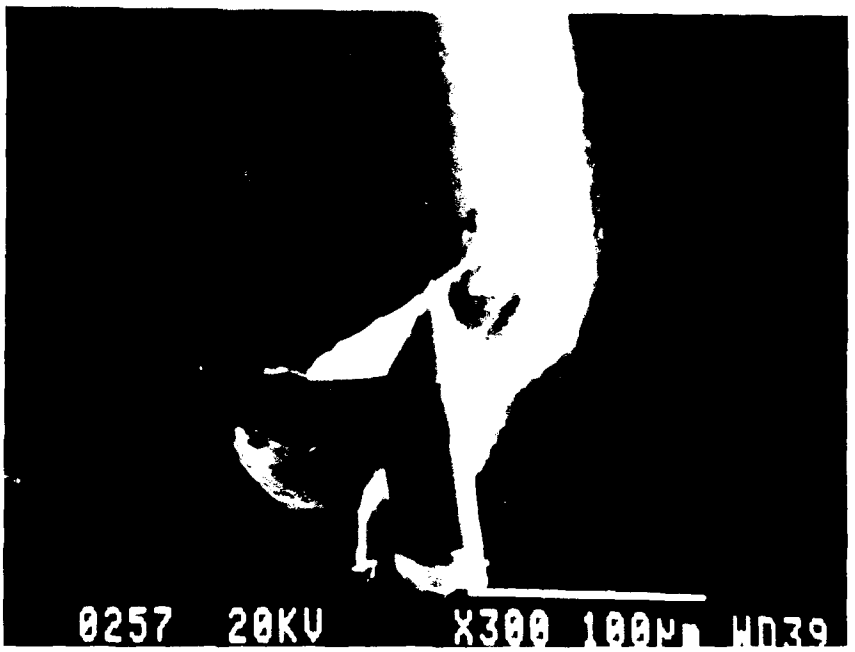

Figure 33. Fiber Series H Tensile Failure Location

Figure 34. Fiber Series E Tensile Failure Location Showing Circumferential Cracks in the Coating

result of thermal residual stress or coating failure during the tensile test, however, no such cracking was noticed on the series E fibers before the tensile testing.

A more typical coating remnant is seen in Figure 35. The coating is the light colored layer covering the upper third of the fiber in the photo; a slight ridge at the bottom of the

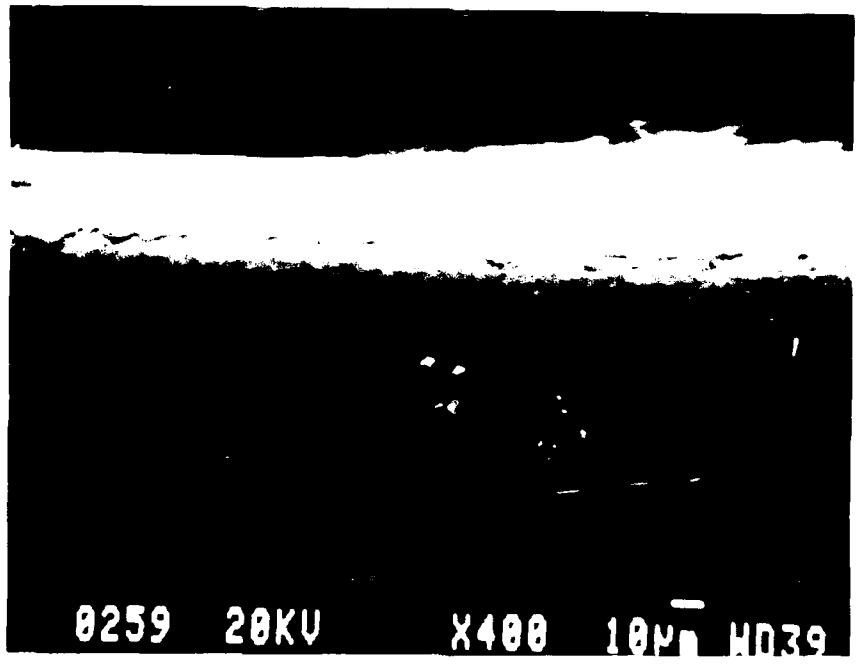

Figure 35. Fiber Series J Coating Remnant

photo may indicate another patch of coating, or that the coating continues around the unseen side of the fiber. It is unknown what caused the coating to fail in this manner, but it may have been tangential stress due to the axial strain (see below).

Clearly, the properties of the alumina coatings used in this experiment and the mechanisms of their failure are still open to a wide range of investigations. More questions were raised than answered by the attempt to characterize the fibers after the tensile tests, but these may suggest useful avenues of investigation.

Two-Dimensional Plane Strain Analysis The best data for the modulus of a coated fiber, both in terms of skew (difference between the mean and median values) and standard deviation is that from fiber series I as noted above. Using this data, the mean elastic modulus of the uncoated fibers in series G, and the material properties given in Table 1 (the Poisson's ratio and coefficient of thermal expansion for the coating are assumed to be the same as for α-alumina), all the elements are in place to complete the two dimensional plane strain analysis of a coated fiber. Summarizing the values to be used for the constants:

$$E_1 = 358.0 \text{ GPa}$$

$$E_2 = 175.8 \text{ GPa}$$

$$\nu_1 = 0.15$$

$$\nu_2 = .022$$

$$\alpha_1 = 3.62 \times 10^{-6}/^{\circ}\text{C}$$

$$\alpha_2 = 7.0 \times 10^{-6}/^{\circ}\text{C}$$

where subscript 1 denotes the fiber and subscript 2 the coating. To get to this point, numerous assumptions have been made both in the derivation of the plane strain equations and in obtaining the fiber and coating moduli. To avoid making any further assumptions, and to further simplify the calculations, the remainder of the analysis will be done for just one fiber series, namely series I. This will produce an illustrative solution and also make the most appropriate use of the experimental data by not generalizing the use of the derived modulus values, but it precludes using the data to try and determine a "critical" coating thickness. Attempting to determine such a quantity would be speculative in any case, as the stress limits of the coating are unknown. From the choice of fiber series I for the analysis, it follows that

$$a = 67.8 \text{ } \mu\text{m}$$

$$b = 69.3 \text{ } \mu\text{m}$$

$$\Delta T = 950 \text{ } ^{\circ}\text{C}$$

Using the above values to compute the thermal residual stresses, the matrix equation (30) is now simply

$$\begin{bmatrix} 2.540\times10^{-3} & -5.814\times10^{-3} \\ -1.180\times10^{-2} & 1.270\times10^{-3} \end{bmatrix} \text{GPa}^{-1} \begin{bmatrix} A_2 \\ C_2 \end{bmatrix} = \begin{bmatrix} 3.230\times10^{-3} \\ 3.230\times10^{-3} \end{bmatrix}$$

The matrix inversion is elementary, and the constants are solved for as

$$\begin{bmatrix} A_2 \\ C_2 \end{bmatrix} = -1.53\times10^{4} \begin{bmatrix} 1.270\times10^{-3} & 1.180\times10^{-2} \\ 5.814\times10^{-3} & 2.540\times10^{-3} \end{bmatrix} \begin{bmatrix} 3.230\times10^{-3} \\ 3.230\times10^{-3} \end{bmatrix} \text{GPa}$$

which gives

$$A_2 = -0.646\ \text{GPa} = -646\ \text{MPa}$$

$$C_2 = -424\ \text{MPa}$$

The thermal residual stress components are now given simply by Equations (18) through (22). Three are constant:

$$\sigma_{r_1} = \sigma_{\theta_1} = A_2\left(1 - \frac{b^2}{a^2}\right) = 29.1\ \text{MPa}$$

$$\sigma_{z_1} = C_2\left(1 - \frac{b^2}{a^2}\right) = 19.1\ \text{MPa}$$

$$\sigma_{z_2} = C_2 = -424.0\ \text{MPa}$$

while two are functions of r:

$$\sigma_{r_2} = A_2\left(1 - \frac{b^2}{r^2}\right)$$

$$\sigma_{\theta_2} = A_2\left(1 + \frac{b^2}{r^2}\right)$$

These functions are plotted against the radius in Figures 36 and 37 below. The vertical lines in each plot indicate the limits of the coating. The (tensile) radial stress goes to zero at the free surface, while the (compressive) tangential stress has its greatest magnitude at the interface. The foregoing can be said without looking at the numbers of course, but the meaning of the numbers—without quantified coating limits, is not clear. Some meaning can perhaps be inferred by calculating the value of A_2 and C_2, and hence $\sigma_{z_2} = C_2$ and the maximum σ_{θ_2} for fiber series C, which did of course show cracking from thermal residual stress. Although this stretches the bounds of cross-series applicability of the

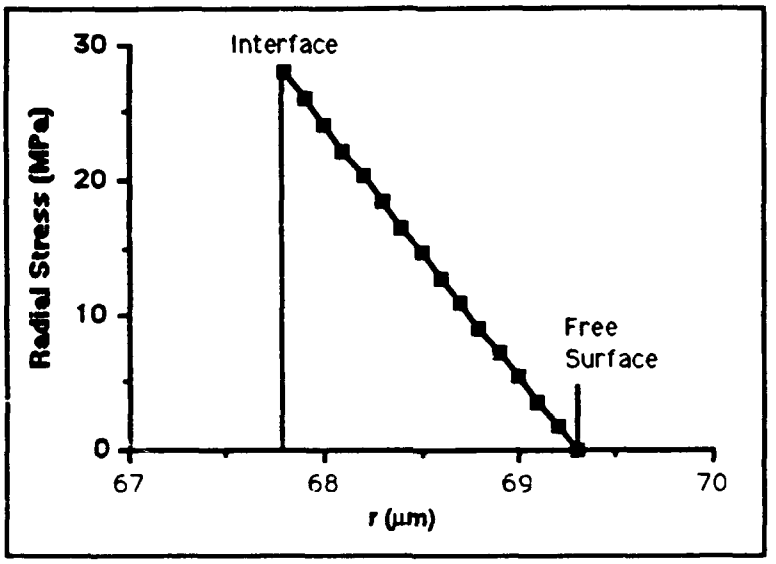

Figure 36. Radial Thermal Residual Stress in the Coating of Fiber Series I

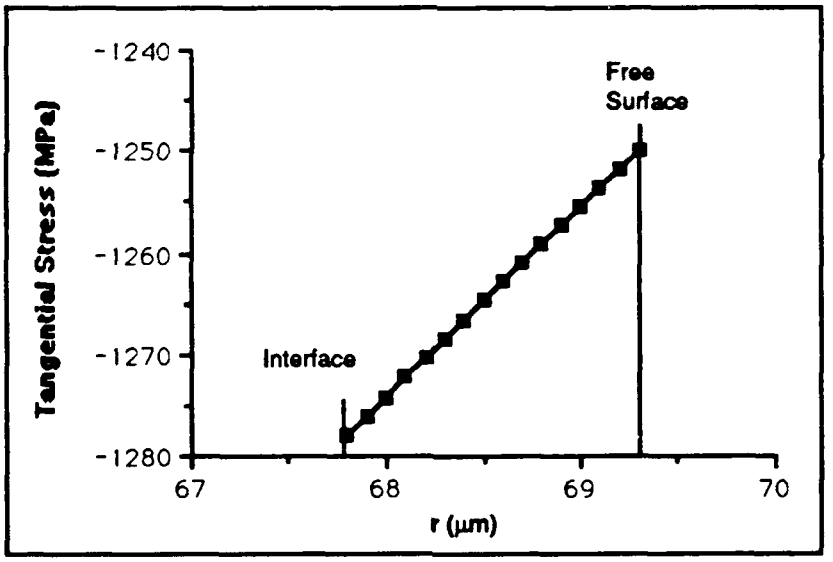

Figure 37. Tangential Thermal Residual Stress in the Coating of Fiber Series I

effective coating modulus, fiber series C was coated at the same temperature, and the calculation may give a rough idea of what the coating can tolerate. The calculations (using the fiber series D fiber modulus) give A_2 = –625 MPa and C_2 = –392 MPa, however, which indicates the stress is higher in the thinner coating. This is perhaps not surprising, but does not help explain the thermal residual stress cracking in fiber series C

at all unless coatings applied at higher sol concentrations are weaker than those applied at lower ones. Equally interesting is the fact that the compressive strength for α-alumina is 2480 MPa (22), which implies that neither fiber series coating would show cracking if it were as strong as α-alumina. This is at least some evidence that the coatings are weaker than α-alumina.

It is also interesting to note that, although the equations for the radial and tangential stresses in the the coating are parabolic in form, the plots in Figures 36 and 37 are essentially linear. This is because the coating thickness is quite small compared to the fiber radius, and the region of interest is on the (essentially) linear portion of the $1 \pm b^2/r^2$ curve. The same is true for the stresses due to an axial strain, calculated below.

Returning to the original goal of showing the stresses in fiber series I, all that remains is to calculate the stress resulting from the axial strain e_z. To do this, one further assumption is necessary, namely a value for strain. In keeping with the method of determining the coating modulus, this will be taken to be the mean value of the strain to failure for fiber series I. (Again, the assumption has been made that everything behaves elastically until the failure point). With $e_z = 0.007879$ (i.e., .7879%), Equation (46) gives

$$C_4 = 1.6358\ \mu m^2$$

and solving for the other constants from Equations (45) and (42),

$$C_3 = -0.001543$$

$$C_1 = -0.001187$$

From Equations (43), (47) (49) and (50) the constant stresses are:

$$\sigma_{rf} = \sigma_{\theta f} \approx -2.19 \text{ MPa}$$

$$\sigma_{zf} \approx 2820.02 \text{ MPa}$$

$$\sigma_{zc} \approx 1406.73 \text{ MPa}$$

The stress components that vary with r can also be calculated and plotted as with the thermal residual stresses. Figure 38 (next page) shows the radial stress in the coating due

to the axial load; the limits of the coating are again marked by vertical lines. At the free surface, the stress goes to zero, as required by one of the boundary conditions. (The numerical value may no be exactly zero unless very high precision is used in the calculations.) Figure 39 shows the tangential stresses; as with the thermal residual

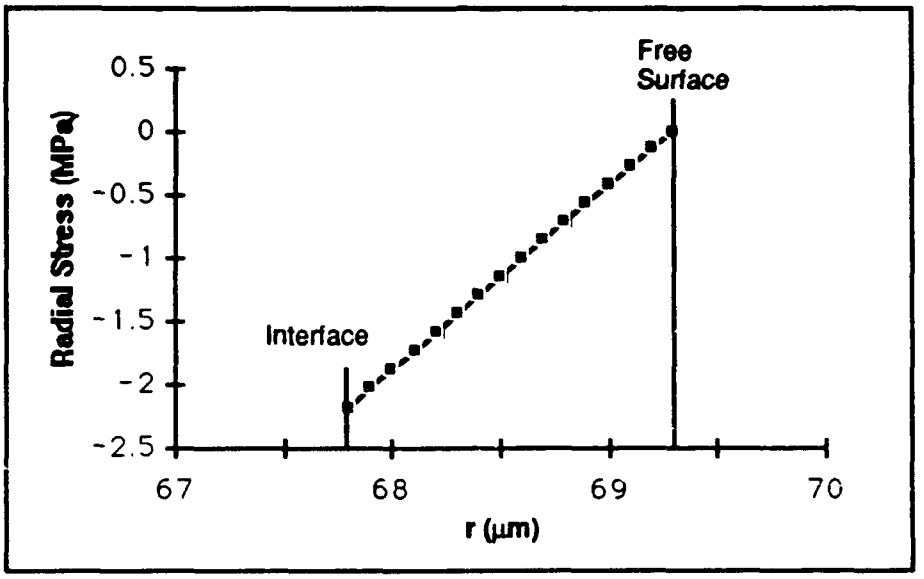

Figure 38. Radial Stress Due to Axial Loading in the Coating of Fiber Series I

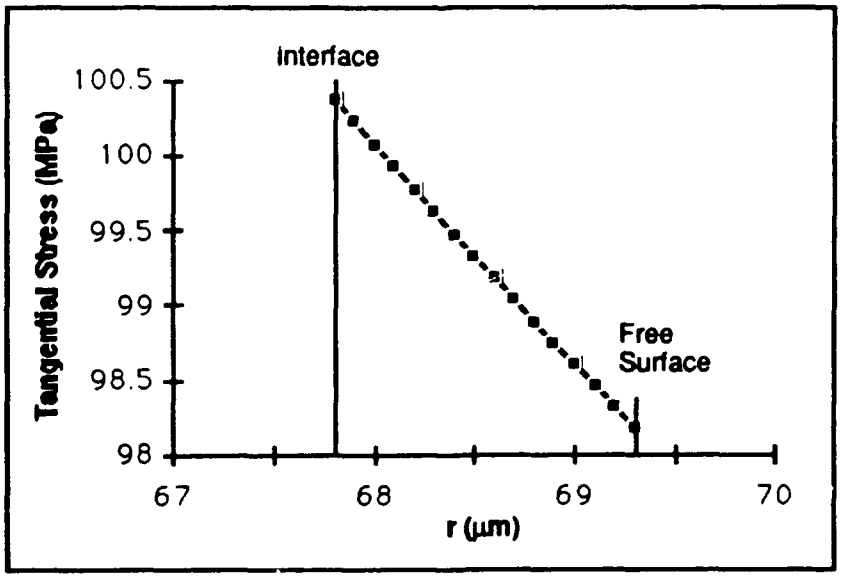

Figure 39. Tangential Stress Due to Axial Loading in the Coating of Fiber Series I

stresses, the tangential stresses due to an an axial strain are orders of magnitude larger than the radial ones. A comparison of Figures 36 and 37 with 38 and 39 respectively also reveals that, in the coating, the thermal residual stresses are an order of magnitude greater than the stresses induced by the axial loading, and in the opposite sense.

The compressive strength of α-alumina was given above as 2480 MPa; its tensile strength is 220 MPa (22). Recognizing that the coating will probably not be as stron as α-alumina, it is apparent that the value of $\sigma_{z_c} \approx 1406.73$ MPa (as calculated on page 81; 982.73 MPa with thermal stress superimposed) is far beyond the likely tensile failure strength of the coating. It is interesting to plot the value of σ_{z_c} versus increasing strain from zero to the failure of the fiber by taking increments of the strain to failure and running them through equations (46), (45), and (50). The result is shown in Figure 40.

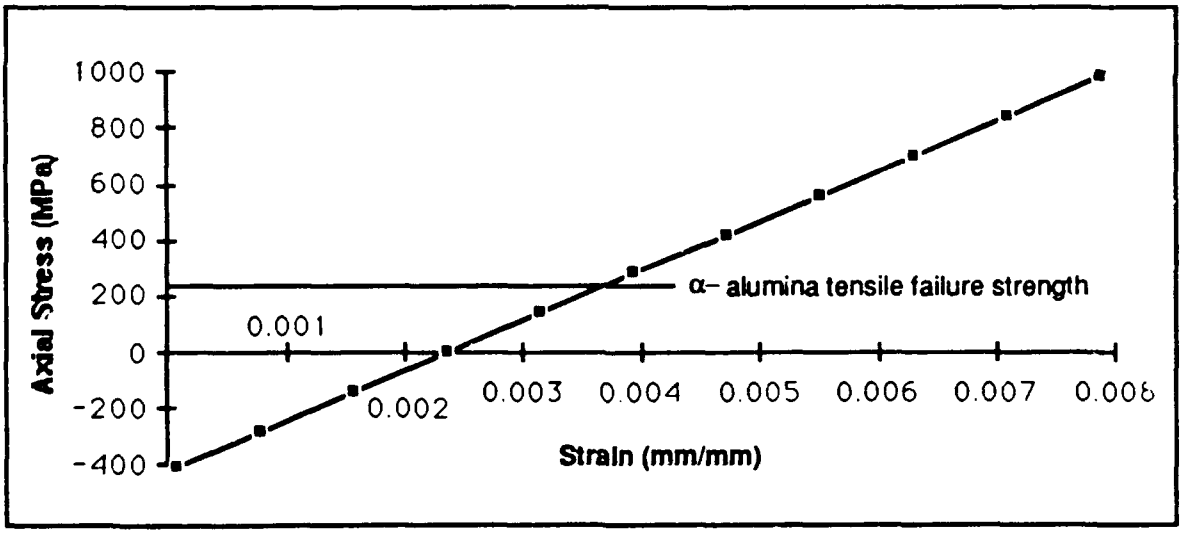

Figure 40. Axial Stress versus Strain in the Coating

If this graph represented what actually occurred, the coating would fail before the fiber had been strained to 50% of its strain to failure, and the numbers calculated for the component stresses due to an axial strain and presented on page 81 and in Figures 38 and 39 would be moot, since the system would have ceased to behave elastically well before fiber failure. If this were in fact the case, however, the maximum tangential stress due to

the axial strain would also be less than 50% of that shown in Figure 39, and it is unlikely that such a low stress could have caused the type of failure shown in Figure 35. If, on the other hand, the tangential stress approached 100 MPa in the coating, it is conceivable that this stress would be enough to cause such a failure (bearing in mind that the tensile failure strength of the coating is likely to be lower than the 220 MPa of α-alumina). Clearly though, more research is needed to determine how the coating actually behaves under load.

The foregoing also suggests another comparison between the two-dimensional plane strain analysis and the experiment, specifically, what do the stress components in the fiber say in terms of failure criteria? The simplest of these, the maximum stress criterion, states that if one component exceeds the failure strength of the material, the material will fail. For the fiber, the axial stress component, which amounts to 2839.1 MPa when the thermal residual stress is superimposed on the stress resulting from the axial strain, is the greatest. The experimental failure strength of the appropriate uncoated fiber (series G) was 29?? .8 MPa, which is less than two standard deviations from this value (Table C-7). Although hardly conclusive, it at least says that the axial strain computed with the two-dimensional analysis is reasonable.

A slightly more sophisticated failure criterion is the Von Mises criteria, which states in terms of the principal stresses (18:75):

$$(\sigma_1 - \sigma_2)^2 + (\sigma_2 - \sigma_3)^2 + (\sigma_3 - \sigma_1)^2 = 2\sigma_{ult}^2$$

Although this is actually a yield criterion, for ceramics the yield point is also effectively the failure point. Equating subscript 1 with the radial direction, 2 with the tangential, and 3 with the axial, and again superimposing the thermal residual stresses on those induced by the axial strain, the principal stresses in the fiber will be:

$$\sigma_1 = 26.9 \text{ MPa}$$

$$\sigma_2 = 26.9 \text{ MPa}$$

$$\sigma_3 = 2839.1 \text{ MPa}$$

The failure strength, according to the Hill-Von Mises criterion, is then 2812.2 MPa, which is still within two standard deviations of the experimental value for fiber series G.

Each of the failure criteria says that the fiber should fail sooner than it actually does, though with less than two standard deviations separating the predicted failure strength from the observed ultimate stress, it is arguable whether the experimental data is sufficiently accurate to show a difference. Assuming that the difference does exist, however, it is most likely due to the assumption in the analysis that the fiber/coating system remains intact and behaves plastically until the point of failure. As mentioned above, it appears likely that the coating does begin to fail before the maximum strain is reached.

A final word on this is in order. Assuming the coating fails well before the fiber does, and subsequently carries almost none of the load, the stress in the fiber will be higher than what is calculated using a constant diameter (of the initial fiber/coating system). This might account for the observed (apparent) decrease in ultimate stress with increasing coating thickness (the effect may in fact be illusory), but it doesn't account for the apparent decrease in strain to failure of coated fibers with increasing coating thickness. Verification and explanation of this phenomenon will require further experiments.

Suggestions and Recommendations

Sol-gel-derived non-α-alumina coatings on silicon carbide fibers do appear to reduce the fibers' ultimate stress, strain to failure, and elastic modulus as determined by tensile testing. Of the three, the effect of alumina coatings on the ultimate stress of a coated fiber is least certain because the coatings are likely to fail before the fiber, with the result that the load is distributed over a smaller area, complicating stress calculations. The change in strain to failure has no such uncertainties, but is less pronounced, while the observed change in modulus (determined from the stress-strain curve) is only valid as long as the computed stress is accurate.

The effect of the alumina coatings appears to be linear with coating thickness, but variations in the data, statistical uncertainties, and the failure of the simple rule of mixtures calculation used to account for the geometry of the sample combine to make either a derivation of an empirical relationship or an approximate rule of thumb impossible. For the same reasons, derivation of accurate coating properties from this experiment was not possible. More extensive tests of the fibers to confirm the trends hinted at by this work and expand the range of sol concentrations, coating thicknesses and heat treating temperatures, as well as a more thorough analytical approach, are needed. To get experimental data with sufficient accuracy and to allow the assumption that the mean values of the data are normally distributed, at least 40 samples should be made of each fiber/coating combination to be tested; this should ensure that more than 30 actual data points are collected for each combination.

It is clear that more work in the characterization of sol-gel derived alumina coatings is in order. This is particularly true for multiple pass coatings; everything from the amount of coating applied per pass at different sol concentrations to the possibility of layering of the coating after multiple passes needs to be examined.

In terms of the potential for applying alumina coatings as a weak interface in a ceramic matrix, the results of this experiment are not encouraging. The push-out tests that were tried did not succeed, and no information gleaned from examining the coatings or the push-out samples indicates that the coating is prone to failure. This suggests an interesting contrast with the SCS-6 fibers: the carbon-rich coating applied to these fibers increases their strength and modulus, apparently through a fault-healing process. At the same time, the carbon coatings serve as an almost ideal weak interface. Alumina appears to do neither of these things. Of course, a direct comparison to SCS-6 isn't possible because of the different structures of alumina and graphitic carbon, but perhaps comparison of alumina to other ceramic materials as a coating might provide some insights: for example (assuming sufficiently good data to say with accuracy) if applying a coating of one type to SCS-0 increases its strength, or decreases it more than alumina does for a given coating thickness, a comparison of this coating to alumina in push-out tests might hint at what sort of a ceramic coating on a fiber would be desirable.

In a different vein, examination of the fibers after testing shows that for the most part the coatings do fail catastrophically at some point during the test, but when that is cannot be determined by this testing method. The two-dimensional plane-strain analysis indicates that they may fail at relatively low strains, but the validity of this result could not be experimentally confirmed. A possibly worthwhile experiment would be to test a coated fiber in a strain stage under a microscope to observe the onset of coating cracking and if possible the characteristic crack distance predicted by the ACK model (1). There is something of a "catch-22" in this problem. It is still unknown at what strain coating cracks might occur, or if in fact the fiber would break before the cracks became visible, so testing in a strain stage would have to proceed by trial and error. Better knowledge of the coating properties, on the other hand, would enable an estimate to be made from these equations as to what load on the coated fiber would be required to exceed the ultimate

stress of the coating. A potential approach to this problem would involve assuming the coating modulus found experimentally (and using the rule of mixtures) was valid and applied to a range of coating thicknesses, assuming that the ultimate stress of the coating could be found in a similar manner, and performing the plane strain analysis to find out under what conditions (thermal stress or applied loads) this assumed ultimate stress would be exceeded. That in turn could serve as the starting point for the strain stage experiment.

Creating a fiber reinforced ceramic composite that will withstand high temperature oxidizing environments continues to be an important goal of ceramics and materials science researchers. This experiment has given little reason to think that alumina coatings are a viable solution, but it does suggest that there is a great deal to learn from examining the behavior of such coatings.

Appendix A: Derivation of Plane Strain Equations

Few things are as confusing and difficult to follow as derivations that skip multiple steps or provide inadequate explanations of steps. Recognizing that the plane strain equations used in this study require little in the way of higher math, but a great deal in terms of algebraic manipulation, a detailed derivation is provided here for those who may be interested.

Problem Set-Up

To begin, consider a fiber of radius a with a coating applied so that the overall radius is b (Figure A-1). Each component of this composite structure will have, in

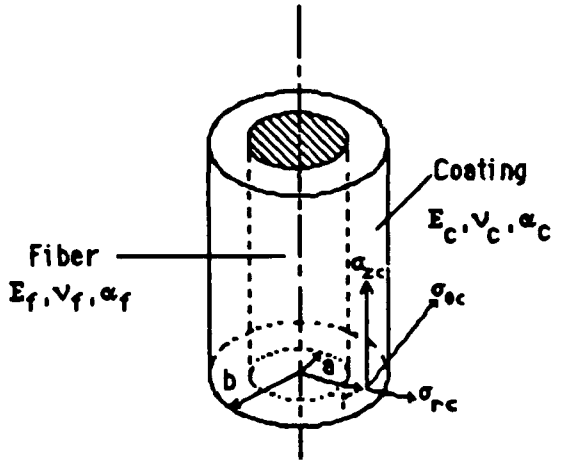

Figure A-1. Sectional View of Coated Fiber

general, different material properties E (Young's modulus), ν (Poisson's ratio) and α (coefficient of thermal expansion). Because of the geometry of the problem, cylindrical coordinates (r, θ, z) are the natural choice. Two types of stresses will be considered: those resulting from a mismatch in thermal expansion coefficients during the coating process (thermal residual stresses), and those resulting from a uniaxial load applied in the z (axial) direction (the tensile tests). In general, a subscript of "f" or "1" will be used to

identify a fiber property, while a subscript of "c" or "2" will be used for coating properties. The assumptions made are that the two materials can be characterized by these elastic properties; that these properties will be independent of temperature; that no debonding or cracking of the coating occurs; and that, because the fibers are very long, the system is axially symmetric. Because of these assumptions, the axial and radial directions are the directions of principal stress, there will be no shear components of the stress, and the axial components will depend only on *r*.

Thermal Residual Stress Equations

The first step is to assume that the stresses take the same form as the Lamé solution for a cylinder under radial stress at the boundary; as given by Reference (21), these are:

$$\sigma_{r_1} = A_1 + \frac{B_1}{r^2} \tag{A.1}$$

$$\sigma_{\theta_1} = A_1 - \frac{B_1}{r^2} \tag{A.2}$$

$$\sigma_{z_1} = C_1 \tag{A.3}$$

$$\sigma_{r_2} = A_2 + \frac{B_2}{r^2} \tag{A.4}$$

$$\sigma_{\theta_2} = A_2 - \frac{B_2}{r^2} \tag{A.5}$$

$$\sigma_{z_2} = C_2 \tag{A.6}$$

It can be seen immediately that $B_1 = 0$; otherwise, stresses would be infinite at the axis of symmetry (r =0). This leaves five constants for which to solve in order to describe the stresses. The axial strains, taking the thermal expansions into account, can be written

$$\begin{aligned} e_r &= \frac{\sigma_r}{E} - \frac{\nu}{E}(\sigma_\theta + \sigma_z) + \alpha\Delta T \\ e_\theta &= \frac{\sigma_\theta}{E} - \frac{\nu}{E}(\sigma_r + \sigma_z) + \alpha\Delta T \\ e_z &= \frac{\sigma_z}{E} - \frac{\nu}{E}(\sigma_r + \sigma_\theta) + \alpha\Delta T \end{aligned} \tag{A.7}$$

from Hooke's law, and as

$$e_r = \frac{du_r}{dr} \qquad e_\theta = \frac{u_r}{r} \qquad e_z = \frac{du_z}{dz} \tag{A.8}$$

from the condition that the strains be derived from two displacement components: u_r in the radial and u_z in the axial direction (the compatibility condition). Since axial symmetry has been assumed, the equations of equilibrium reduce (2) to:

$$\frac{d\sigma_r}{dr} + \frac{\sigma_r - \sigma_\theta}{r} = 0 . \tag{A.9}$$

Now, substituting Equations (A.1) through (A.6) into (A.7), the strains can also be written in terms of the constants. For the coating,

$$\begin{aligned} e_{r_2} &= \frac{A_2}{E_2}(1 - \nu_2) + \frac{B_2}{E_2}\frac{(1 + \nu_2)}{r^2} - \frac{\nu_2}{E_2}C_2 + \alpha_2\Delta T \\ e_{\theta_2} &= \frac{A_2}{E_2}(1 - \nu_2) - \frac{B_2}{E_2}\frac{(1 + \nu_2)}{r^2} - \frac{\nu_2}{E_2}C_2 + \alpha_2\Delta T \\ e_{z_2} &= \frac{A_2}{E_2}(-2\nu_2) + \frac{C_2}{E_2} + \alpha_2\Delta T \end{aligned} \tag{A.10}$$

If u_r is written as

$$u_{r_2} = \left[\frac{A_2}{E_2}(1 - \nu_2) - \frac{\nu_2}{E_2}C_2 + \alpha_2\Delta T\right] r - \frac{B_2}{E_2}\frac{(1 + \nu_2)}{r},$$

then the strain equations (A.10) meet the compatibility condition. Similar equations can be written for the fiber,. for example

$$e_{\theta_1} = \frac{A_1}{E_1}(1 - \nu_1) - \frac{\nu_1}{E_1}C_1 + \alpha_1\Delta T \tag{A.11}$$

by using (A.1) through (A.3) and remembering that $B_1 = 0$.

There are now five constants to evaluate. The appropriate five boundary conditions are:

$$u_{r_1} = u_{r_2} \qquad \text{at } r = a \tag{A.12}$$

$$e_{z_1} = e_{z_2} \qquad \text{at } r = a \tag{A.13}$$

$$\sigma_{r_1} = \sigma_{r_2} \qquad \text{at } r = a \tag{A.14}$$

$$\sigma_{r_2} = 0 \qquad \text{at } r = b \tag{A.15}$$

$$\boxed{C_1 = C_2\left(1 - \frac{b^2}{a^2}\right)} \tag{A.16}$$

Equations (A.12), (A.13) and (A.14) are derived from the requirement for continuity, thus equal radial stresses and equal strains in both materials, at the interface; and Equation

(A.15) from the radial stress at the free surface being zero. Equation (A.16) is already a solution for one of the constants; it comes from the boundary condition that the resultant of the axial stress of a section z = constant of both cylinders must be zero. Writing this condition as an equation:

$$\int_0^{2\pi}\int_0^{a}\sigma_{z_1} r\,dr\,d\theta + \int_0^{2\pi}\int_a^{b}\sigma_{z_2} r\,dr\,d\theta = 0,$$

remembering that the axial stress components are constant, substituting for them from Equations (A.3) and (A.6), and integrating gives

$$\pi a^2 C_1 + \pi\left(b^2 - a^2\right) C_2 = 0,$$

which reduces directly to (A.16).

From Equation (A.15) and Equation (A.4):

$$A_2 + \frac{B_2}{b^2} = 0$$

which gives

$$\boxed{B_2 = -A_2 b^2}. \qquad \text{(A.17)}$$

By applying Equations (A.14) and (A.17) to (A.1) and (A.4),remembering that $B_1 = 0$,

$$\boxed{A_1 = A_2 + \frac{-A_2 b^2}{r^2} = A_2\left(1 - \frac{b^2}{a^2}\right)} \qquad \text{(A.18)}$$

Using Equations (A.16) through (A.18), the equations for the stress components can now be written in terms of just two constants. For the fiber, the expressions become:

$$\sigma_{r_1} = \sigma_{\theta_1} = A_2\left(1 - \frac{b^2}{a^2}\right) \qquad \text{(A.19)}$$

$$\sigma_{z_1} = C_2\left(1 - \frac{b^2}{a^2}\right) \qquad \text{(A.20)}$$

while for the coating

$$\sigma_{r_2} = A_2\left(1 - \frac{b^2}{r^2}\right) \qquad \text{(A.21)}$$

$$\sigma_{\theta_2} = A_2\left(1 + \frac{b^2}{r^2}\right) \qquad \text{(A.22)}$$

$$\sigma_{z_2} = C_2 \qquad \text{(A.23)}$$

The remaining two constants are determined from the displacement boundary conditions, but with considerably more algebra. Applying Equation (A.13) to the *z*-component of the strain for both materials,

$$\frac{A_2}{E_2}(-2\nu_2)+\frac{C_2}{E_2}+\alpha_2\Delta T=\frac{A_1}{E_1}(-2\nu_1)+\frac{C_1}{E_1}+\alpha_1\Delta T. \qquad (A.24)$$

The left side of (A.24) is directly from (A.10), while the right side comes from substituting (A.1) through (A.3) into Equation (A.7). Now substituting (A.16) and (A.18) into (A.24) and rearranging terms

$$2A_2\left[\frac{\nu_2}{E_2}-\frac{\nu_1}{E_1}\left(1-\frac{b^2}{a^2}\right)\right]-C_2\left[\frac{1}{E_2}-\frac{1}{E_1}\left(1-\frac{b^2}{a^2}\right)\right]=(\alpha_2-\alpha_1)\Delta T \qquad (A.25)$$

Another expression involving both C_2 and A_2 comes from equating the displacements in the radial direction at the interface (A.12). This can be done by equating e_θ there (21), with the appropriate expressions given by (A.10) and (A.11), viz,

$$\frac{A_2}{E_2}(1-\nu_2)-\frac{B_2}{E_2}\frac{(1+\nu_2)}{a^2}-\frac{\nu_2}{E_2}C_2+\alpha_2\Delta T=\frac{A_1}{E_1}(1-\nu_1)-\frac{\nu_1}{E_1}C_1+\alpha_1\Delta T \qquad (A.26)$$

which becomes, after again substituting for A_1, B_2 and C_1 and rearranging

$$A_2\left[\frac{(1-\nu_1)}{E_1}\left(1-\frac{b^2}{a^2}\right)-\frac{(1-\nu_2)}{E_2}-\frac{(1+\nu_2)}{E_2}\frac{b^2}{a^2}\right]+C_2\left[\frac{\nu_2}{E_2}-\frac{\nu_1}{E_1}\left(1-\frac{b^2}{a^2}\right)\right]=(\alpha_2-\alpha_1)\Delta T \qquad (A.27)$$

The Equations (A.25) or (A.27) could now be solved for one of the two constants A_2 or C_2 and this expression substituted into the other equation, but this is an extremely tedious task made only slightly easier by the assumption that $n_1 = n_2$ (2). For the purposes of this study, it is better to write (A.25) and (A.27) in matrix form as

$$\begin{bmatrix} 2\left[\frac{\nu_2}{E_2}-\frac{\nu_1}{E_1}\left(1-\frac{b^2}{a^2}\right)\right] & -\left[\frac{1}{E_2}-\frac{1}{E_1}\left(1-\frac{b^2}{a^2}\right)\right] \\ \left[\frac{(1-\nu_1)}{E_1}\left(1-\frac{b^2}{a^2}\right)-\frac{(1-\nu_2)}{E_2}-\frac{(1+\nu_2)}{E_2}\frac{b^2}{a^2}\right] & \left[\frac{\nu_2}{E_2}-\frac{\nu_1}{E_1}\left(1-\frac{b^2}{a^2}\right)\right] \end{bmatrix}\begin{bmatrix} A_2 \\ C_2 \end{bmatrix}=\begin{bmatrix} (\alpha_2-\alpha_1)\Delta T \\ (\alpha_2-\alpha_1)\Delta T \end{bmatrix} \qquad (A.28)$$

This expression may now be solved for A_2 and C_2, and the resulting expressions inserted into Equations (A.19) through (A.23) to get the desired thermal residual stress components.

Stresses Induced by an Axial Load

Since axial symmetry has been assumed, stress and strain will be functions only of r, and the relation for each coordinate axis (with e_z assumed constant) is

$$\begin{aligned} e_r &= \frac{1+\nu}{E}\sigma_r - \frac{\nu}{E}(\sigma_r + \sigma_\theta + \sigma_z) = \frac{\sigma_r}{E} - \frac{\nu}{E}(\sigma_\theta + \sigma_z) \\ e_\theta &= \frac{\sigma_\theta}{E} - \frac{\nu}{E}(\sigma_r + \sigma_z) \\ e_z &= \frac{\sigma_z}{E} - \frac{\nu}{E}(\sigma_r + \sigma_\theta) = \text{constant} \end{aligned} \tag{A.29}$$

These are the same as (A.7), but without the thermal expansion terms, and can be written in matrix form as

$$\begin{bmatrix} e_r & 0 & 0 \\ 0 & e_\theta & 0 \\ 0 & 0 & e_z \end{bmatrix} = \begin{bmatrix} \frac{1}{E} & -\frac{\nu}{E} & -\frac{\nu}{E} \\ -\frac{\nu}{E} & \frac{1}{E} & -\frac{\nu}{E} \\ -\frac{\nu}{E} & -\frac{\nu}{E} & \frac{1}{E} \end{bmatrix} \begin{bmatrix} \sigma_r \\ \sigma_\theta \\ \sigma_z \end{bmatrix} \tag{A.30}$$

which in turn allows the stress components to be solved for as

$$\begin{bmatrix} \sigma_r \\ \sigma_\theta \\ \sigma_z \end{bmatrix} = \begin{bmatrix} \frac{1}{E} & -\frac{\nu}{E} & -\frac{\nu}{E} \\ -\frac{\nu}{E} & \frac{1}{E} & -\frac{\nu}{E} \\ -\frac{\nu}{E} & -\frac{\nu}{E} & \frac{1}{E} \end{bmatrix}^{-1} \begin{bmatrix} e_r & 0 & 0 \\ 0 & e_\theta & 0 \\ 0 & 0 & e_z \end{bmatrix}. \tag{A.31}$$

Inverting the matrix gives

$$\begin{bmatrix} \frac{1}{E} & -\frac{\nu}{E} & -\frac{\nu}{E} \\ -\frac{\nu}{E} & \frac{1}{E} & -\frac{\nu}{E} \\ -\frac{\nu}{E} & -\frac{\nu}{E} & \frac{1}{E} \end{bmatrix}^{-1} = \begin{bmatrix} E + 2\nu^2 K & \nu K & \nu K \\ \frac{\nu E}{1+\nu} + 2\nu^2 K & \frac{E}{1+\nu} + \nu K & \nu K \\ -\frac{\nu E}{1+\nu} + 2\nu K(1-\nu) & -\frac{E}{1+\nu} + K(1-\nu) & K(1-\nu) \end{bmatrix} \tag{A.32}$$

where the bulk modulus $K \equiv \dfrac{E}{(1+\nu)(1-2\nu)}$ (A.33)

This leads directly to a solution for the stress components:

$$\begin{aligned} \sigma_r &= K[(1-\nu)e_r + \nu(e_\theta + e_z)] \\ \sigma_\theta &= K[(1-\nu)e_\theta + \nu(e_r + e_z)] \\ \sigma_z &= K[(1-\nu)e_z + \nu(e_\theta + e_z)] \end{aligned} \tag{A.34}$$

For the plane strain condition, the strains can be written in terms of displacements u_r as:

$$e_r = \frac{du_r}{dr} \qquad e_\theta = \frac{u_r}{r} \qquad e_z = \text{constant.} \tag{A.35}$$

Strain in the axial direction due to the axial loading is assumed constant. Substituting these into Equation (A.34) gives

$$\begin{aligned} \sigma_r &= K\left[(1-\nu)\frac{du_r}{dr} + \nu\frac{u_r}{r} + \nu e_z\right] \\ \sigma_\theta &= K\left[\nu\frac{du_r}{dr} + (1-\nu)\frac{u_r}{r} + \nu e_z\right] \\ \sigma_z &= K\left[\nu\left(\frac{du_r}{dr} + \frac{u_r}{r}\right) + (1-\nu)e_z\right] \end{aligned} \tag{A.36}$$

The only equilibrium equation for this problem is

$$\frac{d\sigma_r}{dr} + \frac{\sigma_r - \sigma_\theta}{r} = 0 \tag{A.37}$$

Substituting Equations (A.36) into Equation (A.37) and simplifying gives a second order differential equation for the radial displacement u_r:

$$\frac{d^2u_r}{dr^2} + \frac{1}{r}\frac{du_r}{dr} - \frac{u_r}{r^2} = 0 \tag{A.38}$$

This has a solution of the form

$$u_r = Cr + \frac{C'}{r} \tag{A.39}$$

which, like the other equations, is valid for either the fiber or the matrix. Consequently, expressions can be written for the radial displacement in each component as:

$$\begin{aligned} u_{r_f} &= C_1 r + \frac{C_2}{r} \\ u_{r_c} &= C_3 r + \frac{C_4}{r}, \end{aligned} \tag{A.40}$$

where the sub-subscript f identifies the fiber and c the coating. Using the boundary conditions of the problem, the constants, displacements, and stress components of the coated fiber under axial stress can now be solved for. The boundary conditions are.

$$u_{r_f} = 0 \qquad \text{at } r = 0 \tag{A.41}$$

$$u_{r_f} = u_{r_c} \qquad \text{at } r = a \tag{A.42}$$

$$\sigma_{r_f} = \sigma_{r_c} \qquad \text{at } r = a \tag{A.43}$$

$$\sigma_{r_c} = 0 \qquad \text{at } r = b \tag{A.44}$$

These boundary conditions are very similar to those used for the thermal residual stress problem. Equation (A.41) comes from the fact that radial displacement must go to zero at the axis of symmetry; Equation (A.42) and (A.43) from the requirement for continuity, thus equal radial stresses and strains in both materials, at the interface; and Equation (A.44) from the radial stress at the free surface being zero.

Applying Equation (A.41) to the first of Equations (A.40) shows that

$$\boxed{C_2 = 0} \tag{A.45}$$

otherwise, u_{r_f} would go to infinity at r = 0. From Equations (A.40) and (A.42)

$$C_1 a + \frac{C_2}{a} = C_3 a + \frac{C_4}{a}$$

which, noting that $C_2 = 0$, reduces to:

$$\boxed{C_1 = C_3 + \frac{C_4}{a^2}} \tag{A.46}$$

Applying the first of Equations (A.40) and Equation (A.45) to the first of Equations (A.36) gives

$$\sigma_{r_f} = K_f(C_1 + \nu_f e_z)$$

or

$$\sigma_{r_f} = K_f\left(C_3 + \frac{C_4}{a^2} + \nu_f e_z\right) \tag{A.47}$$

when Equation (A.46) is used to substitute for C_1.

Using the second of Equations (A.40) in the first Equation (A.36) leads to

$$\sigma_{r_c} = K_c\left(C_3 - \frac{C_4}{r^2}(1 - 2\nu_c) + \nu_c e_z\right) \tag{A.48}$$

Now, applying Equation (A.44) to Equation (A.48) and solving for C_3:

$$\boxed{C_3 = \frac{C_4}{b^2}(1 - 2\nu_c) - \nu_c e_z} \tag{A.49}$$

Equation (A.49) can in turn be plugged into (A.46) to get C_1 in terms of C_4 alone.

The remaining boundary condition, Equation (A.43), is now used to relate Equations (A.47) and (A.48) at r = a:

$$K_f\left(C_3 + \frac{C_4}{a^2} + \nu_f e_z\right) = K_c\left(C_3 - \frac{C_4}{a^2}(1 - 2\nu_c) + \nu_c e_z\right) \qquad (A.50)$$

Substituting from (A.49) fro C_3 and consolidating terms gives an expression for C_4:

$$C_4\left\{\frac{1}{a^2} + \frac{(1 - 2\nu_c)}{b^2}\left[1 + \frac{K_c}{K_f}\left(\frac{b^2 - a^2}{a^2}\right)\right]\right\} = e_z(\nu_c - \nu_f)$$

Recognizing that, for an arbitrary length L, $\pi L(a^2) = V_f$ and $\pi L(b^2 - a^2) = V_c$ (which can be thought of as either unit or specific volumes of the fiber and coating respectively), this expression can be written as:

$$C_4\left\{\frac{1}{a^2} + \frac{(1 - 2\nu_c)}{b^2}\left[1 + \frac{K_c}{K_f}\frac{V_c}{V_f}\right]\right\} = e_z(\nu_c - \nu_f)$$

Putting the term on the left side over a common denominator and solving for C_4 gives:

$$\boxed{C_4 = \frac{e_z(\nu_c - \nu_f)\, a^2\, b^2\, K_f\, V_f}{b^2\, K_f\, V_f + a^2\,(1 - 2\nu_c)(K_f\, V_f + K_c\, V_c)}} \qquad (A.51)$$

All the constants, and thus all the stress components, can now be written in terms of C4 (which itself is made up of known quantities) and *r*. The radial stresses are given by Equations (A.47) and (A.48)—with appropriate substitution for C_3—and the expressions for the tangential stresses, derived from the Equations (A.40) and the second of Equations (A.36), are

$$\sigma_{\theta_f} = K_f(C_1 + \nu_f e_z) = \sigma_{r_f} \qquad (A.52)$$

$$\sigma_{\theta_c} = K_c\left[C_3 + (1 - 2\nu_c)\frac{C_4}{r^2} + \nu_c e_z\right] \qquad (A.53)$$

The axial stresses are also derived from (A.40) and the third of Equations (A.36):

$$\sigma_{z_f} = K_f[(1 - \nu_f)e_z + 2\nu_f C_1] \qquad (A.54)$$

$$\sigma_{z_c} = K_c[(1 - \nu_c)e_z + 2\nu_c C_3] \qquad (A.55)$$

These expressions are used, after numerical computation of the constants, to give the values of the strain components in this thesis.

Equivalently, the expressions can be put in a more familiar form by recognizing that at r = a, the radial pressure – p at the interface will equal σ_{r_c}. Setting – p equal to (A.48) at r = a yields

$$p = K_c \frac{C_4}{b^2}(1 - 2\nu_c)\left(\frac{b^2 - a^2}{a^2}\right) = K_c \frac{C_4}{b^2}(1 - 2\nu_c)\frac{V_c}{V_f} \qquad \text{(A.56)}$$

Substituting for C_4 and manipulating the terms leads to

$$p = \frac{e_z(\nu_c - \nu_f)V_c}{\frac{V_f}{K_c} + \frac{V_c}{K_f} + \frac{1}{G_c}} \qquad \text{(A.57)}$$

where $G_c = E_c/2(1 + \nu_c)$. This is the same expression as Equation (10.30) in (2) if the numerator and denominator are both multiplied by a factor of 2. Using this definition of p, the stress components can be written (2) as

$$\begin{aligned}
\sigma_{rf} &= \sigma_{\theta f} = -p \\
\sigma_{zf} &= E_f e_z - 2\nu_f p \\
\sigma_{r_c} &= p\left(\frac{a^2}{b^2 - a^2}\right)\left(1 - \frac{b^2}{r^2}\right) \\
\sigma_{\theta_c} &= p\left(\frac{a^2}{b^2 - a^2}\right)\left(1 + \frac{b^2}{r^2}\right) \\
\sigma_{z_c} &= E_c e_z + 2\nu_2 p\left(\frac{a^2}{b^2 - a^2}\right)
\end{aligned} \qquad \text{(A.58)}$$

Appendix B: Tensile Test Procedure

The purpose of this Appendix is to provide detailed information on the procedures used in testing the silicon carbide fibers with alumina coatings described in the foregoing thesis, with an eye toward allowing any subsequent experimenters to reproduce the original conditions as closely as possible.

For comparison purposes, a synopsis of the procedures Textron uses to test its silicon carbide fibers is presented first. This procedure is significant, as it highlights the differences between a quality control check and a test suitable for obtaining research-quality data. The information was obtained from Reference ?? in the bibliography, a letter from the Ceramics manager of Textron Specialty materials to Dr Ronald Kerans of the USAF WRDC Materials Laboratory.

Textron Test Procedure. The Textron procedure is a step-by-step approach that is apparently written so that even a person with minimal training can conduct the tests. It begins with instructions on booting up and initializing the test computer and calibrating the load cell. The remainder of the test consists of the following steps:

— visually inspect the spool of fiber for loose winding or multiple ends and the fiber itself for a dullness indicating a lack of sufficient (carbon) coating. Any of these are grounds for rejection of the spool.

— check fiber diameter using a laser micrometer (apparently only one measurement is taken). If the value is not "in spec" (the values vary depending on the specific type of fiber being tested) one or two layers are to be stripped from the tested spool and the value rechecked; if the diameter is again out of spec, the spool is rejected.

— test fibers for machinability by placing ten samples between two pieces of cellophane tape, cutting through them with a paper cutter, and visually inspecting the ends for uneven breakage. Again, if the fibers fail this test, one to two layers of fiber are stripped from the spool and a retest is performed.

— conduct tensile testing. The procedure for this is as follows: ten samples (length unspecified) are pulled to failure in an Instron Universal Test Machine with flat face pneumatic grips. The break load for each is measured and the ultimate stress calculated (in kilopounds per square inch-ksi) and recorded, and if all ten are within spec (above 500 ksi) the spool passes. If any values are not in spec, these are deleted and new tests substituted until either all ten values are in spec or 20 tests have been performed. If this level is reached and some tests are still out of spec, an average ultimate stress is calculated by taking the ten best tests (i.e. the highest values); if this achieves the spec, the fiber is deemed acceptable. If even this fails, one to two layers of fiber are stripped off the spool and the entire process is repeated. At this point, if the fiber again fails the test it is considered unacceptable.

— surface integrity testing is also performed for some fibers; this is done by dipping them in molten aluminum and tensile testing (using the same procedure as above) for an average break load to exceed 12 .0 pounds.

It should be noted that specifications are not given for the SCS-0 fibers (which were used for the experiments in this thesis). Since these fibers are not commercial products, but were provided to the Materials Laboratory for research, this is not surprising. What is more worrisome is that the values given for the "tensile strength"—presumably ultimate stress—of the fibers is almost certainly an average of a few (probably ten) measurements. No information is given on the deviation of the data about this average, nor is there any indication that the numbers are representative of the entire spool (note the instruction, if a measured quantity is "out of spec", to strip off one to two layers of fiber and retest). With no spec to shoot for, the numbers given could have little to no meaning for the segment of fiber that was actually coated with alumina and testing in the experiments for this thesis. With that in mind, (and because fiber modulus is not a given quantity) it became important to test an uncoated fiber from the particular batch that was being coated. It

should also come as no surprise that the ultimate stress obtained from these tests differed significantly from that given by Textron for the particular fiber spools used. These differences are summarized in the table below.

TABLE A1. FIBER NOMINAL VERSUS MEASURED VALUES

Spool ID Number	Textron Diameter (mils)	Measured Diameter (mils)	Textron σult (KSI)	Measured σult (KSI)
14CO-31	5.38	5.38	277	375 *
13CO-366	5.4	5.4	266	340
13CO-368	5.36	5.36	365	423

*uncoated fiber not tested; this value is with an approximately 0.5 μm thick alumina coating.

Thesis Test Procedures. The following is a step-by step procedure for conducting the tensile tests in this experiment, with additional comments on difficulties encountered during the procedure.

1) Turn on the equipment, including the ATS Series 1102B Tensile Test Machine, the LaserMike laser extensometer, and the Z-248 computer. (Note: these usually remained on at all times.) Allow at least 20 minutes for the laser extensometer to warm up.

2) Calibrate the laser extensometer. Procedures for this are contained in (19). This was performed before the tests by Materials Lab personnel, and twice between fiber series by the experimenter as a check; calibration was not found to vary significantly (more than ±0.0002 inch/±5 μm) for the measurements used (gage length and extension of the fiber). It was discovered that although the equipment has an accuracy of ±5 μm for large objects (on the order of tens of mm), it could not be used as a micrometer; that is, it would not record a measurement at all for an object less than 130 μm across, and was very inaccurate for objects nominally 140-150 μm across (the tested fibers).

3) Calibrate the load cell. This was done prior to testing by materials lab personnel.

4) Start the PCDAS 132 software on the Z-248 computer. This software is a customized data acquisition program written for use at the Materials Lab by University of Dayton Research Institute (UDRI) personnel, and modified for these particular experiments by Mr George Hartman of UDRI. It is a menu driven program that prompts for specimen and test information and allows preliminary viewing of the data during and immediately after collection.

5) Ensure that the testing apparatus is in the correct position to begin. This consists of raising the crosshead so that the top edge of the lower pneumatic grip is 1.25 inches from the bottom edge of the upper pneumatic grip. In practice, this distance was measured once, the crosshead displacement indicator zeroed, and the crosshead positioned in subsequent tests so that the indicator again read zero. The particular value of 1.25 inches was chosen to allow the laser extensometer scan (see below) to intersect a small portion of the fiber mounting tab (Figure B-1) above and below the one inch cutout.

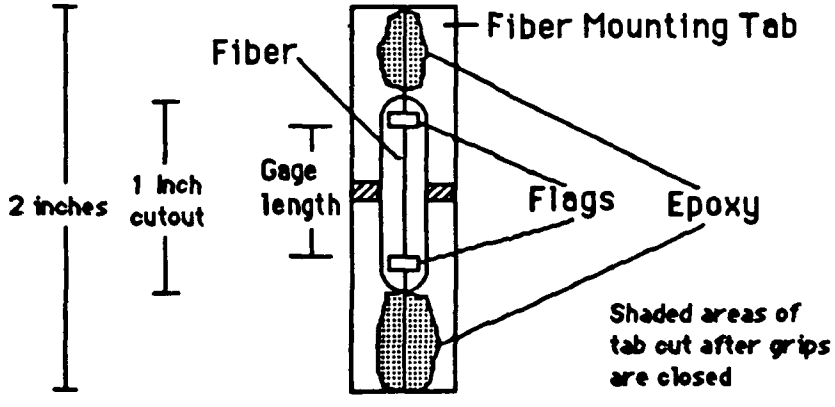

Figure B-1. Tensile Test Sample

6) Choose option 9, "setup LaserMike" from the menu. The user is then prompted for the number of scans to be averaged for a single measurement, for the maximum

extension expected, and for the scan recording code. The values entered for this experiment were 8, 0.2 mm, and S500100 respectively. See the LaserMike manual (19) for a further explanation.

At this point, the fiber is placed in the lower pneumatic grip. Holding an edge of the sample mounting tab parallel to the fiber, position the sample so that the following conditions are met: the fiber is parallel to the laser scan line and as close as possible without blocking the scan (the scan is blocked if laser reflection can be seen from the fiber); approximately 0.125 inches or 3 mm of the tab should be visible between the bottom of the cutout in the tab and the top of the grip. The laser scan line can be positioned on either side of the fiber. When this is done, activate the pneumatic lever closing the lower grip. A steady hand is required, lest the sample be caught in a crooked position by the grip.

Now, if the sample has been positioned properly, the gage length (the distance between the two flags on the fiber) will be displayed on the computer screen (in inches). If the fiber is improperly positioned, the display will read "0.00000"; if that is the case, release the grip and reposition the fiber, then try again. Because of the epoxy attaching the fiber to the cardstock sample tab, the procedure can be repeated several times without damaging the fiber.

Although a gage length is now displayed on the computer screen, this is not necessarily the correct, zero-strain gage length. The reason for this is that the cardstock tabs are not perfectly flat, and in the process of curing, the epoxy may actually put the fiber in slight compression or tension. The effect is undoubtedly small, but for greatest accuracy the gage length should only be recorded for the fiber under zero load. Unloading the fiber is an integral part of the testing process, however, so this is no great inconvenience.

6) Carefully close the upper grip by actuating its lever. This is easier said than done; in closing, the grips actually pull up slightly on the sample, which means that a load will be placed on the sample in the process. By actuating the lever in different ways, the grip closure speed and thus the induced load versus time curve can be varied. Too quick an upper grip closure will result in a rapid rise to a fairly high (4 kg) peak load as observed by multiplying the load cell voltage readout by its full scale (10 volts = 20 pounds) setting; a slower grip closure is generally better, but trial and error has shown that the slowest closure rates can sometimes result in higher peak loads. A good grip closure will result in a peak load of 2.5 kg or less.

Since at this point the load is distributed over the paper tab and the fiber, the portion borne by the fiber is small, and the induced strain (which can be calculated from the change in gage length under this initial load as measured by the laser extensometer readout on the computer screen) is quite small, 0.1 to 0.2%, or about 10 to 20% of the strain to failure for the fiber; for this reason, it was not regularly recorded. Spot checks of the data showed no obvious correlation between initial loading/strain and eventual strain to failure, peak load, or elastic modulus.

Following the peak of the induced load, the load will decrease gradually for a few seconds, then level out. At this point, the testing machine crosshead is raised (since the lower beam of the testing machine is the crosshead, lowering it would put more load on the sample) until the load cell readout is zero. At this point, one side of the sample holding tab is carefully cut in two places to remove an entire section (see Figure B-1) with a pair of scissors. Some loading of the sample is unavoidable during this process, but it is usually small; the greatest risk is bending the tab (and the fiber) at the point where it is held by either grip, since this will usually break the fiber. Now, if the fiber mounted on the sample was under residual tension or compression due to the curing epoxy, the load may be slightly off zero; it should be zeroed again before proceeding (if

the load has become negative, the crosshead will have to be lowered). When the load is again zero, cut the tab on the other side of the fiber in the same way, and again return the load to zero. A representative curve showing the loads induced on the sample during this process is shown in Figure B-2.

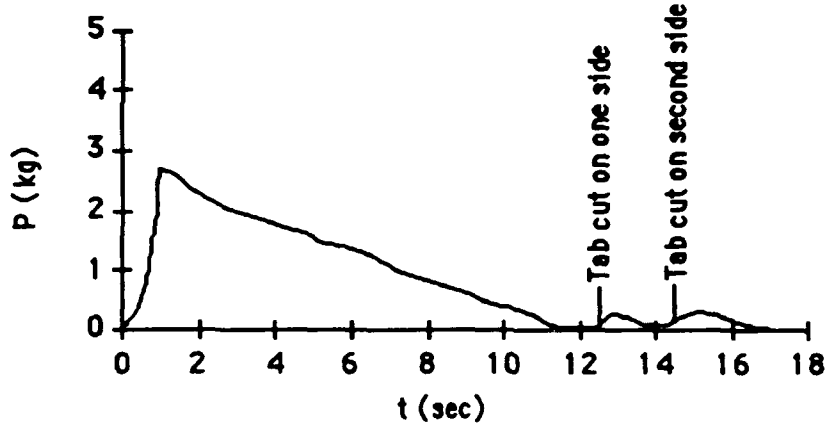

Figure B-2. Representative Initial Load Curve

7) At this point, all load is being borne by the fiber, and if the load cell output is zero, the gage length reading on the computer screen is the desired value. Record this number, and convert it to millimeters for use in subsequent steps.

8) Press the [Carriage return] key on the computer keyboard to return to the PCDAS 132 main menu. From here, choose option 1 and enter data on the sample as prompted. The identifying data requested is self explanatory, the diameter requested should be the fiber diameter as measured earlier, and the "LaserMike gage length" should be the value just recorded. The load corresponding to full scale in the data acquisition program should match the full 10 volt output from the load cell; the only trick here is converting from pounds to kilonewtons (the requested input). A full crosshead displacement voltage is also requested; this was found to be 5.248, but is unimportant if the crosshead displacement data is not being used. All data entered is saved as a default for the next

sample, so in practice, once the initial values are entered, only the new sample number and gage length need to be changed. When all data is entered, the program returns to the main menu.

9) Choose option 2, and enter the filename to which the data will be saved. Note that the program does not save the data automatically, nor does it warn you if you haven't saved data.

10) Choose option 3 and enter the number of data points to acquire, typically 200 . This must be done for every sample, since the program defaults to the number taken for the previous sample. Thus if sample A failed after only 150 data points, the value would default to 150. Sample B, however, might not fail this early, but if the value were still 150, the data acquisition would cease and data would be lost.

11) Choose option 4 and enter the data acquisition time; 100 seconds was used for these tests. Note that this does not necessarily correspond to real time, but is a function of the LaserMike scan rate and the number of data points requested. This value does stay constant, and need only be set once.

12) Choose option 5 and activate the data acquisition channels to be used. LaserMike data is automatically acquired under this setup, so only channel 0 (load) and channel 1 (crosshead displacement if desired) are used. These values also need to be set only at the beginning of a series of tests (when the PCDAS program is started).

13) Choose option 6 to acquire data. Immediately after doing this, activate the crosshead so that it travels downward and loads the fiber. Sit back and enjoy the show until the fiber breaks. This can be directly observed visually, on the computer screen when the load goes to zero, and can usually be heard as a sound somewhere between a snap and a pop.

14) Press {Esc} to end data acquisition when the fiber breaks; the program will return to the main menu. Stop the crosshead's downward motion.

15) Choose option 7 to save the data in the file you designated earlier (step 9). **Be sure to do this!**

16) Remove the two pieces of the sample from the grips and return the crosshead to the initial position. While it is in transit, the raw data can be plotted one channel versus another or versus time. This is particularly useful to see if the laser extensometer data is noisy (possibly indicating flag slippage).

17) Return to step 5 and repeat until all samples are tested.

18) Quit the PCDAS 132 program.

Data Processing. To transform the data from raw voltages to stress, strain and modulus values, the MATE 243 program, also developed by UDRI for the Materials Lab, was used. This program reads the data files created by PCDAS 132 and produces its own files as well as hard copy output. The procedure was as follows.

1) Turn on the computer and start MATE 243.

2) Choose the option to do tensile test analysis.

3) Choose the "Metric Units" option.

4) Choose the option to load data from a file and enter the first file containing data to be analyzed.

5) Choose the "analyze data" option. A screen will be presented showing a stress vs strain plot. These values are calculated from the raw data and the fiber diameter and gage length supplied to PCDAS 132 during data acquisition. You are prompted to choose the beginning and end of valid data. Use this to eliminate spurious data points from before the crosshead moved and after the fiber broke (in the latter case, the strain value can vary widely).

6) The screen will reappear with the invalid data removed. You are now prompted to select the beginning and end points for a least squares curve fit that will be used to compute the elastic modulus. In many cases, this was simple since the curve was linear

from beginning to end. In other cases, however, there was a non-linearity at the beginning or end; as a rule, this portion of the curve is excluded from the least squares fit. In a few cases, there was no obvious portion of the curve to select; to be consistent, points were chosen that would give the highest slope (hence modulUs) while still representing over half of the full stress-strain curve.

7) The computer will draw its least squares fit line over the curve. It now asks you to select the failure point and the yield point, but will default to the point of highest load and the "0.2% offset point" in the stress-strain curve. Since the former is the desired failure point, and yield strength has little or no meaning for silicon carbide fibers, the default values were accepted.

8) A screen of fiber properties is now displayed. This may be captured via a screen dump to the printer, or a more detailed printout, including a plot of the stress strain curve can be obtained. Since the data used in this study were all availabie on the initial screen, the screen dump method was primarily used.

9) At the prompt, enter a filename to save the analyzed data. The menu screen shown for steps 4 and 5 will now appear.

10) Return to step 4 and repeat until all data is analyzed.

11) Quit the program.

Appendix C: Tensile Test Data

TABLE C-1. PROPERTIES OF FIBER SERIES A
(AVERAGE COATING THICKNESS t ≅ 0.5 μm; 1 PASS COATING APPLIED AT 950 ° C, SOL CONCENTRATION 71 g/l)

	Sample #	Gage length (mm)	σ_{ult} (MPa)	Strain to failure (%)	Modulus (GPa)
	2	17.824	1505.9	0.3933	369.44
	3	16.521	2526.1	0.6857	386.23
	4	17.063	1288.8	0.3751	327.85
	5	17.148	1833.8	0.5481	325.94
	6	17.006	2066.1	0.5227	377.97
	7	17.155	1999.3	0.5656	365.87
	8	17.806	1767.0	0.4622	373.58
	9	16.356	2000.8	0.5715	348.35
	10	17.545	2513.9	0.6196	392.69
Total #	9				
		Average:	1944.6	0.5271	363.10
		Median:	1999.3	0.5481	369.44
		Standard Deviation:	387.2	0.0959	22.68
		St Dev of the Mean:	129.1	0.0320	7.56

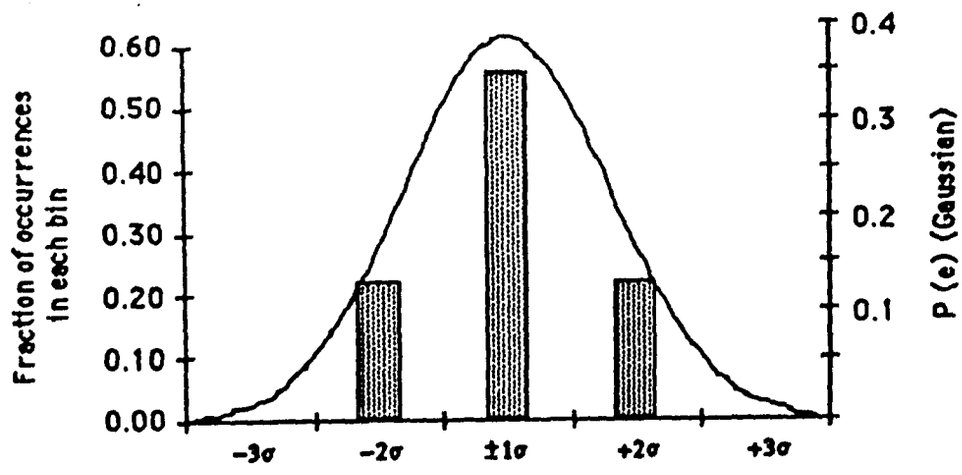

Figure C-1. Fiber A Modulus Measurement Distribution Compared to Gaussian Curve

TABLE C-2. PROPERTIES OF FIBER SERIES B
(AVERAGE COATING THICKNESS t ≅1.5 μm; 3 PASS COATING
APPLIED AT 950 ° C, SOL CONCENTRATION 71 g/l)

Sample #	Gage length (mm)	σ_{ult} (MPa)	Strain to failure (%)	Modulus (GPa)
1	16.867	2256.8	0.6415	343.31
2	18.355	2075.5	0.5701	364.86
3	17.931	1957.6	0.5355	361.73
4	18.110	1945.8	0.5442	342.45
5	17.323	2314.3	0.7156	324.39
6	18.143	1957.6	0.6187	327.78
7	17.365	2063.7	0.6231	346.87
8	16.655	1842.6	0.4972	344.83
9	17.932	1906.0	0.5326	360.91
10	18.343	1875.0	0.5290	347.63
11	16.760	1704.0	0.4577	359.26
13	17.559	1752.7	0.4455	379.53
14	16.540	1524.2	0.4576	325.90
15	18.651	1723.2	0.7436	295.74
16	18.061	2317.0	0.6047	386.54
17	18.049	2436.7	0.6136	381.36
18	17.750	2489.0	0.6983	351.11
19	18.062	2016.4	0.5344	369.91
20	18.311	2396.0	0.6103	373.47
Total # 19				
	Averages:	2029.2	0.5775	351.98
	Median:	2016.4	0.6047	359.26
	Standard Deviation:	266.9	0.0840	22.30
	St Dev of the Mean:	61.2	0.0193	5.12

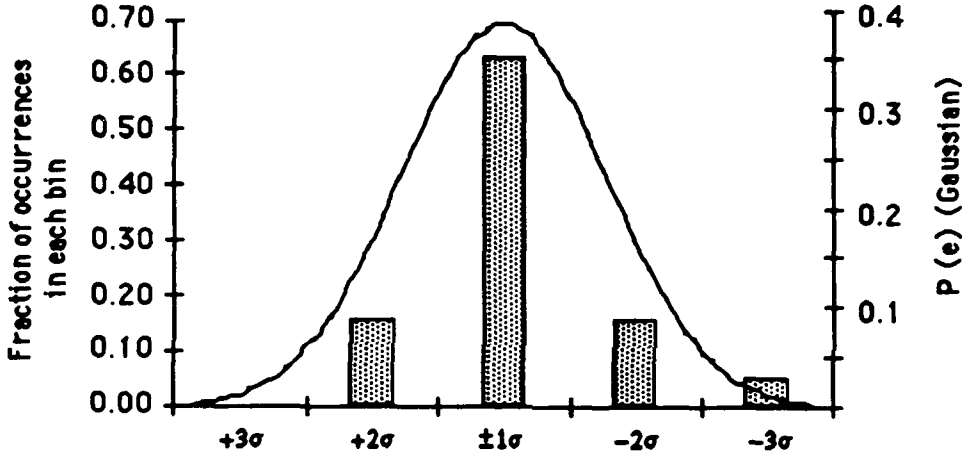

Figure C-2. Fiber B Modulus Measurement Distribution Compared to Gaussian Curve

TABLE C-3. PROPERTIES OF FIBER SERIES C
(AVERAGE COATING THICKNESS t ≡ 3.5 μm; 6 PASS COATING
APPLIED AT 950 ° C, SOL CONCENTRATION 71 g/l)

Sample #	Gage length (mm)	σ_{ult} (MPa)	Strain to failure (%)	Modulus (GPa)
1	19.056	1451.6	0.4745	304.92
2	18.354	2142.2	0.6062	373.02
3	18.704	2284.0	0.5568	392.82
4	18.292	2034.8	0.5443	331.33
5	18.920	1600.9	0.4457	363.62
6	17.967	2292.6	0.6390	353.25
7	18.588	2208.1	0.6368	343.16
8	18.319	2156.5	0.6184	345.30
9	18.305	1547.9	0.4357	349.36
10	18.284	1722.6	0.4779	353.19
11	17.820	1989.0	0.5815	331.55
12	16.704	1559.4	0.4592	349.49
13	17.279	1373.2	0.4234	316.88
14	17.303	1850.1	0.6371	297.01
15	17.175	1840.1	0.5235	343.44
16	19.055	2234.7	0.6025	372.22
17	19.041	2231.8	0.6296	367.11
18	18.212	1863.2	0.5356	349.55
19	17.837	2302.1	0.6522	356.18
20	17.796	2175.4	0.5709	386.43
Total # 20				
Averages:		1943.0	0.5525	348.99
Median:		2011.9	0.5638	349.52
Standard Deviation:		301.4	0.0748	23.92
St Dev of the Mean:		67.4	0.0167	5.35

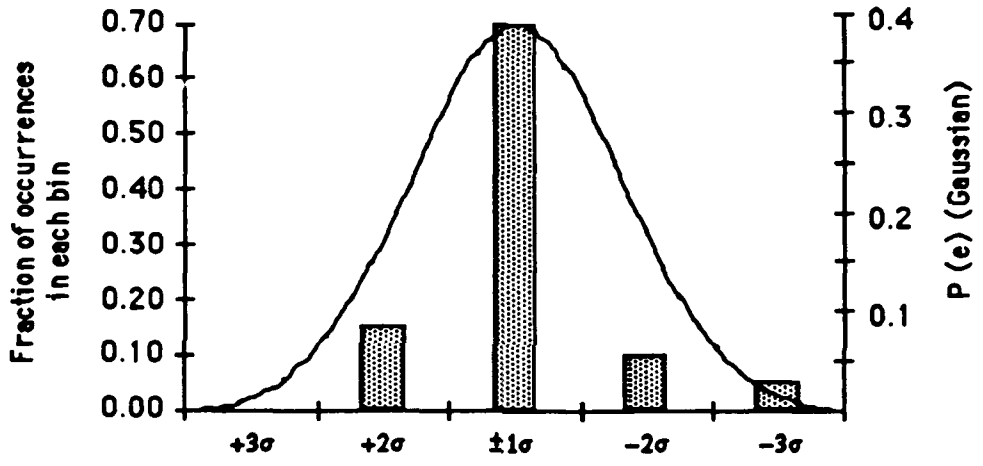

Figure C-3. Fiber C Modulus Measurement Distribution Compared to Gaussian Curve

TABLE C-4. PROPERTIES OF FIBER SERIES D
(AVERAGE COATING THICKNESS t ≅ 0 μm;
UNCOATED FIBER; BASIS FOR SERIES A – C)

	Sample #	Gage length (mm)	σ_{ult} (MPa)	Strain to failure (%)	Modulus (GPa)
	1	17.900	3017.4	0.7918	368.23
	2	17.626	2159.5	0.5736	357.70
	3	18.706	1976.7	0.5051	377.06
	4	18.506	1581.7	0.4310	370.28
	5	18.199	1953.1	0.4997	370.00
	6	16.575	2730.0	0.7723	348.81
	7	17.209	1914.8	0.5048	374.04
	8	18.854	2788.9	0.6709	402.23
	9	17.698	1975.2	0.4908	385.49
	10	17.714	2470.5	0.4933	386.45
	11	18.120	2911.3	0.7878	361.98
	12	18.346	2482.3	0.6175	383.24
	13	18.760	2610.6	0.6390	396.19
Total #	13				
		Averages:	2351.7	0.5983	375.52
		Median:	2470.0	0.5736	374.04
		Standard Deviation:	434.2	0.1207	14.54
		St Dev of the Mean	120.4	0.0335	4.03

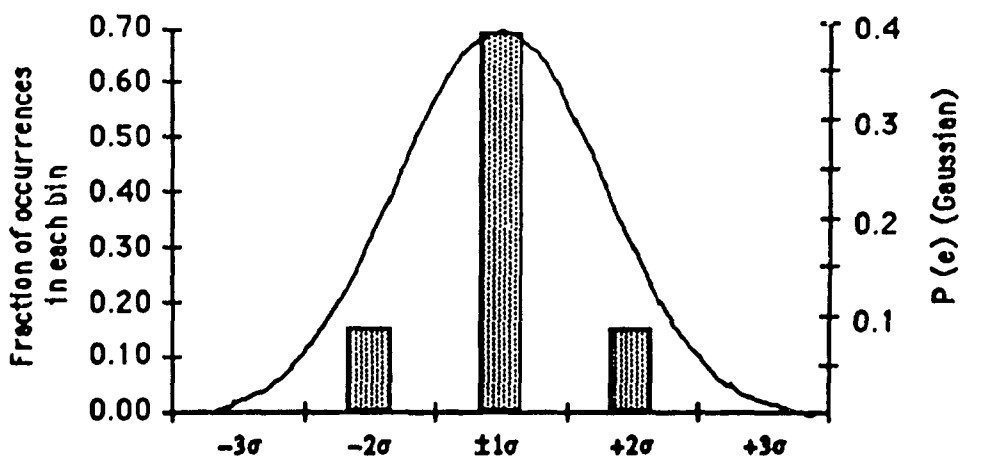

Figure C-4. Fiber D Modulus Measurement Distribution Compared to Gaussian Curve

TABLE C-5. PROPERTIES OF FIBER SERIES E
(AVERAGE COATING THICKNESS t ≅ 0.5 μm; 2 PASS COATING
APPLIED AT 800 ° C, SOL CONCENTRATION 71 g/l)

	Sample #	Gage length (mm)	σ_{ult} (MPa)	Strain to failure (%)	Modulus (GPa)
	1	18.100	1249.4	0.3368	389.19
	2	17.642	2549.6	0.7458	363.28
	3	18.708	2745.8	0.7766	347.33
	4	17.943	2686.2	0.8182	341.96
	5	18.198	2835.8	0.8347	335.96
	6	18.621	2243.1	0.6438	344.00
	7	17.241	2506.0	0.7985	337.03
	8	18.102	2289.6	0.6062	381.14
	9	18.203	2538.0	0.8930	312.26
	10	18.092	2719.6	0.7272	366.46
	11	18.002	2276.0	0.5870	395.14
	12	18.319	3017.4	0.7876	384.52
	13	18.787	2570.8	0.7274	355.90
	14	18.743	3017.4	0.7589	399.61
	15	18.618	2645.9	0.7094	367.26
	16	19.108	2821.4	0.6992	389.48
	17	18.807	2800.7	0.7401	383.14
	18	18.504	3017.4	0.8236	374.54
	19	18.349	2671.5	0.7392	374.16
Total #	19				
		Averages:	2589.6	0.7239	365.39
		Median:	2671.5	0.7401	367.26
		Standard Deviation:	389.6	0.1179	23.19
		St Dev of the Mean:	89.4	0.0270	5.32

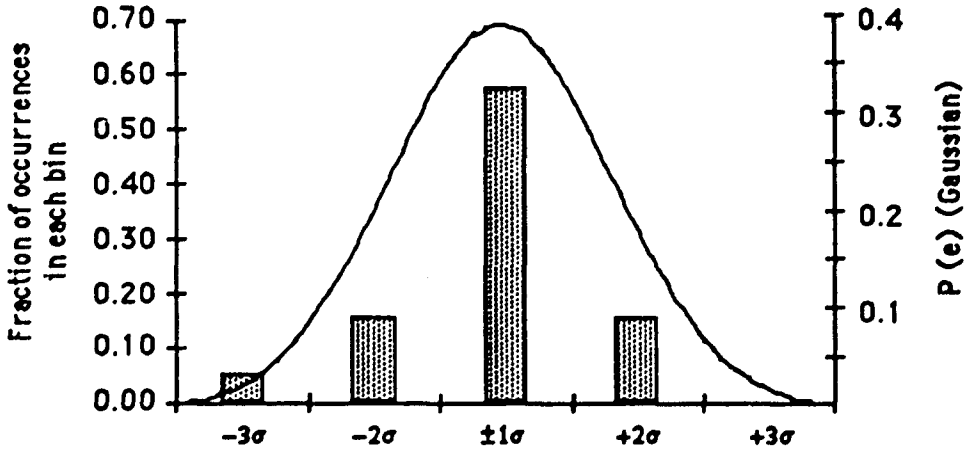

Figure C-5. Fiber E Modulus Measurement Distribution Compared to Gaussian Curve

TABLE C-6. PROPERTIES OF FIBER SERIES F
(AVERAGE COATING THICKNESS t ≅ 1.0 μm; 4 PASS COATING
APPLIED AT 800 ° C, SOL CONCENTRATION 71 g/l)

Sample #	Gage length (mm)	σ_{ult} (MPa)	Strain to failure (%)	Modulus (GPa)
1	17.738	2361.6	0.7131	331.43
3	18.307	2622.7	0.7742	332.46
4	18.910	2611.4	0.8140	329.90
5	18.387	2381.3	0.8040	299.76
6	17.810	2710.2	0.9185	310.21
7	18.357	2567.6	0.9852	302.91
8	17.730	2258.5	0.8108	300.57
9	18.721	2450.5	0.8738	317.85
10	16.894	2973.8	0.8720	348.96
11	17.777	2551.7	0.6858	362.48
12	18.450	2149.4	0.5589	362.45
13	17.309	2192.3	0.6134	369.54
14	18.556	2690.6	0.7611	347.81
15	18.599	1608.1	0.4179	358.99
16	17.960	2026.2	0.5883	347.22
17	18.245	2518.8	0.6905	353.73
18	18.206	2192.3	0.5106	381.31
Total # 17				
Averages:		2403.9	0.7289	338.68
Median:		2450.5	0.7611	347.22
Standard Deviation:		307.7	0.1487	24.81
St Dev of the Mean:		74.6	0.0361	6.02

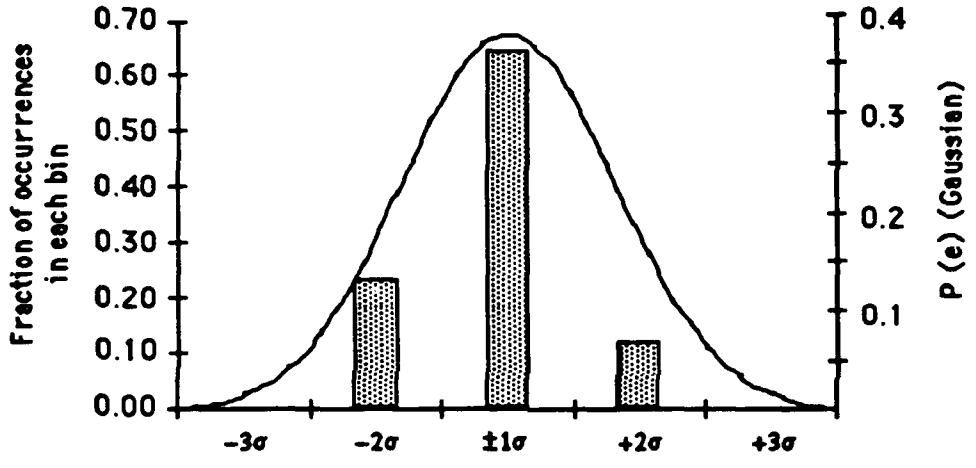

Figure C-6. Fiber F Modulus Measurement Distribution Compared to Gaussian Curve

TABLE C-7. PROPERTIES OF FIBER SERIES G
(AVERAGE COATING THICKNESS t ≡ 0 μm;
UNCOATED FIBER; BASIS FOR SERIES H – M)

	Sample #	Gage length (mm)	σ_{ult} (MPa)	Strain to failure (%)	Modulus (GPa)
	4	18.422	2851.3	0.7832	362.11
	6	18.122	2451.1	0.7106	349.43
	7	18.871	3080.0	0.8588	374.78
	8	17.884	3087.6	0.7713	387.02
	9	19.502	2582.0	0.7463	355.57
	10	18.171	3214.0	0.9184	352.09
	11	16.873	2949.1	0.8550	371.20
	12	18.081	2684.3	0.7487	356.37
	13	17.056	3358.4	1.0141	357.85
	14	17.802	3433.6	0.9717	348.76
	15	18.399	3316.3	0.9277	362.19
	16	16.884	2849.8	0.9222	334.61
	17	17.512	2257.0	0.6136	365.89
	18	17.742	2837.8	0.8031	357.58
	19	17.528	2997.3	0.8318	360.30
	20	17.179	3057.5	0.8309	361.09
	21	17.937	2269.0	0.6712	351.52
	22	17.823	2539.9	0.7610	329.25
	23	17.417	3198.9	0.9406	367.60
	24	17.786	3319.3	0.9026	367.24
	25	18.519	3153.8	0.8984	361.90
	26	18.212	2416.5	0.6444	380.63
	27	16.161	3027.4	0.9304	326.12
	28	17.629	2952.1	0.9466	341.28
	29	17.815	3207.9	0.9253	365.20
	30	17.579	2928.1	0.8569	361.12
Total #	26				
		Averages:	2923.8	0.8379	358.03
		Median:	2974.7	0.8559	360.70
		Standard Deviation:	330.1	0.1039	13.99
		St Dev of the Mean:	64.7	0.0204	2.74

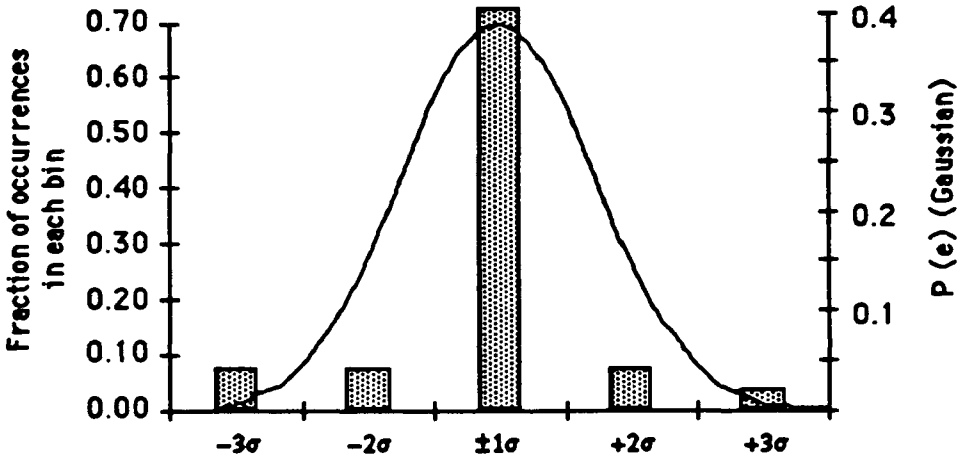

Figure C-7. Fiber G Modulus Measurement Distribution Compared to Gaussian Curve

TABLE C-8. PROPERTIES OF FIBER SERIES H
(AVERAGE COATING THICKNESS t ≡ 0.5 μm; 4 PASS COATING
APPLIED AT 950 ° C, SOL CONCENTRATION 36 g/l)

Sample #	Gage length (mm)	σ_{ult} (MPa)	Strain to failure (%)	Modulus (GPa)
1	17.482	2739.9	0.8252	324.63
2	18.083	2813.7	0.8077	352.98
3	17.673	2887.5	0.8537	347.51
4	18.408	3082.3	0.9756	348.58
5	17.779	2574.5	0.7515	360.86
6	18.067	2695.6	0.7929	345.29
7	18.348	3005.6	0.7739	384.51
8	19.044	3055.8	0.8803	348.21
9	18.659	2772.3	0.8467	360.19
10	18.821	2798.9	0.8178	378.02
11	18.761	3129.6	0.8976	358.04
12	17.227	2497.8	0.7667	359.95
13	18.375	2742.8	0.7216	395.00
14	17.789	2884.5	0.8639	361.70
15	17.769	2353.1	0.6633	378.16
16	19.133	2621.8	0.8231	357.63
17	17.224	2710.3	0.8538	358.11
18	17.843	2483.0	0.7417	375.77
20	17.984	2860.9	0.8418	349.44
21	18.669	3318.5	0.9524	352.04
22	18.593	1857.1	0.6393	322.55
23	17.238	3200.4	0.9769	342.17
24	18.412	2406.2	0.6580	363.22
25	18.354	2914.1	0.8954	360.33
26	17.013	2964.2	0.8495	356.83
27	17.490	3182.7	0.9309	350.26
28	18.409	2858.0	0.8623	365.98
29	17.905	2757.6	0.8256	361.80
Total # 28				
Averages:		2791.7	0.8246	357.85
Median:		2806.3	0.8337	358.50
Standard Deviation:		297.5	0.0869	15.36
St Dev of the Mean:		56.2	0.0164	2.90

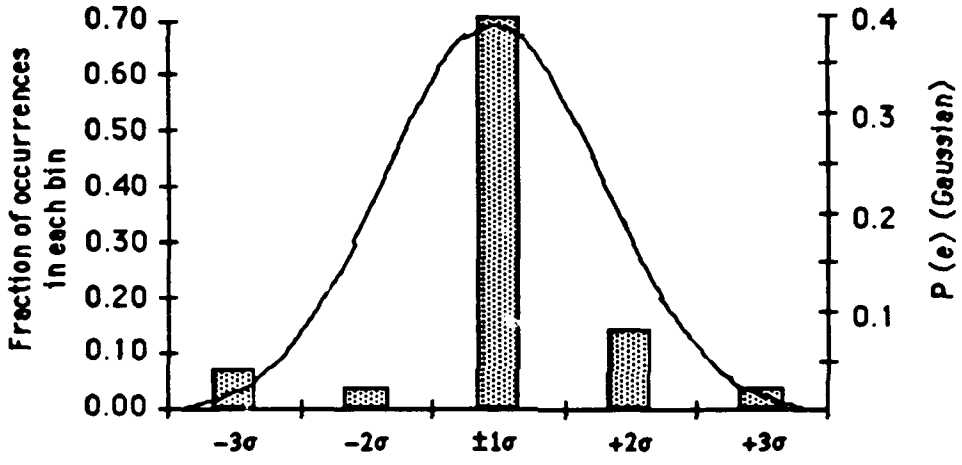

Figure C-8. Fiber H Modulus Measurement Distribution Compared to Gaussian Curve

TABLE C-9. PROPERTIES OF FIBER SERIES I
(AVERAGE COATING THICKNESS t ≅ 1.5 μm; 8 PASS COATING
APPLIED AT 950 ° C, SOL CONCENTRATION 36 g/l)

	Sample #	Gage length (mm)	σ_{ult} (MPa)	Strain to failure (%)	Modulus (GPa)
	1	17.717	2374.0	0.7599	357.64
	2	16.973	2414.4	0.7812	354.01
	3	17.964	2573.1	0.7423	336.41
	4	18.043	2893.3	0.8897	339.68
	5	17.626	2786.5	0.8949	341.54
	6	17.946	2881.7	0.8719	349.76
	7	17.296	2893.3	0.9105	327.18
	8	18.943	2697.1	0.7884	367.15
	9	17.512	2613.5	0.8659	333.66
	10	19.218	2982.7	0.8631	356.47
	11	18.689	1872.1	0.5885	349.69
	12	17.538	2203.8	0.6503	355.34
	13	18.476	1990.4	0.6406	378.28
	14	17.865	2754.8	0.8645	353.16
	15	17.674	2296.2	0.7114	347.32
	16	17.380	2501.0	0.7176	352.94
	17	16.974	2694.2	0.8096	350.29
	18	18.063	3002.9	0.8311	360.33
	19	17.409	2613.5	0.7864	357.40
	20	18.405	2278.8	0.7094	355.48
	21	17.830	2552.9	0.8191	346.98
	22	18.285	2723.1	0.7640	357.37
	23	17.645	2446.2	0.7673	348.34
	24	18.145	1805.8	0.6229	340.42
	25	17.479	2916.3	0.9519	345.40
	26	17.672	2446.2	0.7560	361.07
	27	18.661	2175.0	0.7105	338.12
	28	18.120	2855.8	0.8859	352.39
	29	17.311	2682.7	0.8936	341.89
Total #	29				
		Averages:	2549.0	0.7879	350.20
		Median:	2613.5	0.7864	350.29
		Standard Deviation:	319.5	0.0925	10.37
		St Dev of the Mean:	59.3	0.0172	1.93

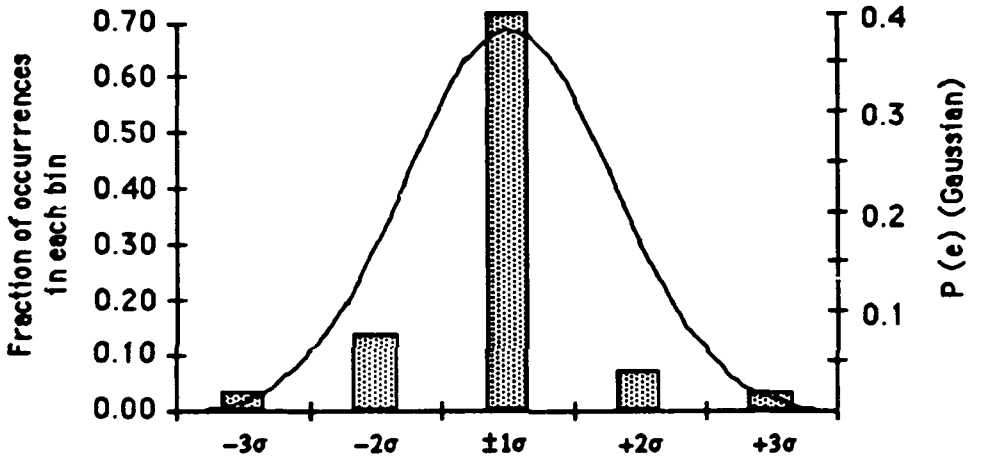

Figure C-9. Fiber I Modulus Measurement Distribution Compared to Gaussian Curve

TABLE C-10. PROPERTIES OF FIBEP. SERIES J
(AVERAGE COATING THICKNESS t ≅ 2.5 μm; 12 PASS COATING
APPLIED AT 950 ° C, SOL CONCENTRATION 36 g/l)

	Sample #	Gage length (mm)	σ_{ult} (MPa)	Strain to failure (%)	Modulus (GPa)
	1	18.163	2314.0	0.7566	353.55
	2	18.425	2435.0	0.7706	352.62
	3	18.057	2710.9	0.8327	348.89
	4	16.778	2547.7	0.8765	322.64
	5	17.307	1936.8	0.6560	329.96
	6	17.729	2373.1	0.7235	329.95
	7	16.731	1821.4	0.5648	323.89
	8	17.202	2252.1	0.7530	344.56
	9	17.736	2133.8	0.6359	327.01
	10	17.824	2305.6	0.7111	346.31
	11	17.236	2010.0	0.6072	333.60
	12	18.053	2249.3	0.6711	356.58
	13	16.929	1894.6	0.6031	307.80
	14	17.816	1990.3	0.6088	328.95
	15	17.953	2525.1	0.7541	339.25
	16	17.487	2063.5	0.6217	364.92
	17	17.771	2409.7	0.7518	357.59
	18	16.731	2691.2	0.8608	338.02
	19	18.243	2066.3	0.6572	349.14
	20	17.804	1843.9	0.6249	308.40
	21	18.264	2556.1	0.7871	363.22
	22	18.396	2297.1	0.6614	351.49
	23	17.431	2297.1	0.6922	326.98
	24	18.120	2100.1	0.6728	360.52
	25	17.532	1883.3	0.6476	343.80
	26	18.324	2378.7	0.6862	349.27
	27	16.931	2325.3	0.7996	342.62
	28	18.359	2330.9	0.6530	350.34
	29	17.796	2494.2	0.8892	311.70
	30	17.842	2671.5	0.8712	330.21
Total #	30				
		Averages:	2263.6	0.7134	339.79
		Median:	2301.4	0.6892	343.21
		Standard Deviation:	254.9	0.0898	15.57
		St Dev of the Mean:	46.5	0.0164	2.84

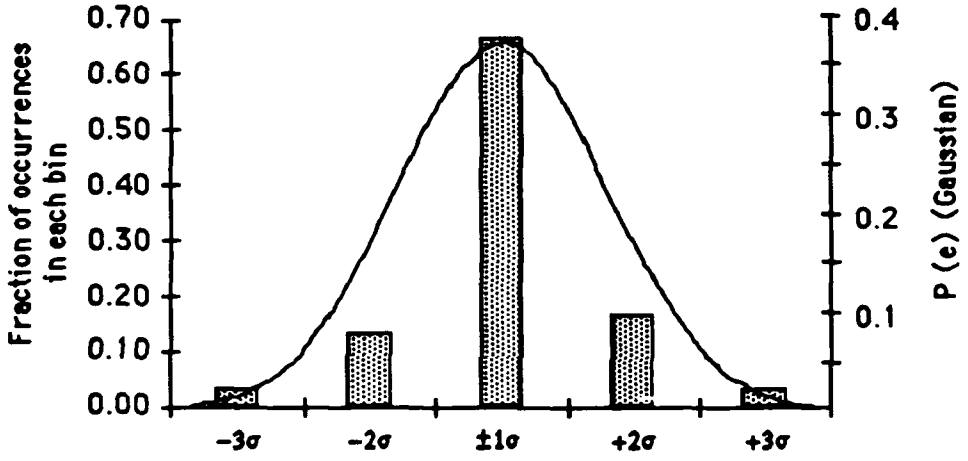

Figure C-10. Fiber J Modulus Measurement Distribution Compared to Gaussian Curve

TABLE C-11. PROPERTIES OF FIBER SERIES K
(AVERAGE COATING THICKNESS t ≡ 0.5 μm; 4 PASS COATING
APPLIED AT 800 ° C, SOL CONCENTRATION 36 g/l)

Sample #	Gage length (mm)	σ_{ult} (MPa)	Strain to failure (%)	Modulus (GPa)
1	17.616	3030.7	0.8925	367.40
2	18.115	3378.6	1.0769	326.78
3	17.208	2744.7	0.7927	354.83
4	18.029	3198.7	0.9172	373.78
5	18.571	2582.6	0.7509	341.60
6	17.457	3225.3	0.9763	355.94
7	16.167	2880.3	0.8185	388.68
8	17.750	3104.4	0.9187	367.03
9	17.133	3133.9	0.9043	370.82
10	17.516	3048.4	0.8237	360.26
11	17.938	2352.6	0.6995	365.02
12	17.621	2980.6	0.9211	348.13
13	16.830	2939.3	0.9402	348.64
14	17.014	3402.1	1.0495	355.67
15	17.264	2995.3	0.9696	336.62
16	17.564	2759.4	0.8590	328.52
17	17.518	3139.8	0.9830	342.15
18	17.087	3018.9	0.8874	363.63
19	18.747	2865.6	0.8441	358.01
20	17.878	2644.5	0.8127	359.06
21	17.715	3036.6	0.8646	358.43
22	17.485	3027.7	0.8948	354.25
23	18.082	3113.2	0.9426	365.46
24	17.353	3242.9	0.9602	360.64
25	17.326	3133.9	0.9573	351.49
26	18.224	3163.3	0.9060	366.02
27	17.864	2895.1	0.8090	378.07
28	17.446	2818.4	0.9114	314.27
29	17.796	2898.0	0.8407	362.70
30	18.276	2753.6	0.8283	366.35
Total # 30				
Averages:		2983.6	0.8918	356.34
Median:		3029.2	0.9051	359.66
Standard Deviation:		227.5	0.0813	15.43
St Dev of the Mean:		41.5	0.0148	2.82

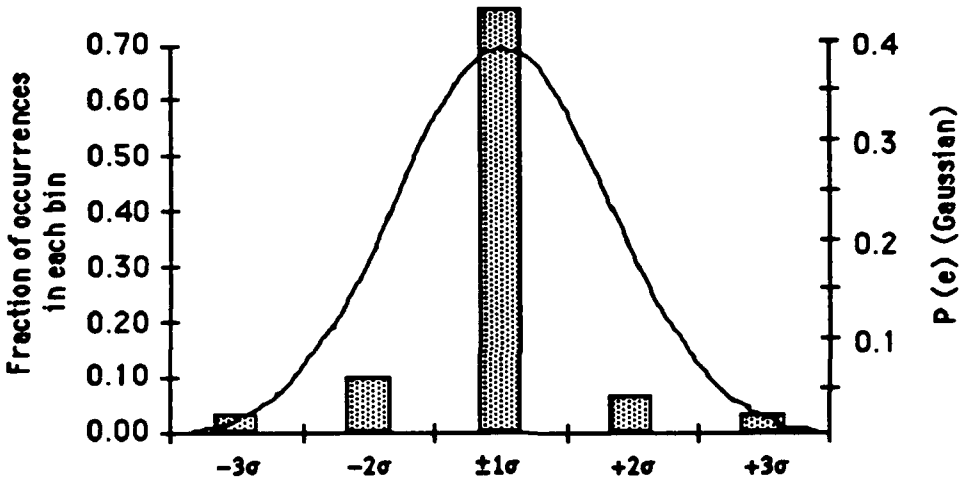

Figure C-11. Fiber K Modulus Measurement Distribution Compared to Gaussian Curve

TABLE C-12. PROPERTIES OF FIBER SERIES L
(AVERAGE COATING THICKNESS t ≡ 1.5 μm; 8 PASS COATING
APPLIED AT 800 ° C, SOL CONCENTRATION 36 g/l)

Sample #	Gage length (mm)	σ_{ult} (MPa)	Strain to failure (%)	Modulus (GPa)
1	17.063	2431.6	0.6788	367.55
2	17.672	2707.5	0.7704	354.36
3	17.512	2276.4	0.7020	366.51
4	18.259	2543.7	0.7679	361.17
5	17.945	2865.6	0.8351	361.14
6	17.693	2492.0	0.7149	351.29
7	17.533	3000.7	1.0518	315.34
8	18.029	2083.8	0.4931	381.88
9	17.594	2687.4	0.8143	372.82
10	16.980	3075.4	0.9125	348.05
11	16.718	2773.6	0.5865	433.53
12	18.654	2920.2	0.8878	356.13
13	17.600	2785.1	0.8197	349.12
14	17.827	2675.9	0.6896	439.16
15	17.522	3130.0	1.0234	327.45
16	17.379	2644.3	0.8126	359.05
17	16.903	2256.3	0.7033	319.52
19	18.627	2770.8	0.7936	375.69
20	17.794	2621.3	0.7498	379.36
21	17.993	3118.5	0.9034	364.63
22	17.549	2877.1	0.9061	343.27
23	18.175	2739.1	0.8497	362.42
24	17.177	2762.1	0.8488	356.95
25	17.734	3015.1	0.8536	351.20
26	17.634	3038.1	1.0947	313.96
27	18.357	2664.4	0.8524	346.75
28	18.085	2917.3	0.9691	342.74
18*	16.563	2566.7	1.4906	180.16
Total # 27				
Averages:		2736.0	0.8180	359.30
Median:		2762.1	0.8197	356.95
Standard Deviation:		262.1	0.1322	27.95
St Dev of the Mean:		50.4	0.0254	5.38

* not included in count, average, median or standard deviations

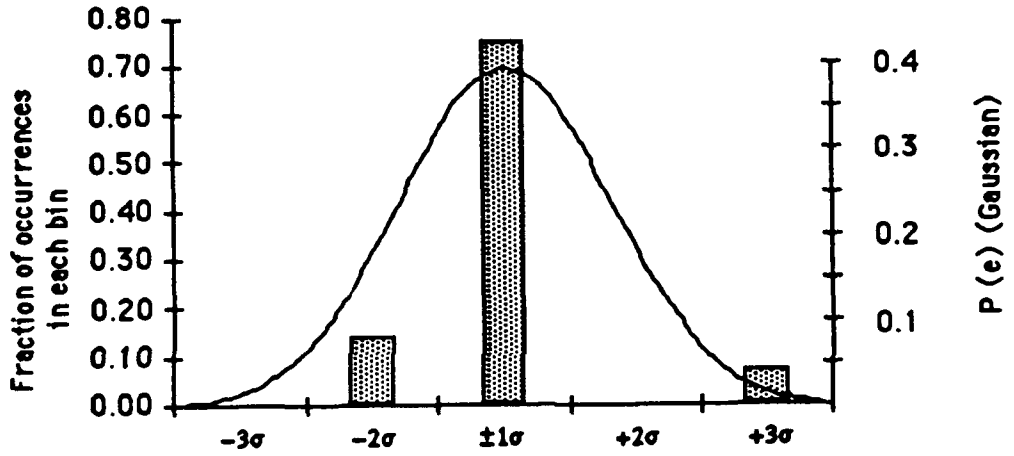

Figure C-12. Fiber L Modulus Measurement Distribution Compared to Gaussian Curve

TABLE C-13. PROPERTIES OF FIBER SERIES M
(AVERAGE COATING THICKNESS t ≡ 2.5 μm; 12 PASS COATING
APPLIED AT 800 ° C, SOL CONCENTRATION 36 g/l)

Sample #	Gage length (mm)	σ_{ult} (MPa)	Strain to failure (%)	Modulus (GPa)
1	17.501	2020.3	0.6473	335.93
2	17.346	2222.6	0.6560	355.66
3	17.631	2472.7	0.7780	338.13
4	18.293	2166.4	0.6526	368.62
5	16.857	2658.1	0.9011	327.51
6	18.300	2391.2	0.7134	345.73
7	17.962	2464.3	0.7410	365.72
8	17.245	2554.2	0.8249	346.50
9	16.942	2961.6	0.9026	345.38
10	17.919	2753.7	0.9384	324.18
11	16.911	2607.6	0.8591	331.42
12	16.774	2725.6	0.8843	337.21
13	16.509	2717.1	0.9231	327.87
14	16.436	2658.1	0.8252	343.01
15	16.847	2512.0	0.8232	328.03
16	17.841	2807.1	0.8827	330.26
17	18.998	2483.9	0.8370	343.95
19	18.216	2562.6	0.7362	362.04
20	17.215	2512.0	0.8145	362.27
21	17.628	2762.1	0.8415	329.75
22	17.532	2585.1	0.8953	320.10
24	16.934	2222.6	0.9510	306.01
25	18.452	2599.1	0.8342	335.54
27	17.673	2559.8	0.7129	359.44
28	16.778	1039.7	0.3724	333.12
18*	17.686	2219.8	0.5658	451.91
26*	16.580	2127.1	0.8242	274.51
Total # 25				
Averages:		2480.8	0.7979	340.14
Median:		2559.8	0.8252	337.21
Standard Deviation:		361.1	0.1236	15.27
St Dev of the Mean:		72.2	0.0247	3.05

* not included in count, average, median or standard deviations

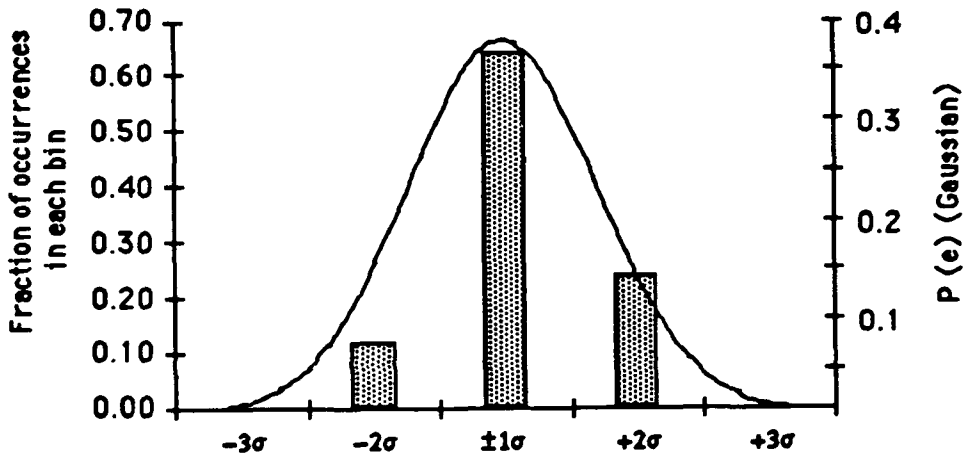

Figure C-13. Fiber M Modulus Measurement Distribution Compared to Gaussian Curve

Bibliography

1. Aveston, J. *et al.* "Single and multiple fracture," *The properties of fibre composites, Conference Proceedings*, London: IPC Science and Technology Press Ltd. 15-26. 4 November 1971.

2. Chawla, K. K. *Composite Materials.* New York: Springer Verlag, 1987.

3. Chiao, Y-H. and D. R. Clarke. "Residual Stress Induced Fracture in Glass-Sapphire Composites: Planar Geometry," *Acta Metallica Materialia, 38*: 251-258 (February 1990).

4. Clarke, D. R. and Y-H. Chiao. "Residual Stress Induced Fracture in Glass-Sapphire Composites: Cylindrical Geometry," *Acta Metallica Materialia, 38*: 259-267 (February 1990).

5. Evans, A. G. *et al.* "On Crack Path Selection and the Interface Fracture Energy in Bimaterial Systems," *Acta metallica, 37*: 3249-3254 (December 1989).

6. Foulds, William, Manager, Ceramics. Personal Correspondence to Ronald J. Kerans. Textron Specialty Materials, Lowell, MA, 27 December 1988.

7. Goettler, R. W. and K. T. Faber. "Interfacial Shear Stresses in Fiber-Reinforced Glasses," *Composites Science and Technology, 37*:129-147 (1989).

8. Hay, R. S. and E. E. Hermes. "Sol-Gel Coatings on Continuous Ceramic Fibers," submitted to *Ceramic Engineering and Science Proceedings.*

9. Hay, R. S. *et al.* "Microstructure and Phase Evolution in Sol-Gel Derived YAG Thin Films," *Ceramic Transactions—Ceramic Thin and Thick Film, 11*: 243-258 (1990).

10. Hsueh, Chun-Hway. "Analytical Evaluation of Interfacial Shear Strength for Fiber-Reinforced Ceramic Composites," *Journal of the American Ceramic Society, 71*: 490-493 (June 1988).

11. Kerans, Ronald J. *et al.* "The Role of the Fiber–Matrix Interface in Ceramic Composites," *American Ceramic Society Bulletin, 68*: 429-442 (February 1989).

12. Kerans, Ronald J. and Triplicane A. Parthasarathy. "Theoretical Analysis of the Fiber Pull-Out and Push-Out Tests," submitted to the *Journal of the American Ceramic Society*, 6 April 1990.

13. Lehman, Richard L. and Cheryl A Doughan. "Carbon Coated Alumina Fiber/Glass Matrix Composites," *Composites Science and Technology, 37*: 149-164 (1990).

14. Lu, Mei-Chien and Chun-Hway Hsueh. "Effects of Friction in Ceramic Coating/Fiber Composites," *Journal of Composite Materials, 24*: 572-593 (June 1990).

15. Luh, Ellice Y. and Anthony G. Evans. "High-Temperature Mechanical Properties of a Ceramic Matrix Composite," *Journal of the American Ceramic Society, 70*: 466-469 (July 1987).

16. Mah, T. *et al.* "High-Temperature Mechanical Behavior of Fiber-Reinforced Glass-Ceramic-Matrix Composites," *Journal of the American Ceramic Society, 68*: C-248–C-251 (September 1985).

17. McClave, James T. and Frank H. Dietrich II. *Statistics*. San Francisco: Dellen Publishing Company, 1988.

18. Mendelson, A. *Plasticity: Theory and Application*. New York: MacMillan, 1968.

19. *Model 501-00 Operator's Manual*. Manual Number 90925, LaserMike, Inc., Dayton, OH, November 1987.

20. Pach, Ladislav *et al.* "Nucleation of alpha alumina in boehmite gel," *Journal of the Materials Research Society, 5*: 278–285 (February 1990).

21. Poritsky, Hillel. "Analysis of Thermal Stresses in Sealed Cylinders and the Effect of Viscous Flow During Anneal," *Physics 5*: 406-412 (December 1934).

22. "Technical Data," *Ceramic Source '90, a Publication of The American Ceramic Society, Inc, 5*: 314-321 (1990).

23. Young, Hugh D. *Statistical Treatment of Experimental Data*. New York: McGraw-Hill, 1962.

24. Zhang, Wenchao. " Computation of Stress Fields in Unidirectional *n*-Phase Fibrous Composites under Longitudinal and Transverse Loads," *Computers and Structures, 34*: 647-653 (April 1990).

Vita

Capt Christian C. Daehnick [redacted] grew up in the Pittsburgh, Pennsylvania suburb of Allison Park. He completed high school in 1978 and enrolled in the Massachusetts Institute of Technology, graduating from there in 1982 with a Bachelor of Science degree in Aeronautical and Astronautical Engineering. He was also a distinguished graduate of the Air Force ROTC program, and received a regular commission in the United States Air Force. Entering active duty, he was assigned to the Foreign Technology Division at Wright-Patterson Air Force Base in Dayton, Ohio as a weapons analyst for two years before being transferred to that organization's Berlin (Germany) Liaison Office. He was selected as an inspector for the US-USSR Intermediate-Range Nuclear Forces (INF) Treaty, and made several trips to the Soviet Union in 1988 as a member of the inspection team that checked the accuracy of the technical data supplied by the Soviets on their weapons. Capt Daehnick also holds a Master of Arts degree in International Affairs from the University of Dayton and is a Distinguished Graduate of the Air Force Squadron Officers School. He is married to the former [redacted] of Dallas, Texas.

Permanent Address: 2996 Clearview Rd
Allison Park, PA 15101

REPORT DOCUMENTATION PAGE

Form Approved
OMB No 0704-0188

1. AGENCY USE ONLY (Leave blank)	2. REPORT DATE	3. REPORT TYPE AND DATES COVERED
	December 1990	Master's Thesis

4. TITLE AND SUBTITLE
MATERIAL PROPERTIES OF SILICON CARBIDE FIBERS WITH CONTINUOUSLY APPLIED SOL-GEL ALUMINA COATINGS

5. FUNDING NUMBERS

6. AUTHOR(S)
Christian C. Daehnick, Captain, USAF

7. PERFORMING ORGANIZATION NAME(S) AND ADDRESS(ES)
Air Force Institute of Technology
WPAFB OH 45433-6583

8. PERFORMING ORGANIZATION REPORT NUMBER
AFIT/GA/ENY/90D-03

9. SPONSORING/MONITORING AGENCY NAME(S) AND ADDRESS(ES)

10. SPONSORING/MONITORING AGENCY REPORT NUMBER

11. SUPPLEMENTARY NOTES

12a. DISTRIBUTION/AVAILABILITY STATEMENT
Approved for public release; distribution unlimited

12b. DISTRIBUTION CODE

13. ABSTRACT (Maximum 200 words)

An investigation was conducted to determine the effect of non-alpha-alumina coatings applied under varying conditions on some of the properties of silicon carbide fibers. Limited characterization of the coatings by optical, scanning elctron, and transmitted elctron microscopy as well as energy-dispersive x-ray analysis was performed. Tensile tests were used to determine changes in elastic modulus, ultimate strength, and strain to failure of the coated fibers relative to uncoated fibers. The coatings were found to lower the mean value of the measured properties as their thickness increased, but the measurements were not accurate enough to determine if this corresponded to a simple rule of mixtures relationship or not. For the same reason, no definitive statements can be made about the properties of the coating itself. A two-dimensional plane-strain analysis incorporating thermal residual stresses was also performed to determine possible failure points.

14. SUBJECT TERMS	15. NUMBER OF PAGES
Alumina, Silicon Carbide, Ceramics, Ceramic Composites, Ceramic Fibers, Tensile Testing, Elastic Proprties	146
	16. PRICE CODE

17. SECURITY CLASSIFICATION OF REPORT	18. SECURITY CLASSIFICATION OF THIS PAGE	19. SECURITY CLASSIFICATION OF ABSTRACT	20. LIMITATION OF ABSTRACT
Unclassified	Unclassified	Unclassified	UL